BIODEGRADABLE POLYURETHANE SCAFFOLDS AND DELIVERY SYSTEMS FOR REGENERATION OF BONE TISSUE

By

Bing Li

Dissertation

Submitted to the Faculty of the

Graduate School of Vanderbilt University

in partial fulfillment of the requirements

for the degree of

DOCTOR OF PHILOSOPHY

in

Chemical Engineering

August, 2010

Nashville, Tennessee

Approved:

Professor Scott A. Guelcher

Professor Jamey D. Young

Professor Jeffrey M. Davidson

Professor Kenneth A. Debelak

Professor Paul E. Laibinis

To my beloved wife, Hong, infinitely supportive

ACKNOWLEDGEMENTS

This work would not have been possible without the financial support of the Orthopaedic Trauma Research Program (DOD-W81XWH-07-1-0211), the Armed Forces Institute of Regenerative Medicine (sub-contract from the Rutgers-Cleveland Clinic Consortium Award DOD-W81XWH-08-2-0034), the National Institute on Aging (AG-06528), Vanderbilt University School of Engineering, the Vanderbilt Center for Bone Biology, the Department of Veterans Affairs, and the US Army Institute of Surgical Research.

I am grateful to all of those with whom I have had the pleasure to work during the projects. I would especially like to thank Dr. Scott Guelcher. As my mentor, he has taught me more than I could ever give him credit for here. He has shown me, by his example, what a good researcher and person should be. I would thank Dr. Joseph Wenke and Kate Brown at Institute of Surgical Research for the great work on the rat femoral segmental defect studies; Dr. Jeff Davidson at Department of Pathology for the help with the rat dermal wound study; Toshitaka Yoshii for the rat femoral plug defect study; and Dr. Daniel Perrien at Center for Bone Biology for his help with histomorphometry in the segmental defect studies. I would also thank Andrea Hafeman in Guelcher's lab for her help with material characterizations.

Nobody has been more important to me in the pursuit of this PhD than my loving and supportive wife, Hong. I am also grateful for my parents and family members, whose love and guidance are with me in whatever I pursue.

TABLE OF CONTENTS

INDEX OF FIGURES

INDEX OF TABLES

CHAPTER I

INTRODUCTION

Infection is the most common factor compromising bone wound healing. The current standard of care for infected bone fractures is a staged approach, comprising a first step of infection control using non-degradable PMMA beads loaded with antibiotics followed by a second step of grafting to promote bone formation. While complications may also arise from the wound healing process, it is critical to control infection in the graft as well. The present study aims to replace the current two-stage therapy with a single surgical procedure allowing both infection control and wound healing to take place simultaneously, which is achieved by delivering both antibiotic and growth factor from biodegradable polyurethane scaffolds composites in a sustained manner.

Infection control and bone wound healing

Infection complication in bone wound

Infection is defined as the imbalance between host tissue and microorganisms, which occurs when the number of organisms exceeds 10^5 per gram tissue (1), and it can be caused by tissue damage (such as skin wound, burns, and bone fracture) and surgical procedures including device implantation (2). Complications by wound infection are detrimental to bone tissue healing; therefore the number of organisms present in tissue has to be under a certain level in order to allow the wound healing process to occur normally. In severe, high energy bone wounds with a large surface area of soft tissue exposure, infection is the leading cause of morbidity and it can lead to undesirable consequences such as delay of

union, non-union, and amputation (3). A study on type III tibial fractures caused by combat injuries shows that while gram negative bacteria may be relatively easy to treat and clear in the initial stage of the wounds, subsequent evidence of infection is mainly complicated by gram positive organisms (3), indicating the necessity of long-term control of serious infections.

Infection control

In practice, poly(methyl methacrylate) (PMMA) cement beads or spacers have been used as a local antibiotic delivery platform, which has been shown to decrease infections in a number of clinical studies (4-6). Compared with systemic parenteral treatment, local antibiotic treatment can achieve much higher concentrations at the contaminated site, resulting in more efficient infection control and reduced systemic toxicity concerns (7-9). A study comparing the local use of gentamycin-PMMA beads to long-term, systemic parenteral gentamycin in the treatment of infected non-unions suggested similar success rates in patients (10). Additionally, systemic parenteral treatment has been reported to result in greater treatment failure compared with local antibiotic treatment (8). Therefore, the local antibiotic delivery strategy is comparable to or better than systemic parenteral antibiotic treatment.

However, since PMMA does not biodegrade, it must be removed during an additional surgical step and cannot be allowed to remain in the wound bed during definitive closure. Furthermore, the antibiotic release efficiency is typically low (e.g., <25% cumulative release), the burst release is high (>60% of the released antibiotic is within the first day), and the antibiotics are below therapeutic levels within a week or two (11-14). Cases of secondary infectious complications have been reported (15), which have been attributed to

insufficient sustained release of the antibiotic. Furthermore, too low a concentration of antibiotic may induce antibiotic resistance of bacteria (16).

Resorbable calcium phosphates and sulfates have also been investigated for local antibiotic delivery. Calcium sulfate pellets impregnated with antibiotic (Osteoset T, Wright Medical) have been shown to be effective in treating osteomyelitis in animals and humans (17-19). These biomaterials are biodegradable and osteoconductive, but calcium sulfate has been associated with seromas and drainage problems (20).

Bone wound healing

The bone wound healing process involves the action and interaction of many cells regulated by biochemical and mechanical signals. Generally, for non-critical size defects, the process of bone healing involves the migration and proliferation of pluripotent mesenchymal stem cells to the site of injury, and the formation of a stabilizing callus from these cells that subsequently chondrifies and ossifies (21).

Once the infection is under control, the PMMA beads are surgically removed, and the wound will then be treated with bone graft materials, such as natural or synthetic scaffolds. Clinically, rhBMP-2 delivered from a collagen sponge (INFUSE® Bone Graft, Medtronic Sofamor Danek) is an FDA-approved therapy for posterior-lateral spine, lower leg (tibia), and certain dental applications. However, since the protein is adsorbed on the surface of the collagen sponge, this delivery system results in a bolus release of growth factor in the first several hours (22), a property that may contribute to the requirement of high rhBMP-2 dosages in clinical applications (23, 24). Due to the fact that BMP-2 is a potent morphogen, there are safety issues such as ectopic bone formation associated with administering high levels of the drug (25, 26).

Importance of infection control during bone grafting

While treatment with antibiotic-laden PMMA beads may effectively control infection in the wound bed prior to bone grafting, cases of secondary infectious complications have been reported (15) which have been attributed to the absence of locally delivered antibiotics.

Additionally, although generally effective at promoting bone growth, the bone graft is essentially a foreign material placed into an avascular and often contaminated defect and could thus possibly function as a nidus for infection.

Neovascularization or angiogenesis plays important role in the regeneration of bone defects (27-30), that can require three to six weeks as suggested in some studies (28, 30). Therefore, it is desirable to control the infection in contaminated bone wounds to allow angiogenesis to occur normally.

Biodegradable polyurethanes for tissue regeneration

Biodegradable polymers have been used extensively as scaffolds to support tissue regeneration. The main advantages include the ability to tune mechanical properties, degradation kinetics, and release kinetics for various purposes. Suitable pore morphologies can be achieved to facilitate tissue ingrowth. The degradable polymers must meet specific requirements in order to be useful for orthopaedic injuries/diseases, such as mechanical support during tissue growth, undergo controlled degradation to biocompatible breakdown products, support controlled release of biologics, and provide an osteoconductive and osteoinductive micro environments (31). What's more, the developments of *in situ* polymerizable compositions in the form of an injectable liquid/paste are becoming more

and more attractive in tissue engineering applications (32, 33). Many of the presently available degradable polymers fail to fulfill all of the above requirements. For example, in situ polymerizable systems based on polypropylene fumarate (34) and polyanhydride chemistry (32, 35) have been reported, respectively; however, such polymer systems have limited mechanical properties that may hinder their orthopaedic applications.

Compared with currently available scaffolds and delivery systems, polyurethane (PUR) scaffolds offer many advantages in the design of injectable and biodegradable polymer compositions. PURs have been investigated as degradable scaffolds due to their excellent potential in tuning polymer structure to achieve mechanical properties and biodegradability to suit a variety of applications (36-41). Porous, biodegradable, and biocompatible PUR scaffolds support attachment, growth, and differentiation of osteoprogenitor cells *in vitro*, and biodegrade to nontoxic products *in vivo* (38, 42-44). Moreover, the physical and biological properties, as well as the degradation rate, of PUR scaffolds can be tuned to targeted values through the choice of intermediates used in the synthesis (43, 45). PUR scaffolds can be used as injectables through a two-component liquid system which cures *in situ* to form a solid with tough elastomeric mechanical properties (38, 41). The moderate exotherm during polymerization does not adversely affect the surrounding tissue. Also, the mechanical and physical properties can be tuned to the requirements of the targeted application. The resulting polymer scaffolds allow for diffusion of nutrients, providing a cytocompatible environment that guide cell attachment, growth, and differentiation. Lastly, the scaffolds also serve as a delivery device for drugs that promote cell infiltration and tissue remodeling (46). PUR scaffolds have been used for controlled delivery of many drugs successfully (46-48), and the release profiles can be

controlled through adopting various strategies. Dual release can also be achieved through embedding two different drugs in the same scaffold (49).

Growth factors and antibiotic for bone wound healing

Platelet-derived growth factor (PDGF-BB)

Growth factors are polypeptides that transmit signals through cell surface receptors to modulate cellular activities. They regulate cellular proliferation, differentiation, migration, adhesion, and gene expression (50). PDGF, a dimer consisting of two disulfide-bonded peptide chains (A or B), is a mitogenic and angiogenic protein that can promote fibroblast growth (51). The homo dimer PDGF-BB is the most active isoform for promoting wound repair (52). New bone formation was significantly enhanced by PDGF when adsorbed on hydroxyapatite micro crystals (53). PDGF-BB is unique among several growth factors in enhancing both granulation tissue volume and the degree of re-epithelialization (54), stimulating granulation tissue formation in both normal and diabetic rats (55). PDGF delivered in a collagen gel to treat tibial oeteotomies in rabbits enhanced functional fracture repair and stimulated osteogenesis significantly (56). PDGF delivered with the osteoporosis drug alendronate was also reported to substantially increase bone density (57).

Bone morphogenetic proteins (BMP-2)

Bone morphogenetic proteins (BMPs) are currently attracting the most commercial and clinical interest. Homodimeric BMP-2 is a member of the transforming growth factor beta (TGF-beta) superfamily that induces bone formation and regeneration, and the osteoinductive capacity of BMP-2 has been demonstrated in preclinical models and evaluated in clinical trials (58). Many of the animal models used to evaluate the capacity of

BMP-2 to heal bone defects have utilized critical-size defects, and healing of long bone critical-size defects by BMP-2 has been demonstrated in species including rats, rabbits, dogs, sheep and non-human primates (59). Systemic administration of rhBMP-2 increases mesenchymal stem cell activity and reverses ovariectomy-induced and age-related bone loss in two different mouse models (60), indicating that BMP-2 may be utilized for the treatment of osteoporosis. Recent studies show that rhBMP-2 delivered in an injectable calcium phosphate carrier or with a liposome carrier accelerates bone healing in a rabbit ulna osteotomy model and a rat femur bone defect model (61, 62). BMP-2 is shown to be efficacious in several fusion applications, including intervertebral and lumbar posterolateral fusion (63). BMP-2 has also been shown to induce new dentine formation and BMP-2 is an effective bone inducer around dental implants for periodontal reconstruction (64).

Recombinant human BMP-2 delivered in a collagen sponge is an FDA approved therapeutic for posterior-lateral spine fusion (InFuse-Sofamor/Danek-Medtronic); however, it results in a bolus release of growth factor in the first several hours (22). Due to the fact that BMP-2 is a morphogen and functions in later stages of cell growth to promote cell differentiation into osteoblasts (65), long-term release is desired to achieve an ideal effect in promoting bone fracture healing. Injection of BMP-2 in a calcium phosphate carrier at one or two weeks after surgery is more effective than injection within one day to enhance osteotomy-site healing in primates (66). The delayed injection approach delivered BMP-2 at later time points when a sufficient number of cells had infiltrated the implant. Since BMP-2 is a morphogen but not a mitogen, it exerts its function more potentially when more cells are present. This is the reason that achieving a sustained release of BMP-2 is desired.

Other studies have suggested that BMP-2 plays an important role at early stages in the healing process. BMP-2 is involved in promoting angiogenesis (67) and migration of human

mesenchymal progenitor cells (MPCs) (68). It may also serve as the trigger in the fracture healing cascade as demonstrated by its early maximal expression on day 1 as measured in a mouse tibial fracture model (69). Taken together, these previous studies suggest that both a burst and sustained release of rhBMP-2 are beneficial. A burst release of rhBMP-2 is anticipated to increase cellular migration and promote angiogenesis, while sustained release is anticipated to promote differentiation of the responding cells and thus more new bone formation.

The antibiotic: vancomycin

Open bone fractures are often exposed to infections, and the healing often requires administration of antibiotics to fight against micro-organism besides reconstruction of the damaged bone. Ideally, the delivery system should deliver antibiotic well above the effective antibacterial concentration in a sustained manner (2). It has been suggested that release of antibiotic at concentrations exceeding the minimum inhibitory concentration (MIC) for 6 – 8 weeks is desirable for treatment of osteomyelitis (70).

Vancomycin, a tricyclic glycopeptide antibiotic, is an effective therapy for treating serious infections caused by gram-positive bacteria such as Staphylococcus aureus (71, 72). Vancomycin has less negative effects on osteoblasts and skeletal cells than other commonly used antibiotics *in vitro* (73, 74), and it does not impede bone growth in fractures *in vivo* (75). A number of strategies have been developed for the delivery of vancomycin from polymers, such as poly(trimethylene carbonate)-based surface-eroding delivery systems (76) and nanoparticles presenting vancomycin on the surface (77).

The exact structure of vancomycin was determined by Williams and Kalman in 1977 (78), and the acid-base chemistry of the glycopeptide molecule, such as protonation macroconstants, the isoelectric point, and the distribution of its differently prononated

species under different pH, was revealed by Takacs-Novak et al in 1993 (79). Vancomycin contains six functional groups which undergoes protonation-deprotonation as a function of pH, and they are: three phenolate groups with pKa values of 12.0, 10.40, and 9.59 respectively, one secondary amino group with a pKa value of 8.89, one primary amino group with a pKa value of 7.75, and one carboxylate group with a pKa value of 2.18 (79, 80). Vancomycin carries two positive charges under strong acidic condition when pH < 2.0, and bears four negative charges in strong basic solution when pH > 13.0. The isoelectric point of vancomycin was found at pH 8.3 where it has no net charge, that is also where the molecule has the lowest solubility, and this property can be used to tune drug release profiles.

Design of this work

Rationale

Conventional clinical treatment for infected bone wounds is a staged procedure, wherein the infection control step is separated from the subsequent wound healing step. The non-degradable PMMA beads loaded with antibiotic used in the first step must be removed and replaced with a bone graft to allow bone wound healing to occur. Therefore, the bone graft lacks infection control, potentially leading to secondary complications.

The hypothesis of this study is that the biodegradable composite polyurethane scaffolds incorporating both growth factor rhBMP-2 and antibiotic vancomycin (PUR/BMP-2/V) would control infection and enhance new bone formation in an infected rat femoral segmental defect simultaneously. The scaffolds biodegrade *in vivo* to non-cytotoxic products, eliminating the secondary removal surgical procedure, and the degradation rate would be controlled through adjusting the composition of the scaffold to match the rate of bone wound healing. The composite biomaterial is biocompatible, which supports

attachment, proliferation, and differentiation of osteoprogenitor cells. The long term effective release of vancomycin is anticipated to protect the graft from infection, a prerequisite for normal tissue ingrowth, and the sustained release of BMP-2 would facilitates cell recruitment and differentiation thus promoting bone tissue regeneration.

Drug delivery concerns in bone regeneration

Neovascularization

Blood vessel formation is a prerequisite for bone healing (27, 28), and angiogenesis is essential for bone regeneration in segmental defects (29, 30). It has been shown that vascularization of the fracture callus in sheep progressed during the first three weeks of healing (28), and another study has suggested that complete vascularization of implanted scaffolds may require up to six weeks (30).

Therefore, in contaminated bone wounds, it is desirable to maintain a therapeutic level of antibiotic for at least 3 – 6 weeks to control the infection until substantial vascularization occurs in the wound bed.

Cellular events

Conceptually, the process of bone wound healing involves several cellular regulated stages including inflammation, callus differentiation, ossification, and remodeling (21). It is a complex process that involves the immigration, proliferation, and differentiation of a number of different cell types including inflammatory cells, angioblasts, fibroblasts, chondroblasts, and osteoblasts, which synthesize and release bioactive substances of extracellular matrix components such as collagen and growth factors (81). After the initial inflammatory stage wherein macrophages transported from the blood remove any dead tissue and generate the initial granulation tissue, the undifferentiated mesenchymal cells

migrating from the surrounding soft tissue will proliferate in the fracture site, and generate a stabilizing callus (82). In the next stage, depending on the biological requirements and mechanical conditions, mesenchymal cells will differentiate into chondrocytes, osteoblasts, or fibroblasts. These differentiated cells begin to synthesize the extracellular matrix of their corresponding tissue (81). Intramembranous woven bone is produced by osteoblasts and cartilage is formed by chondrogenesis, followed by endochondral ossification until a bony bridge is formed. The remodeling of the fracture site to restore the original structure and shape will occur thereafter which takes ~ one year which is much longer than the previous steps that takes only several weeks depending on the animal species (81).

The ideal growth factor delivery profile would match the biological functions. For the growth factor to promote cellular events involved in bone healing, the release profile must be controlled so that a modest release at the early stage would recruit cell migration, and a sustained release at longer time points would be responsible for the promotion of cell differentiation and new bone formation.

Drug delivery strategies

Adsorption on polymer surface

Polymer scaffolds are immersed in a solution of the drug for a certain period, followed by drying to allow adsorption of drugs on the polymer surfaces. This is the strategy adopted by InFuse (collagen adsorbed with high dose of BMP-2, a product clinically used for bone regeneration therapy) which results in a bolus release within the first several hours and no sustained release. The bolus release system requires a high growth factor dosage which is expensive and also has side effects such as ectopic bone formation.

Drug/excipients powder

In an alternative approach, the drug is directly incorporated in the PUR scaffold by mixing it with the polyol component before polymerization. Appropriate amounts of the drug carrier excipients such as glucose and a protein stabilizer such as heparin are present as well to help maintain growth factor activity and control the release profile. Compared with the adsorption method, this approach incorporates the drug within scaffold walls instead of adsorbing it on the surface, achieving a more sustained release profile as a result of the introduction of the polymer diffusion barrier.

PLGA microspheres encapsulation

Poly (lactic-co-glycolic acid) (PLGA) are among the most commonly used family of biodegradable polymers. The drug release profile from PLGA microspheres is controlled by many factors, such as molecular weight, hydrophilicity, morphology, and size etc (83). One strategy that has been used extensively is to include low molecular weight poly(ethylene glycol) (PEG) segments that can enhance the release profile by modification of the PLGA microspheres' morphology of the microspheres such as improving the porosity and internal hydrophilicity (84). Incorporating the microspheres in a PUR scaffold accomplishes a controlled drug release system that can also serve as a template for cell infiltration and tissue ingrowth.

Encapsulation of the drug into PLGA microparticles of at an average size of 100 μm which is larger than the dimension of PUR scaffold walls, followed by embedding of microspheres in the PUR scaffold is anticipated to achieve a decreased burst and sustained release of the drug. Encapsulation of the drug in PLGA microparticles at an average size of 1 μm, which is significantly lower than the dimension of PUR scaffold walls, followed by

embedding of microspheres in the PUR scaffold is anticipated to result in no exposed particle surface, achieving a further decreased burst and sustained release of the drug.

Growth factor can also bind to the surfaces of heparin-modified PLGA microspheres, which are then coated with gelatin, and embedded in PUR scaffolds. By adopting this strategy, the burst release is expected to be decreased (22, 85).

Tuning drug hydrophilicity

The change in drug hydrophilicity is anticipated to alter its water solubility, thereby potentially changing its release profile from the scaffolds. Commercially available vancomycin hydrochloride salt is highly hydrophilic, with a water solubility of around 200 mg/ml. The conversion of vancomycin hydrochloride salt to vancomycin free base at pH 8 (where the molecule has no net charge and is more hydrophobic) resulted in significantly decreased solubility of less than 20 mg/ml. The decreased drug hydrophilicity is expected to result in more controlled release during early days and more sustained release profile thereafter.

Specific aims

The ultimate technical aim of the study is to fabricate implantable PUR composite scaffolds incorporating growth factor and antibiotic. The biodegradable porous PUR scaffold is able to support osteoprogenitor cell attachment, proliferation, and differentiation. The outcome of the present study will serve as the basis for future development of injectable therapies and provide an alternative strategy for the treatment of infected bone wound healing.

Delivery of active growth factor from reactive system

Tasks: Design and develop a family of PUR-PDGF-BB composite biomaterials that promote cell proliferation and promote excisional wound healing, thus proving that PUR is appropriate for active growth factor delivery.

a. Evaluate the *in vitro* release profile and activity of PDGF-BB released from PUR scaffold when incorporated as a powder in presence of excipients (glucose and heparin), or when PDGF-BB is bound to heparin-modified PLGA microspheres and granulated in gelatin followed by incorporation in PUR.
b. Test the performance of PUR incorporated with PDGF-BB when implanted into rat skin excisional wounds.

Expected outcomes: The PUR scaffold will support cell attachment and proliferation, and biodegrade at a controlled rate. Bioactive PDGF-BB will be released to the extracellular matrix to promote cell proliferation, and enhance skin excisional wound healing compared with blank PUR scaffold.

Controlled release of BMP-2 from PUR

Task: Design and develop a family of PUR-BMP-2 composite biomaterials with different release profiles that promote cell migration and differentiation, and enhance new bone formation in rat femoras.

a. Evaluate the *in vitro* release profile and activity of rhBMP-2 when incorporated as a powder in presence of excipients (glucose and heparin), or encapsulated in PLGA microspheres at average sizes of 100 μm (L) and 1 μm (S) respectively followed by incorporation in PUR.
b. Test the performance of PUR incorporated with rhBMP-2 when implanted into rat femoral plug defects.

c. Test the performance of PUR incorporated with rhBMP-2 when implanted into rat critical size femoral segmental defects using collagen sponge adsorbed with rhBMP-2 as clinical control.

Expected outcomes: Different strategies of incorporating BMP-2 into PUR scaffold will yield different release profiles. PUR/BMP-2 scaffolds are anticipated to yield a high burst release of BMP-2, which is not the optimal release profile, but addition of BMP-2 as a powder prior to mixing will facilitate clinical off-label use. Encapsulation of BMP-2 in large particles will decrease the burst and result in a more sustained release. Encapsulation of BMP-2 in small particles will almost suppress the burst release completely and yield a sustainable release for at least one month because the small particles are embedded inside the scaffold walls. PUR/BMP-2 scaffolds which are controlled delivery systems, would improve new bone formation relative to the collagen sponge BMP-2 control which has a bolus release of BMP-2, and the different release strategies would result in different new bone formation profiles *in vivo* which helps elucidating the role of growth factor release at different stages.

Sustained release of vancomycin from PUR

Task: Design and develop a family of PUR-vancomycin composite biomaterials with different release profiles that inhibit bacteria growth *in vitro* and control infection in an infected rat femoral segmental defect.

a. Evaluate the *in vitro* release profile and activity of Vancomycin hydrochloride (V-HCl) and Vancomycin free base (V-FB) when incorporated in PUR.
b. Test the performance of PUR/V-HCl and PUR/V-FB when implanted into infected rat critical size femoral segmental defects using PMMA/V-HCl cement beads as clinical control.

Expected outcomes: Different strategies of incorporating vancomycin into PUR scaffold will yield different release profiles. The decreased drug hydrophilicity is expected to result in more controlled release during early days and more sustained release profile thereafter. The enhanced release profile was expected to result in better infection control *in vivo* which is at lease comparable to the clinical used PMMA beads.

Dual delivery of BMP-2 and Vancomycin from PUR

Task: Design and develop a PUR-BMP-2-V composite biomaterial that controls infection and improves bone regeneration simultaneously in an infected rat femoral segmental defect.

a. Evaluate the *in vitro* release profiles of both BMP-2 and vancomycin from PUR-BMP-2-V composite with optimized release kinetics in previous aims
b. Evaluate the composite in a non-infected rat femoral segmental defect to study the antibiotic effect on new bone formation promoted by BMP-2.
c. Evaluate the PUR-BMP-2-V composite in an infected rat femoral segmental defect to study the synergistical effect of both vancomycin and BMP-2 on promoting infected bone wound healing, using collagen-BMP-2 as controls.

Expected outcomes: Treatment with the proposed PUR-BMP-2-V composite will enhance infected bone wound healing relative to the collagen sponge BMP-2 control. PUR-BMP-2-V composite is expected to perform better than PUR-BMP-2 due to the infection control by sustained release of vancomycin.

References

1. Sussman C, Bates-Jensen BM. Wound care:va collaborative practice manual for physical therapists and nurses. 2nd ed: Aspen Publishers, Gaithersburg, Md; 2001.

2. Zilberman M, Elsner JJ. Antibiotic-eluting medical devices for various applications. J Control Release. 2008 Sep 24;130(3):202-15.

3. Johnson EN, Burns TC, Hayda RA, Hospenthal DR, Murray CK. Infectious complications of open type III tibial fractures among combat casualties. Clin Infect Dis. 2007 Aug 15;45(4):409-15.

4. Ostermann PA, Seligson D, Henry SL. Local antibiotic therapy for severe open fractures. A review of 1085 consecutive cases. J Bone Joint Surg Br. 1995 Jan;77(1):93-7.

5. Ristiniemi J, Lakovaara M, Flinkkila T, Jalovaara P. Staged method using antibiotic beads and subsequent autografting for large traumatic tibial bone loss: 22 of 23 fractures healed after 5-20 months. Acta Orthop. 2007 Aug;78(4):520-7.

6. Moehring HD, Gravel C, Chapman MW, Olson SA. Comparison of antibiotic beads and intravenous antibiotics in open fractures. Clin Orthop Relat Res. 2000 Mar(372):254-61.

7. Duncan CP, Masri BA. The role of antibiotic-loaded cement in the treatment of an infection after a hip replacement. Instr Course Lect. 1995;44:305-13.

8. Nelson CL, Evans RP, Blaha JD, Calhoun J, Henry SL, Patzakis MJ. A comparison of gentamicin-impregnated polymethylmethacrylate bead implantation to conventional parenteral antibiotic therapy in infected total hip and knee arthroplasty. Clin Orthop Relat Res. 1993 Oct(295):96-101.

9. Hanssen AD, Spangehl MJ. Practical applications of antibiotic-loaded bone cement for treatment of infected joint replacements. Clin Orthop Relat Res. 2004 Oct(427):79-85.

10. Calhoun JH, Henry SL, Anger DM, Cobos JA, Mader JT. The treatment of infected nonunions with gentamicin-polymethylmethacrylate antibiotic beads. Clin Orthop Relat Res. 1993 Oct(295):23-7.

11. Adams K, Couch L, Cierny G, Calhoun J, Mader JT. *In vitro* and *in vivo* evaluation of antibiotic diffusion from antibiotic-impregnated polymethylmethacrylate beads. Clin Orthop Relat Res. 1992 May(278):244-52.

12. Kuechle DK, Landon GC, Musher DM, Noble PC. Elution of vancomycin, daptomycin, and amikacin from acrylic bone cement. Clin Orthop Relat Res. 1991 Mar(264):302-8.

13. Mader JT, Calhoun J, Cobos J. *In vitro* evaluation of antibiotic diffusion from antibiotic-impregnated biodegradable beads and polymethylmethacrylate beads. Antimicrob Agents Chemother. 1997 Feb;41(2):415-8.

14. Nelson CL, Griffin FM, Harrison BH, Cooper RE. *In vitro* elution characteristics of commercially and noncommercially prepared antibiotic PMMA beads. Clin Orthop Relat Res. 1992 Nov(284):303-9.

15. Malchau H, Herberts P, Eisler T, Garellick G, Soderman P. The Swedish Total Hip Replacement Register. J Bone Joint Surg Am. 2002;84-A Suppl 2:2-20.

16. Thomes B, Murray P, Bouchier-Hayes D. Development of resistant strains of Staphylococcus epidermidis on gentamicin-loaded bone cement *in vivo*. J Bone Joint Surg Br. 2002 Jul;84(5):758-60.

17. Beardmore AA, Brooks DE, Wenke JC, Thomas DB. Effectiveness of local antibiotic delivery with an osteoinductive and osteoconductive bone-graft substitute. J Bone Joint Surg Am. 2005 Jan;87(1):107-12.

18. Gitelis S, Brebach GT. The treatment of chronic osteomyelitis with a biodegradable antibiotic-impregnated implant. J Orthop Surg (Hong Kong). 2002 Jun;10(1):53-60.

19. McKee MD, Wild LM, Schemitsch EH, Waddell JP. The use of an antibiotic-impregnated, osteoconductive, bioabsorbable bone substitute in the treatment of infected long bone defects: early results of a prospective trial. J Orthop Trauma. 2002 Oct;16(9):622-7.

20. McLaren AC. Alternative materials to acrylic bone cement for delivery of depot antibiotics in orthopaedic infections. Clin Orthop Relat Res. 2004 Oct(427):101-6.

21. Bailon-Plaza A, van der Meulen MCH. A mathematical framework to study the effects of growth factor influences on fracture healing. Journal of Theoretical Biology. 2001 Sep 21;212(2):191-209.

22. Jeon O, Song SJ, Kang SW, Putnam AJ, Kim BS. Enhancement of ectopic bone formation by bone morphogenetic protein-2 released from a heparin-conjugated poly(L-lactic-co-glycolic acid) scaffold. Biomaterials. 2007;28(17):2763-71.

23. Boyne PJ, Marx RE, Nevins M, Triplett G, Lazaro E, Lilly LC, et al. A feasibility study evaluating rhBMP-2/absorbable collagen sponge for maxillary sinus floor augmentation. Int J Periodontics Restorative Dent. 1997 Feb;17(1):11-25.

24. Howell TH, Fiorellini J, Jones A, Alder M, Nummikoski P, Lazaro M, et al. A feasibility study evaluating rhBMP-2/absorbable collagen sponge device for local alveolar ridge preservation or augmentation. Int J Periodontics Restorative Dent. 1997 Apr;17(2):124-39.

25. Hoffmann A, Weich HA, Gross G, Hillmann G. Perspectives in the biological function, the technical and therapeutic application of bone morphogenetic proteins. Appl Microbiol Biotechnol. 2001 Oct;57(3):294-308.

26. Hogan BL. Bone morphogenetic proteins: multifunctional regulators of vertebrate development. Genes Dev. 1996 Jul 1;10(13):1580-94.

27. Gung YW, Cheng CK, Su CY. A stereomorphologic study of bone matrix apposition in HA-implanted cavities observed with SEM, being prepared by a microvascular cast and freeze-fracture method. Med Eng Phys. 2003 Sep;25(7):565-71.

28. Lienau J, Schmidt-Bleek K, Peters A, Haschke F, Duda GN, Perka C, et al. Differential regulation of blood vessel formation between standard and delayed bone healing. J Orthop Res. 2009 Sep;27(9):1133-40.

29. Li R, Stewart DJ, von Schroeder HP, Mackinnon ES, Schemitsch EH. Effect of cell-based VEGF gene therapy on healing of a segmental bone defect. J Orthop Res. 2009 Jan;27(1):8-14.

30. Geiger F, Bertram H, Berger I, Lorenz H, Wall O, Eckhardt C, et al. Vascular endothelial growth factor gene-activated matrix (VEGF165-GAM) enhances osteogenesis and angiogenesis in large segmental bone defects. J Bone Miner Res. 2005 Nov;20(11):2028-35.

31. Ma PX, Choi JW. Biodegradable polymer scaffolds with well-defined interconnected spherical pore network. Tissue Eng. 2001 Feb;7(1):23-33.

32. Burkoth AK, Anseth KS. A review of photocrosslinked polyanhydrides: in situ forming degradable networks. Biomaterials. 2000 Dec;21(23):2395-404.

33. Gunatillake P, Mayadunne R, Adhikari R. Recent developments in biodegradable synthetic polymers. Biotechnol Annu Rev. 2006;12:301-47.

34. Temenoff JS, Mikos AG. Injectable biodegradable materials for orthopedic tissue engineering. Biomaterials. 2000 Dec;21(23):2405-12.

35. Poshusta AK, Burdick JA, Mortisen DJ, Padera RF, Ruehlman D, Yaszemski MJ, et al. Histocompatibility of photocrosslinked polyanhydrides: a novel in situ forming orthopaedic biomaterial. J Biomed Mater Res A. 2003 Jan 1;64(1):62-9.

36. Guelcher S, Srinivasan A, Hafeman A, Gallagher K, Doctor J, Khetan S, et al. Synthesis, *In vitro* degradation, and mechanical properties of two-component poly(ester urethane)urea scaffolds: Effects of water and polyol composition. Tissue Engineering. 2007;13(9):2321-33.

37. Guelcher SA. Biodegradable polyurethanes: Synthesis and applications in regenerative medicine. Tissue Engineering Part B-Reviews. 2008;14(1):3-17.

38. Guelcher SA, Patel V, Gallagher KM, Connolly S, Didier JE, Doctor JS, et al. Synthesis and *in vitro* biocompatibility of injectable polyurethane foam scaffolds. Tissue Engineering. 2006;12(5):1247-59.

39. Gorna K, Gogolewski S. Biodegradable polyurethanes for implants. II. *In vitro* degradation and calcification of materials from poly(epsilon-caprolactone)-poly(ethylene oxide) diols and various chain extenders. Journal of Biomedical Materials Research. 2002;60(4):592-606.

40. Gorna K, Gogolewski S. Preparation, degradation, and calcification of biodegradable polyurethane foams for bone graft substitutes. Journal of Biomedical Materials Research Part A. 2003;67A(3):813-27.

41. Bonzani IC, Adhikari R, Houshyar S, Mayadunne R, Gunatillake P, Stevens MM. Synthesis of two-component injectable polyurethanes for bone tissue engineering. Biomaterials. 2007 Jan;28(3):423-33.

42. Guan JJ, Sacks MS, Beckman EJ, Wagner WR. Synthesis, characterization, and cytocompatibility of efastomeric, biodegradable poly(ester-urethane)ureas based on poly(caprolactone) and putrescine. Journal of Biomedical Materials Research. 2002;61(3):493-503.

43. Zhang JY, Beckman EJ, Hu J, Yang GG, Agarwal S, Hollinger JO. Synthesis, biodegradability, and biocompatibility of lysine diisocyanate-glucose polymers. Tissue Engineering. 2002;8(5):771-85.

44. Zhang JY, Beckman EJ, Piesco NP, Agarwal S. A new peptide-based urethane polymer: synthesis, biodegradation, and potential to support cell growth *in vitro*. Biomaterials. 2000;21(12):1247-58.

45. Adhikari R, Gunatillake PA, Griffiths I, Tatai L, Wickramaratna M, Houshyar S, et al. Biodegradable injectable polyurethanes: synthesis and evaluation for orthopaedic applications. Biomaterials. 2008 Oct;29(28):3762-70.

46. Hafeman AE, Li B, Yoshii T, Zienkiewicz K, Davidson JM, Guelcher SA. Injectable biodegradable polyurethane scaffolds with release of platelet-derived growth factor for tissue repair and regeneration. PharmRes. 2008;25(10):2387-99.

47. Simmons A, Padsalgikar AD, Ferris LM, Poole-Warren LA. Biostability and biological performance of a PDMS-based polyurethane for controlled drug release. Biomaterials. 2008;29(20):2987-95.

48. Boateng JS, Matthews KH, Stevens HNE, Eccleston GM. Wound healing dressings and drug delivery systems: A review. Journal of Pharmaceutical Sciences. 2008;97(8):2892-923.

49. Suzuki A, Terai H, Toyoda H, Namikawa T, Yokota Y, Tsunoda T, et al. A biodegradable delivery system for antibiotics and recombinant human bone morphogenetic protein-2: A potential treatment for infected bone defects. J Orthop Res. 2006 Mar;24(3):327-32.

50. Nimni ME. Polypeptide growth factors: targeted delivery systems. Biomaterials. 1997 Sep;18(18):1201-25.

51. Ross R, Glomset J, Kariya B, Harker L. A platelet-dependent serum factor that stimulates the proliferation of arterial smooth muscle cells *in vitro*. ProcNatlAcadSciUSA. 1974;71(4):1207-10.

52. Pierce GF, Mustoe TA. Pharmacological Enhancement of Wound-Healing. Annual Review of Medicine. 1995;46:467-81.

53. McGill JJ, Strates BS, McGuire MH. Stimulation of Osteogenesis by Platelet Derived Growth-Factor and A Transforming Growth-Factor. Clinical Research. 1991;39(3):A788.

54. Mustoe TA, Pierce GF, Morishima C, Deuel TF. Growth Factor-Induced Acceleration of Tissue-Repair through Direct and Inductive Activities in a Rabbit Dermal Ulcer Model. Journal of Clinical Investigation. 1991 Feb;87(2):694-703.

55. Grotendorst GR, Martin GR, Pencev D, Sodek J, Harvey AK. Stimulation of Granulation-Tissue Formation by Platelet-Derived Growth-Factor in Normal and Diabetic Rats. Journal of Clinical Investigation. 1985;76(6):2323-9.

56. Nash TJ, Howlett CR, Martin C, Steele J, Johnson KA, Hicklin DJ. Effect of Platelet-Derived Growth-Factor on Tibial Osteotomies in Rabbits. Bone. 1994;15(2):203-8.

57. Mitlak BH, Finkelman RD, Hill EL, Li J, Martin B, Smith T, et al. The effect of systemically administered PDGF-BB on the rodent skeleton. J Bone Miner Res. 1996 Feb;11(2):238-47.

58. Chen D, Zhao M, Mundy GR. Bone morphogenetic proteins. Growth Factors. 2004 Dec;22(4):233-41.

59. Murakami N, Saito N, Horiuchi H, Okada T, Nozaki K, Takaoka K. Repair of segmental defects in rabbit humeri with titanium fiber mesh cylinders containing recombinant human bone morphogenetic protein-2 (rhBMP-2) and a synthetic polymer. J Biomed Mater Res. 2002 Nov;62(2):169-74.

60. Turgeman G, Zilberman Y, Zhou S, Kelly P, Moutsatsos IK, Kharode YP, et al. Systemically administered rhBMP-2 promotes MSC activity and reverses bone and cartilage loss in osteopenic mice. J Cell Biochem. 2002;86(3):461-74.

61. Li RH, Bouxsein ML, Blake CA, D'Augusta D, Kim H, Li XJ, et al. rhBMP-2 injected in a calcium phosphate paste (alpha-BSM) accelerates healing in the rabbit ulnar osteotomy model. J Orthop Res. 2003 Nov;21(6):997-1004.

62. Matsuo T, Sugita T, Kubo T, Yasunaga Y, Ochi M, Murakami T. Injectable magnetic liposomes as a novel carrier of recombinant human BMP-2 for bone formation in a rat bone-defect model. J Biomed Mater Res A. 2003 Sep 15;66(4):747-54.

63. Sandhu HS. Bone morphogenetic proteins and spinal surgery. Spine (Phila Pa 1976). 2003 Aug 1;28(15 Suppl):S64-73.

64. Cochran DL, Wozney JM. Biological mediators for periodontal regeneration. Periodontol 2000. 1999 Feb;19:40-58.

65. Tatsuyama K, Maezawa Y, Baba H, Imamura Y, Fukuda M. Expression of various growth factors for cell proliferation and cytodifferentiation during fracture repair of bone. European Journal of Histochemistry. 2000;44(3):269-78.

66. Seeherman H, Li R, Bouxsein M, Kim H, Li XJ, Smith-Adaline EA, et al. rhBMP-2/calcium phosphate matrix accelerates osteotomy-site healing in a nonhuman primate model at multiple treatment times and concentrations. J Bone Joint Surg Am. 2006 Jan;88(1):144-60.

67. de Jesus Perez VA, Alastalo TP, Wu JC, Axelrod JD, Cooke JP, Amieva M, et al. Bone morphogenetic protein 2 induces pulmonary angiogenesis via Wnt-beta-catenin and Wnt-RhoA-Rac1 pathways. J Cell Biol. 2009 Jan 12;184(1):83-99.

68. Fiedler J, Roderer G, Gunther KP, Brenner RE. BMP-2, BMP-4, and PDGF-bb stimulate chemotactic migration of primary human mesenchymal progenitor cells. J Cell Biochem. 2002;87(3):305-12.

69. Cho TJ, Gerstenfeld LC, Einhorn TA. Differential temporal expression of members of the transforming growth factor beta superfamily during murine fracture healing. J Bone Miner Res. 2002 Mar;17(3):513-20.

70. Ambrose CG, Gogola GR, Clyburn TA, Raymond AK, Peng AS, Mikos AG. Antibiotic microspheres: preliminary testing for potential treatment of osteomyelitis. Clin Orthop Relat Res. 2003 Oct(415):279-85.

71. Lee SH, Lee JE, Baek WY, Lim JO. Regional delivery of vancomycin using pluronic F-127 to inhibit methicillin resistant Staphylococcus aureus (MRSA) growth in chronic otitis media *in vitro* and *in vivo*. J Control Release. 2004 Apr 16;96(1):1-7.

72. Stigter M, Bezemer J, de Groot K, Layrolle P. Incorporation of different antibiotics into carbonated hydroxyapatite coatings on titanium implants, release and antibiotic efficacy. J Control Release. 2004 Sep 14;99(1):127-37.

73. Edin ML, Miclau T, Lester GE, Lindsey RW, Dahners LE. Effect of cefazolin and vancomycin on osteoblasts *in vitro*. Clin Orthop Relat Res. 1996 Dec(333):245-51.

74. Antoci V, Jr., Adams CS, Hickok NJ, Shapiro IM, Parvizi J. Antibiotics for local delivery systems cause skeletal cell toxicity *in vitro*. Clin Orthop Relat Res. 2007 Sep;462:200-6.

75. Haleem AA, Rouse MS, Lewallen DG, Hanssen AD, Steckelberg JM, Patel R. Gentamicin and vancomycin do not impair experimental fracture healing. Clinical Orthopaedics and Related Research. 2004 Oct(427):22-4.

76. Kluin OS, van der Mei HC, Busscher HJ, Neut D. A surface-eroding antibiotic delivery system based on poly(trimethylene carbonate). Biomaterials. 2009 Jun 3.

77. Kell AJ, Stewart G, Ryan S, Peytavi R, Boissinot M, Huletsky A, et al. Vancomycin-modified nanoparticles for efficient targeting and preconcentration of Gram-positive and Gram-negative bacteria. ACS Nano. 2008 Sep 23;2(9):1777-88.

78. Williams DH, Kalman J. Structural and mode of action studies on the antibiotic vancomycin. Evidence from 270-MHz proton magnetic resonance. J Am Chem Soc. 1977 Apr 13;99(8):2768-74.

79. Takacsnovak K, Noszal B, Tokeskovesdi M, Szasz G. Acid-Base Properties and Proton-Speciation of Vancomycin. International Journal of Pharmaceutics. 1993 Feb 5;89(3):261-3.

80. Claudius JS, Neau SH. Kinetic and equilibrium characterization of interactions between glycopeptide antibiotics and sodium carboxymethyl starch. International Journal of Pharmaceutics. 1996 Nov 22;144(1):71-9.

81. Doblare M, Garcia JM, Gomez MJ. Modelling bone tissue fracture and healing: a review. Engineering Fracture Mechanics. 2004 Sep;71(13-14):1809-40.

82. Einhorn TA. The cell and molecular biology of fracture healing. Clinical Orthopaedics and Related Research. 1998 Oct(355):S7-S21.

83. Kang F, Singh J. Effect of additives on the release of a model protein from PLGA microspheres. AAPS PharmSciTech. 2001;2(4):30.

84. Cleek RL, Ting KC, Eskin SG, Mikos AG. Microparticles of poly(DL-lactic-co-glycolic acid)/poly(ethylene glycol) blends for controlled drug delivery. Journal of Controlled Release. 1997 Oct 13;48(2-3):259-68.

85. Jeon O, Kang SW, Lim HW, Chung JH, Kim BS. Long-term and zero-order release of basic fibroblast growth factor from heparin-conjugated poly(L-lactide-co-glycolide) nanospheres and fibrin gel. Biomaterials. 2006;27(8):1598-607.

CHAPTER II

THE EFFECT OF THE LOCAL DELIVERY OF PLATELET-DERIVED GROWTH FACTOR FROM REACTIVE TWO-COMPONENT POLYURETHANE SCAFFOLDS ON THE HEALING IN RAT SKIN EXCISIONAL WOUNDS

Abstract

A key tenet of tissue engineering is the principle that the scaffold can perform the dual roles of biomechanical and biochemical support through presentation of the appropriate mediators to surrounding tissue. While growth factors have been incorporated into scaffolds to achieve sustained release, there are a limited number of studies investigating release of biologically active molecules from reactive two-component polymers, which have potential application as injectable delivery systems. Here I report the sustained release of platelet-derived growth factor (PDGF) from a reactive two component polyurethane. The release of PDGF was bi-phasic, characterized by an initial burst followed by a period of sustained release for up to 21 days. Despite the potential for amine and hydroxyl groups in the protein to react with the isocyanate groups in the reactive polyurethane, the *in vitro* bioactivity of the released PDGF was largely preserved when added as a lyophilized powder. PUR/PDGF scaffolds implanted in rat skin excisional wounds accelerated wound healing relative to the blank PUR control, resulting in almost complete healing with reepithelization at day 14. The presence of PDGF attracted both fibroblasts and mononuclear cells, significantly accelerating degradation of the polymer and enhancing formation of new granulation tissue as early as day 3. The ability of reactive two-component PUR scaffolds to

promote new tissue formation *in vivo* through local delivery of PDGF may present compelling opportunities for the development of novel injectable therapeutics.

Introduction

Wound healing is a tightly orchestrated sequence of events that is driven by intercellular communication via cytokines and growth factors. When healing goes awry, many of the consequences can be attributed to the alteration of these signaling mechanisms, and deficient wound healing can be corrected, in part, by administration of signal molecules to sites of tissue repair. Reorganization of damaged tissue requires restoration of appropriate architecture and biomechanical properties. Supplementing the tissue defect with biocompatible scaffolds that may be derived from natural or synthetic sources can augment this aspect. A key tenet of tissue engineering is the principle that the scaffold — like the native extracellular matrix — can perform the dual roles of biomechanical and biochemical support through presentation of the appropriate mediators to surrounding tissue.

PDGF is a co-factor with vascular endothelial growth factor (VEGF) for stable angiogenesis (1). It is chemotactic and mitogenic for bone cells, mesenchymal stem cells, ligament, dermal fibroblasts, and fibroblast-like cells derived from the periodontal ligament and gingiva (2-4). PDGF-BB is the most widely understood and utilized isoform for wound healing applications, and it has been reported to stimulate and enhance new tissue formation in both bone and soft tissue models (5-8). Inasmuch as PDGF-BB is a universal ligand for the PDGF receptor, it has achieved moderate commercial success as a component of Regranex™, a carboxymethylcellulose (CMC) gel formulation of 100μg/ml rhPDGF-BB (for simplicity referred to as PDGF). Due to the bolus release of PDGF from the CMC gel, this topical agent, which is approved for treatment of diabetic foot ulcers, must be applied daily

or more frequently at high concentrations. In contrast, preclinical studies have shown that a sustained release of PDGF enhances cellular infiltration and new tissue formation relative to a bolus release. In a mid-sagittal dorsal incision model in the rat, a nearly linear sustained release (e.g., up to 14 days) of PDGF from nanofibrous scaffolds (9) was reported to enhance new tissue formation at days 7 and 14 (8), while a bolus release (e.g., complete release after 4h) had a negligible effect (8, 10). Likewise, gene delivery of PDGF has produced positive effects by sustained, low level release (11).

To address the clinical need for an improved delivery device for sustained release of PDGF, we are investigating the potential of polyurethane (PUR) scaffolds. Porous, biodegradable, and biocompatible PUR scaffolds have been reported to support cellular infiltration and new tissue formation in sub-cutaneous (12-15), cardiovascular (16, 17), and bone models (18, 19). Furthermore, these materials have been shown to biodegrade at a controlled rate to nontoxic products *in vitro* (16, 17, 20, 21) and *in vivo* (14-16, 22) to non-cytotoxic decomposition products. In addition to its function as a matrix supporting the ingrowth of cells and new tissue, the PUR scaffold can also function as a drug delivery system (23, 24). Biodegradable PUR scaffolds have been used for controlled release of growth factors such as bFGF (25) and PDGF-BB (12). A distinct advantage of polyurethane scaffolds is the potential to inject the materials as a reactive liquid mixture which adheres to host tissue, conforms and expands to fill irregularly shaped wounds, and cures in situ to form an elastic porous scaffold (12, 26). A polyisocyanate (or NCO-terminated prepolymer) mixed with a polyol (hydroxyl functionality) reacts to form a polymer network incorporating urethane linkages. Water reacts with the polyisocyanate to form a disubstituted urea and carbon dioxide, which functions as a blowing agent, thereby introducing pores into the material.

In a previous study, we have reported the release of PDGF from PUR scaffolds, wherein radiolabeled PDGF was incorporated as a dry powder into PUR scaffolds that were prepared from hexamethylene diisocyanate trimer (HDIt). The release profile was characterized by a burst followed by a period of sustained release, and the cumulative release of PDGF was found to be independent of the dosage (12). However, the bioactivity of the released PDGF was not assessed. Proteins such as PDGF contain active hydrogens, such as primary amine and hydroxyl groups, which can potentially react with the polyisocyanate, thereby denaturing the protein. Therefore, in this study, we used two strategies for delivering PDGF from PUR scaffolds to address the need to preserve the bioactivity of the released PDGF. In the first approach, PDGF was incorporated into PUR scaffolds as a powder in the presence of excipients (heparin and glucose). In the second approach, PDGF was bound to PLGA microspheres through heparin, the microspheres were coated with a gelatin layer to form granules, and the granules were then incorporated into PUR scaffold. The gelatin coating was hypothesized to protect active hydrogens (e.g., primary amine and hydroxyl groups) in the growth factors from reacting with the polyisocyanate component of the PUR. We have measured the *in vitro* release kinetics of PDGF from two-component reactive PUR scaffolds, as well as the *in vitro* biological activity of released PDGF, using both strategies. Considering that there were no substantial differences in either the release profile or the biological activity of released PDGF between the two strategies, the simpler approach of adding PDGF as a powder was selected for *in vivo* experiments. PUR scaffolds with and without PDGF were implanted in excisional wounds in Sprague-Dawley rats. We reasoned that the initial burst release of PDGF would attract mesenchymal cells into the scaffold, while the sustained release of PDGF would promote tissue remodeling in the later stages of the healing process. PUR+PDGF scaffolds implanted in rats promoted substantial ingrowth of cells as early as day 3 post-implantation, followed by extensive new tissue formation and scaffold

degradation at day 7 and almost complete healing at day 14. Interestingly, PDGF not only enhanced ingrowth of cells and new tissue, but also accelerated scaffold degradation relative to the negative control. Thus the ability of PUR scaffolds to deliver biologically active PDGF at sustained low levels for several weeks presents potentially compelling opportunities for these materials as a combined scaffold and delivery system for regenerative medicine.

Materials & Methods

Materials

Polyvinyl alcohol (PVA), glycolide, and D,L-lactide were obtained from Polysciences (Warrington, PA). The tertiary amine catalyst TEGOAMIN33, which comprises a solution of 33 wt% triethylene diamine (TEDA) in dipropylene glycol, was received from Goldschmidt (Hopewell, VA) as a gift. Polyethylene glycol (PEG, 600 Da) was purchased from Alfa Aesar (Ward Hill, MA). Dichloromethane (DCM), methanol, trifluoroacetic acid (TFA) and glucose were from Acros Organics (Morris Plains, NJ). Hexamethylene diisocyanate trimer (HDIt, Desmodur N3300A) was received as a gift from Bayer Material Science (Pittsburgh, PA). PDGF-BB was received as a gift from Amgen (Thousand Oaks, CA). Sodium iodide (Na125I) for radiolabeling was purchased from New England Nuclear (part of Perkin Elmer, Waltham, MA). Stannous octoate catalyst was received from Nusil technology (Overland Park, KS). 1-ethyl-3-(3-dimethylaminopropyl)-carbodiimide hydrochloride (EDC) was from Advanced ChemTech (Louisville, Kentucky). Reagents for cell culture were all purchased from HyClone (Logan, UT). All other reagents were purchased from Sigma-Aldrich (St. Louis, MO). Prior to use, glycerol and PEG 600 were dried at 10 mm Hg for 3 hours at 80 ºC, and ε-caprolactone was dried over anhydrous magnesium sulfate, while all other materials were used as received.

Radiolabeling of PDGF-BB

PDGF-BB was labeled with radioactive iodine (^{125}I) using IODO-BEADS Iodination Reagent (Pierce Biotechnology, Rockford, IL) in accordance with previously published techniques (12). IODO-beads containing approximately 1 mCi $Na^{125}I$ were incubated in 1 ml reaction buffer for 5 minutes under room temperature, followed by addition of 50 μg PDGF to the reaction solution and incubation for another 25 minutes. The solution was then removed from the IODO-BEADS reaction tube and the Iodine-labeled PDGF (125I-PDGF) was separated in a Sephadex disposable PD-10 desalting column (Sigma-Aldrich). Eluted fractions were collected and Cobra II Autogamma counter (Packard Instrument Co, Meridien, CT) was adopted to determine the fractions containing the ^{125}I-PDGF.

Amine-terminated poly(L-lactide-co-glycolide) synthesis

Hydroxyl-terminated poly(L-lactide-co-glycolide) (PLGA-OH, 50/50 lactide/glycolide, MW 20,000) copolymers were synthesized by ring-opening polymerization of D,L-lactide and glycolide using a dried polycaprolactone triol (MW 300) starter in the presence of stannous octoate catalyst as described previously (20, 22). The polymer was then dissolved in DCM and reacted with N-t-Boc-glycine (4 mM) and DMAP (1.2 mM). To this mixture 4 mM of DCC (N,N'-Dicyclohexylcarbodiimide) was added, and the reaction mixture stirred in ice/water bath for 24 h. After filtering the dicyclohexylurea by-product, the filtrate was precipitated in methanol, filtered, and dried. The amine groups were de-protected by reacting the polymer in a solution of TFA in DCM for 3 h to remove the t-Boc groups, followed by precipitation in methanol, filtration, and drying. Structure of the the PLGA-NH2 was verified by NMR (Bruker 300 MHz).

Fabrication of PLGA-Heparin-PDGF microspheres

A microcapillary device was used to generate the PLGA-NH2 microspheres (27). An oil phase comprising a solution of PLGA-NH2 in DCM (5% wt) was fed to the concentric tube (0.1 inch in diameter), while an aqueous carrier stream (2% w/v PVA) surrounded the emerging jet of the PLGA-NH2/DCM solution, which was sprayed into a solution of 2% PVA. After stirring ~3 hour to evaporate the DCM, the particles were filtered, washed with deionized water, and lyophilized for 24 h. The particle size was measured to be 50 μm using an Olympus BX60 microscope.

Heparin (activity: 170 USPU/mg) was covalently bound to the surfaces of PLGA-NH2 microspheres using standard carbodiimide techniques (10, 28). Briefly, heparin (0.33 g/g PLGA-NH2) was incubated with PLGA-NH2 microspheres in a pH 5.5 buffer solution (0.1M MES containing 0.5M NaCl). To activate the –COOH groups of the heparin, NHS (6 mmol) and EDC (6 mmol) were added to the solution, followed by reaction in an ice water bath for 24 h. The resulting PLGA-Hp microspheres were filtered, washed, and lyophilized. The amount of heparin conjugated to the microsphere surface was measured to be 0.15 wt% using the toluidine blue method (28). PDGF-BB (labeled and/or non-labeled) was loaded onto PLGA-Hp microspheres by incubating in PBS for 1 h, followed by centrifugation to separate the particles. The loading efficiency was measured to be 80% by ELISA (R&D systems).

Gelatin coating of PLGA-Heparin-PDGF microspheres

PLGA-Heparin-PDGF microspheres (210 mg) were mixed with 70 μl gelatin solution (5%) and forced through a 300-μm sieve to yield gelatin coated granules. The granules were then dried at 4 °C for 2 days.

Polyurethane scaffold synthesis and characterization

Polyester triols (900 Da) were prepared from a glycerol starter and a backbone comprising 60wt% ε-caprolactone, 30wt% glycolide, and 10wt% D,L-lactide as published previously (20, 22). The reaction was carried out by mixing these components in a 100-ml reaction flask with mechanical stirring under argon in the presence of stannous octoate (0.1 wt%) catalyst for 40 hours at 140 ºC. The product was then dried under vacuum at 80 ºC overnight. PUR scaffolds were synthesized by one-shot reactive liquid molding of hexamethylene diisocyanate trimer (HDIt; Desmodur N3300A) and a hardener comprising polyol (half polyester triol 900-Da and half PEG 600-Da), 1.5 parts per hundred parts polyol (pphp) water, 4.5 pphp TEGOAMIN33 tertiary amine catalyst, 1.5 pphp sulfated castor oil stabilizer, and 4.0 pphp calcium stearate pore opener. The isocyanate was added to the hardener, mixed for 30 seconds in a Hauschild SpeedMixer™ DAC 150 FVZ-K vortex mixer (FlackTek, Inc., Landrum, SC), and the resulting liquid mixture poured into a cylindrical mold where it cured as a free-rise foam after ~20 min (20, 22). The targeted index (the ratio of NCO to OH equivalents times 100) was 115.

Scanning electron microscopy (Hitachi S-4200 SEM, Finchampstead, UK) was utilized to measure the pore size and determine the internal pore morphology of the polyurethane scaffolds. The core porosity was calculated from the measure density as reported previously (20). The glass transition temperature (Tg) of the scaffolds was evaluated by dynamic mechanical analysis (DMA) in compression mode with a temperature sweep of -80 ºC to 100 ºC, at a frequency of 1 Hz, 20-μm amplitude, 0.3-% strain, and 0.2-N static force (12).

Incorporation of protein in the polyurethane scaffold

BSA-FITC (2.5 μg) was co-dissolved with varying amounts of glucose (0 mg, 0.5 mg, 2 mg, or 5 mg) and the resulting solution lyophilized. The lyophilized powder was added to

the hardener component before mixing with the isocyanate to prepare the PUR scaffolds (each scaffold weighed 100 mg). For the foams including BSA-FITC in solution, the appropriate amount of BSA-FITC was dissolved in the water and the resulting solution added to the hardener. Prior to reaction with the isocyanate, 0.5 mg glucose powder was also added to the hardener. PDGF-BB (2.5 μg, labeled and/or non-labeled) was co-dissolved and lyophilized with excipients (heparin, glucose, or a combination of both) in order to stabilize the protein during lyophilization and scaffold synthesis. The heparin dosage was 50 μg per foam and the glucose dosage 2 mg per 100 mg scaffold. As described above, the lyophilized powder was added to the hardener component before mixing with the isocyanate to prepare the PUR scaffolds. For the foams containing gelatin-coated granules, 15wt% granules were mixed well with the hardener components before reacting with isocyanate.

In vitro release

An appropriate amount of sample (PLGA particles, gelatin-coated granules, and scaffolds) was immersed in 1 ml release medium (α-MEM containing 1% BSA) contained in polypropylene vials sealed by O-rings. The total protein amount in the release system was controlled at 2.5 μg by adding the appropriate mass of PUR foam to the medium. α-MEM and BSA were included to mimic the cellular growth environment and minimize adsorption of PDGF onto the scaffolds and vials.

For the PUR foam samples containing BSA-FITC, the medium was refreshed from each vial at the time points as indicated in the figures, and the released BSA-FITC concentration was measured by emission fluorescence at 530 nm after excitation at 485 nm using a BIO-TEK FL600 microplate fluorescence reader.

For the samples containing PDGF-BB, the medium was refreshed every 24 h. An extra centrifugation step was required before changing the medium of the particle and granule samples. The PDGF concentration was determined by either Human PDGF-BB Quantikine ELISA kit (R&D systems, Minneapolis, MN), or with a Cobra II Autogamma counter (Packard Instrument Co, Meridien, CT) for radio-labeled protein.

In vitro cell proliferation assay with released PDGF

MC3T3 mouse osteoblast precursor cells were seeded in 96-well plates at 1000 cells/well and incubated with α-MEM cell culture media containing 10% serum to promote cell attachment. After 24h, the media were replaced by media containing 0.5% serum and the PDGF releasates (or controls) were added at dosages of 3 and 10 ng/ml. Cell numbers were measured using a CyQUANT NF Cell Proliferation Assay kit from Invitrogen (Carlsbad, CA) at time points of 24 and 72h.

In vivo rat skin excisional wound test

The PUR/PDGF scaffolds were cut into 6mm × 2mm discs and implanted into 8mm full-thickness excisional wounds in the dorsal skin of adult male Sprague-Dawley rats. The loading of PDGF-BB in the scaffold was 0 μg (control), 1.8 μg (11.5 μg/ml scaffold), and 18 μg (11.5 μg/ml scaffold). Each was replicated 6 times. The rats were sacrificed 3, 7, and 14 days post-implantation. The harvested implants were fixed in formalin for 24 h, embedded in paraffin, and processed for histological evaluation with Mallory's trichrome staining and hematoxylin & eosin (H&E) staining. Quantitative analysis of polymer degradation and granulation tissue formation was performed using Image Pro 6.2 (Media Cybernetics) by measuring the area percentage of both polymer and new tissue within the scaffold based on trichrome images.

Results

In vitro release of BSA-FITC from PUR/BSA-FITC scaffolds

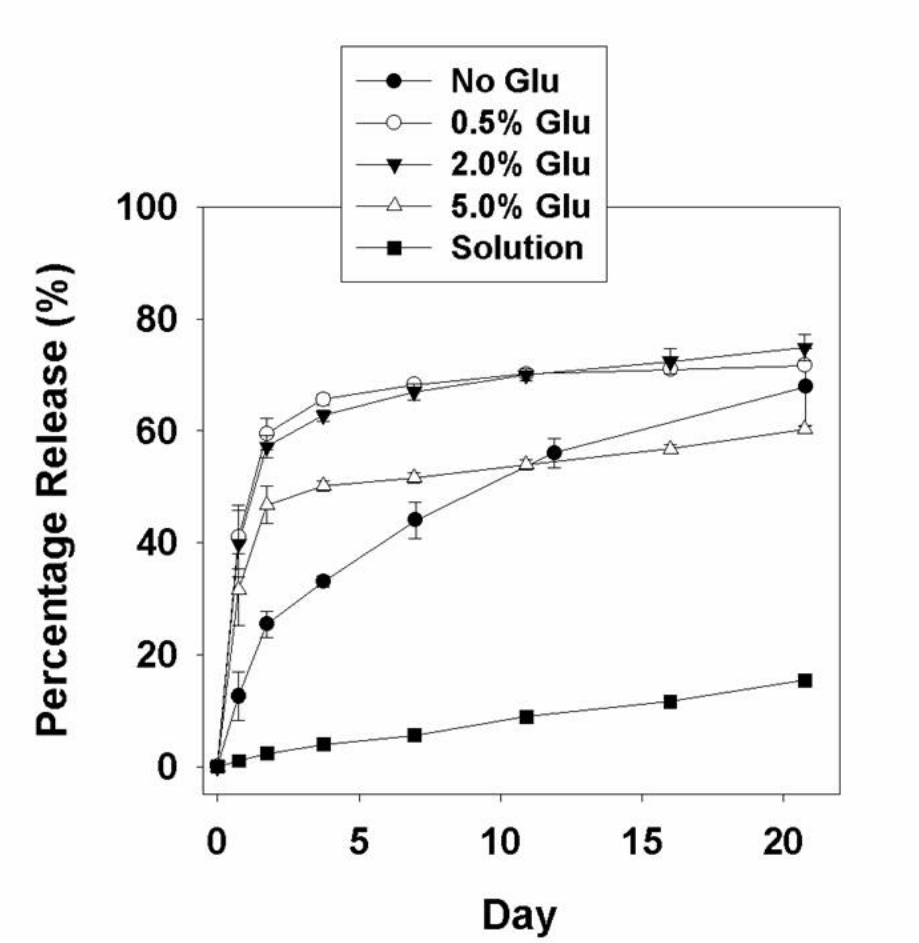

Figure II-1 *In vitro* release profile of BSA-FITC from polyurethane scaffold. BSA-FITC was incorporated in the scaffold as solution in presence of 0.5% glucose, and as powder in presence of different weight percentages of glucose. Each data point represents the mean of three determinations ±SD.

Previous studies have shown that dissolved proteins and peptides with active hydrogens (e.g., hydroxyl groups and amines) react with the polyisocyanate and are covalently bound to the polyurethane (29-31). Reaction of hydroxyl and amine groups in the dissolved protein with isocyanate groups will result in the formation of urethane and

urea bonds, which hydrolyze very slowly. Furthermore, reaction of the protein may result in denaturation and loss of biological activity. I therefore hypothesized that addition of the protein in solution would result in low cumulative release. To test this hypothesis, BSA-FITC was dissolved in water and added to the hardener component prior to mixing with HDIt. As shown in Figure II-1, the cumulative release of BSA-FITC was <20% after 21 days, thereby suggesting that a substantial portion of the BSA reacts with the polyisocyanate and is covalently bound to the scaffold.

To protect the protein from reacting with the polyisocyanate, BSA-FITC was lyophilized with a varying amount of glucose excipient and then added to the hardener as a powder. As shown in Figure II-1, the total amount of protein released was significantly higher when added as a powder compared to addition in solution. The glucose dosage played an important role in the release profile; the presence of 0.5% and 2% glucose increased the total amount released after 21 days and increased the initial burst release. However, further increasing the glucose dosage to 5% decreased the total release.

In vitro release of PDGF-BB from PUR scaffolds

Preliminary PDGF release experiments were performed in the absence of glucose excipient in an attempt to minimize the burst release and maximize the sustained release. Even more so than the PUR/BSA-FITC scaffolds, addition of PDGF as a powder without the glucose excipient resulted in negligible protein release (data not shown), which may be due to conformational and other biochemical differences between BSA-FITC and PDGF. Based upon the data in Figure II-1, 2 wt% glucose was added to the scaffolds to increase the cumulative release of PDGF. The release profile was monitored by two methods. In the first approach, PDGF was radioiodinated and a gamma counter was used to monitor the release kinetics. Release of PDGF was also measured by ELISA assay using the liquid releasates.

Both methods yielded similar release profiles (Figure II-2), characterized by a burst release on the first day. The ELISA assay detected a lower total release of 70%, compared with 85% for the 125I labeling method, which likely results from denaturation of some fraction of the released protein that cannot be detected by the antibody.

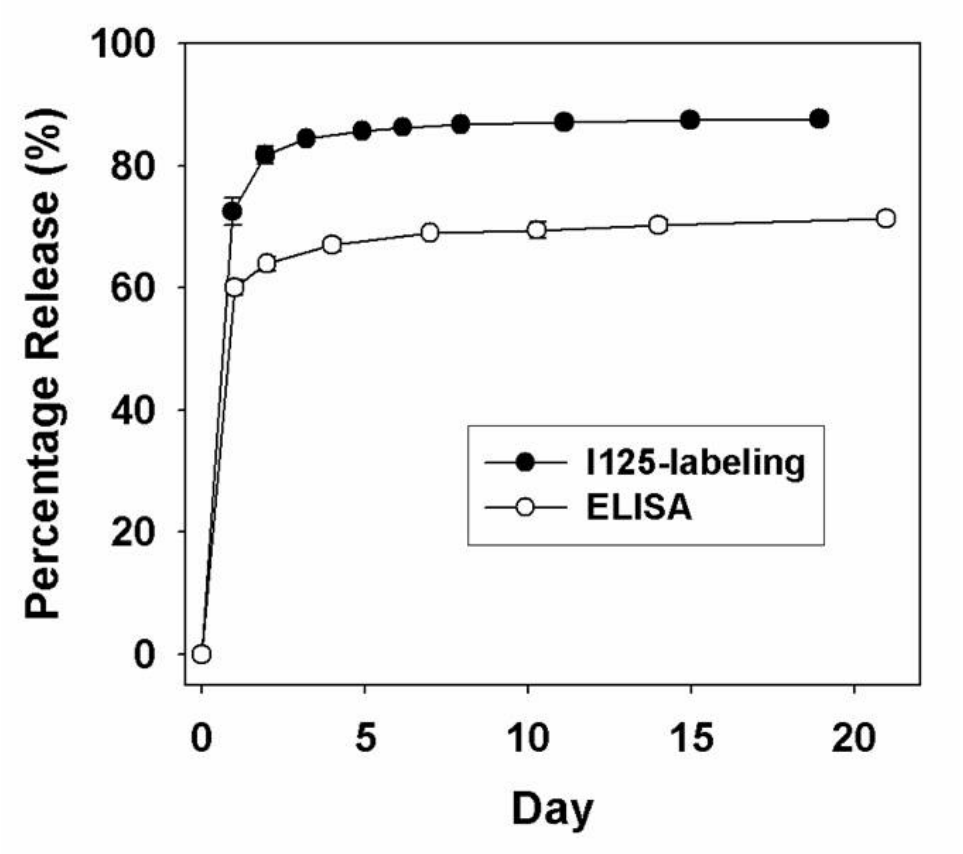

Figure II-2 *In vitro* release profile of PDGF from polyurethane scaffold including PDGF powder (PUR-PDGF) in the presence of 0.05% heparin and 2% glucose. The release kinetics was measured by gamma counting and ELISA respectively.

To mitigate the burst release, another strategy was adopted to achieve controlled release of PDGF from polyurethane scaffolds. Heparin was bound to the surface of microparticles made from amine-terminated PLGA (at the average size of 50 μm) using

standard carbodiimide techniques. PDGF was then loaded onto the particle surface through heparin binding.

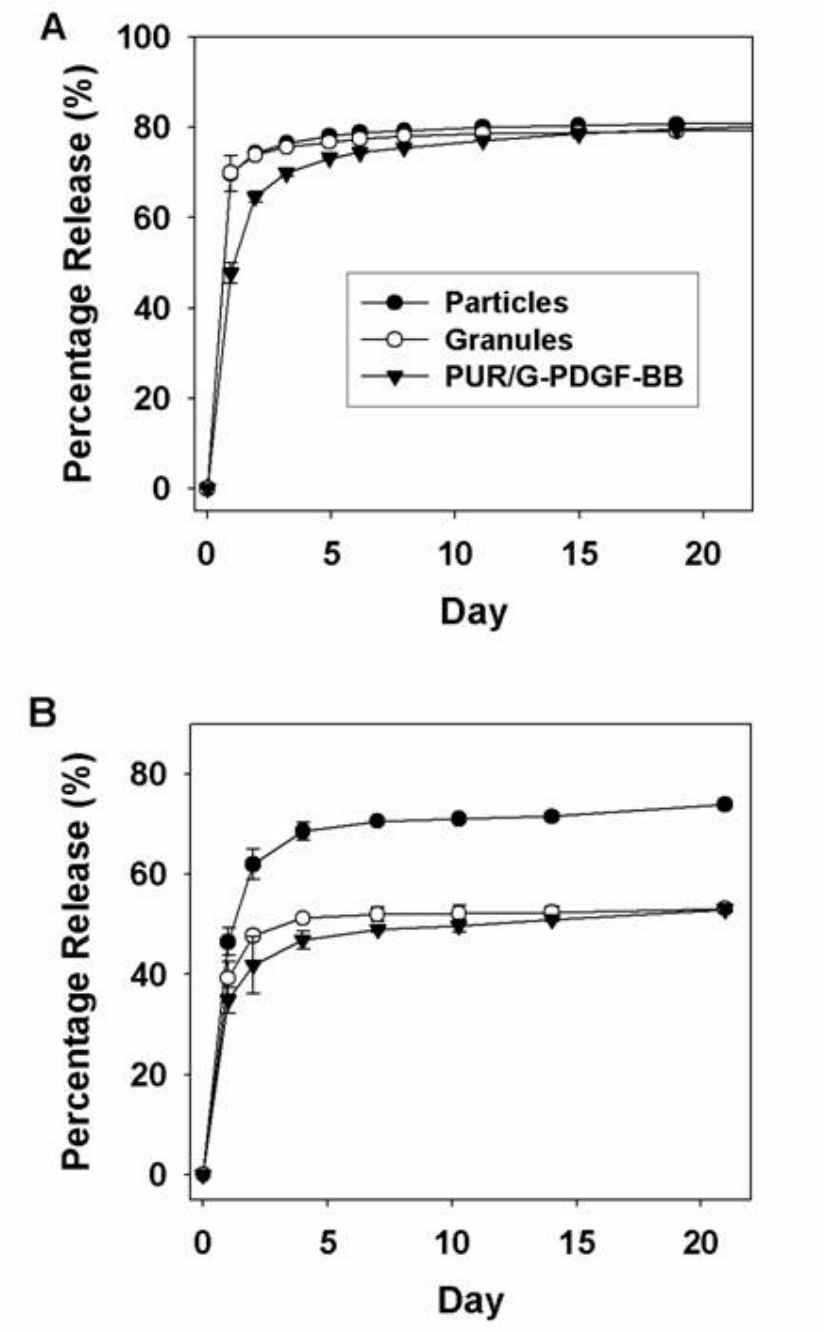

Figure II-3 *In vitro* release profile of PDGF from PLGA particles, granules and polyurethane scaffolds containing granules (PUR/G-PDGF). The release kinetics was determined by (A) gamma reading and (B) ELILSA.

As shown in Figure II-3, the total release of PDGF from the particles alone at day 21 was determined to be 80% and 72% by ^{125}I labeling and ELISA respectively. However, when the PLGA-Heparin-PDGF microparticles were incorporated in the polyurethane scaffold, less than 10% of the total protein was released over 21 days (data not shown), a finding which suggests that the surface-immobilized protein reacted with the polyisocyanate. To protect the protein on the surface of the PLGA microspheres from chemical modification, the microspheres were granulated by mixing the particles with a small amount of gelatin solution followed by forcing the mixture through a 48-mesh sieve to form 110-μm granules. The granules were then added to the hardener component before reacting with isocyanate to form PUR/G-PDGF polyurethane scaffolds. The PDGF release from gelatin-coated granules was similar to that of heparin-PLGA particles when detected by ^{125}I labeling (Figure II-3A), but release was lower when measured by ELISA (Figure II-3B). Compared with the release profiles from PUR/PDGF scaffolds (Figure II-2 and Figure II-3), the PUR/G-PDGF scaffolds exhibited lower burst and more sustained release when measured by radioiodination. However, when measured by ELISA, the total release was lower for the PUR/G-PDGF scaffolds, which again suggests that the isocyanate reaction may adversely affect the activity of the protein, despite the presence of a gelatin coating.

In vitro cell proliferation assay of released PDGF

To assess the *in vitro* bioactivity of PDGF released from the polyurethane scaffolds, releasates at days 1, 3, and 7 from PUR/PDGF and PUR/G-PDGF scaffolds, and at day 1 and 3 from particles and granules, were lyophilized and reconstituted to the same PDGF concentration, as determined by ELISA. The releasates were then tested for mitogenic activity using MC3T3 cells. After plating, the serum content was decreased from 10% to 0.5% to reduce background, and the reconstituted releasates were added at dosages of 3

and 10 ng/ml. Fresh PDGF acted as a positive control. Cell numbers were measured at time points of 24 and 72 h by staining the DNA and measuring fluorescence on a plate reader.

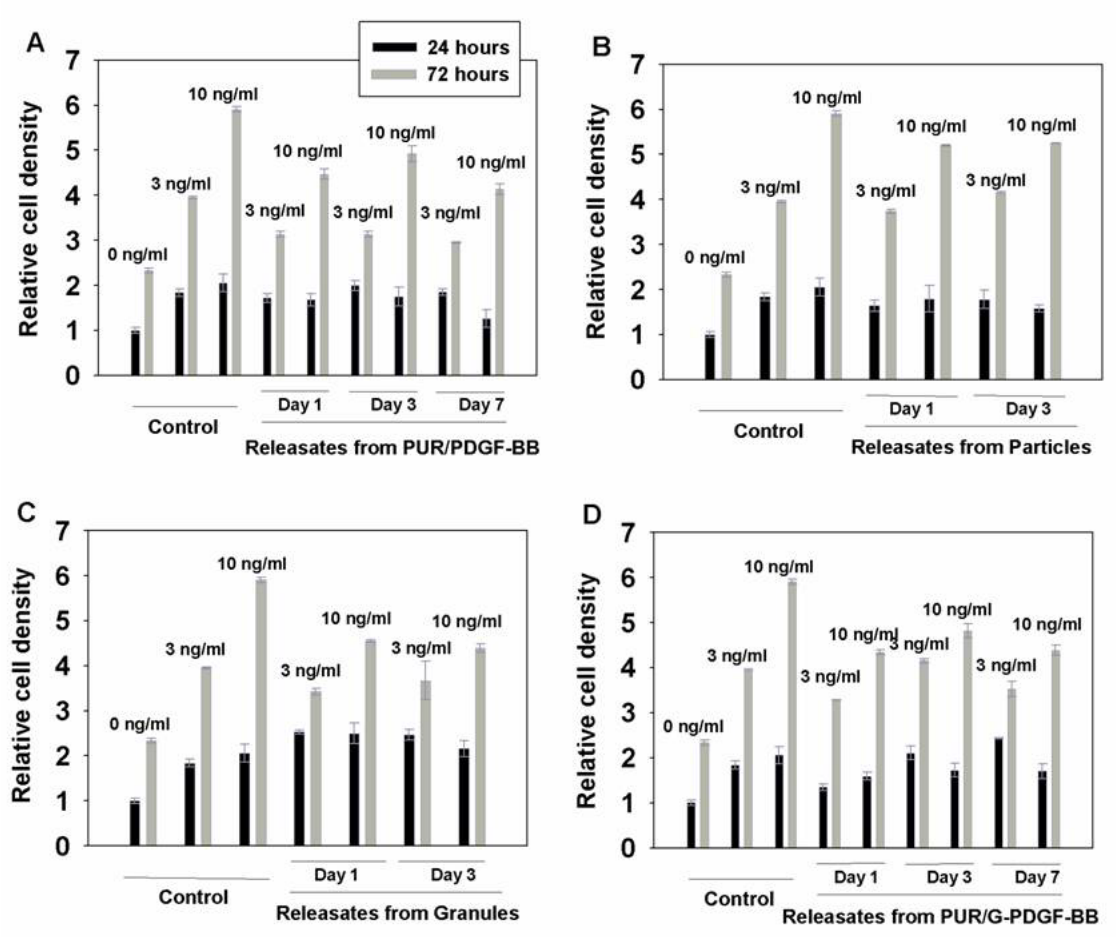

Figure II-4 *In vitro* cell counts measured for MC3T3 cells incubated in PDGF releasates from (A) PUR/PDGF scaffolds, (B) microspheres incorporating PDGF, (C) granules, and (D) PUR/G-PDGF scaffolds. MC3T3 cells were treated with varying dosages of PDGF (0, 3, and 10 ng/ml) for 24 and 72 hours after attachment of the cells to the surface of the well plates. The control treatment comprised fresh PDGF. CyQUANT assay was carried out to measure cell number.

Figure II-4 shows that the released PDGF from all the samples tested (PUR/PDGF, particles, granules, and PUR/G-PDGF) was biologically active, promoting proliferation of MC3T3 cells in a time-dependent manner. At the 72h time point, a statistically significant,

dose-dependent effect was observed. There was no statistically significant difference in the samples at the 24h time point. While the addition of released PDGF yielded statistically significant higher cell numbers compared to the negative control, the cell numbers were less than the positive control. For the PUR/PDGF material, the data of the cell proliferation assay indicated that the released PDGF exhibited ~20% decreased activity.

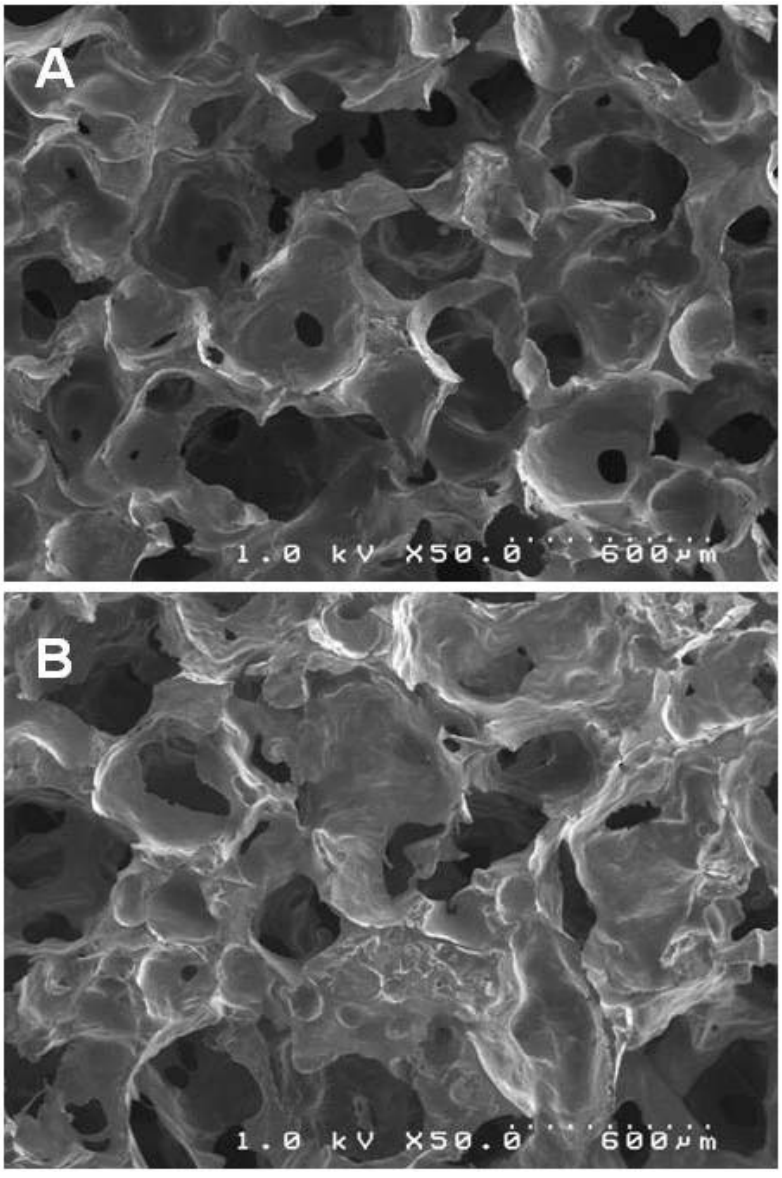

Figure II-5 Scanning electronic microscopic images of polyurethane scaffold containing (A) 2% glucose, and (B) 15% granules.

Porosity and mechanic properties of polyurethane scaffolds

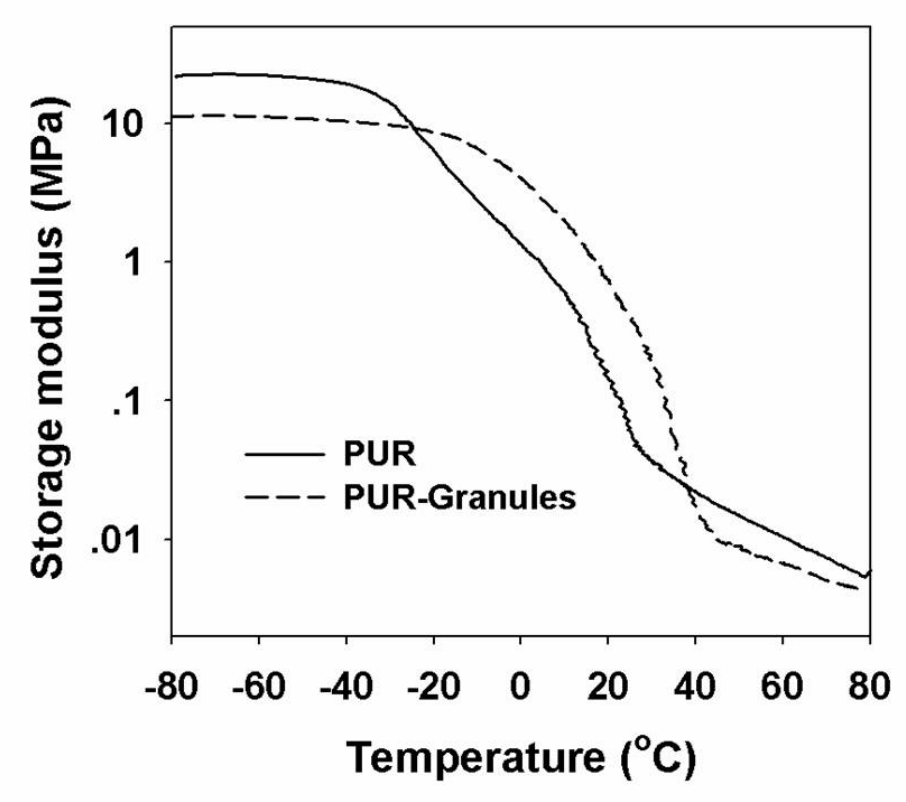

Figure II-6 Temperature sweeps of (A) PUR, and (B) PUR/G scaffolds (DMA).

The polyurethane scaffold containing 2% glucose (Figure II-5A) was porous with interconnected pores as evidenced by SEM imaging. The pore size was polydisperse and on the order of several hundred microns. The presence of 15 wt% granules in the PUR scaffold (Figure II-5B) did not substantially change the internal pore morphology. PUR/G scaffolds had a slightly lower density, thus the core porosity was higher than that of the PUR. The porosities of PUR and PUR/G scaffolds were calculated to be 87.4% and 85.2% respectively (Table II-1). As shown in Figure II-6, both materials exhibit glass transitions (Tg) less than 37°C, with Tg measured to be 24.5°C and 34.0°C for PUR and PUR/G respectively (Table II-1). The scaffolds exemplify the characteristics associated with rubbery elastomers,

including the glassy region below Tg, the glass transition region, and the rubbery plateau region above Tg.

Table II-1 PUR scaffold properties: density, porosity, and glass transition temperature (measured by DMA). The data for PUR containing 2 wt% glucose (PUR) and 15 wt% granules (PUR-Granules) are listed.

	Density ($kg \cdot m^{-3}$)	Porosity (vol-%)	Tg (°C)
PUR	178.4 ± 8.9	85.2 ± 0.7	24.5 ± 0.6
PUR-Granules	152.2 ± 7.4	87.4 ± 0.6	34.0 ± 1.7

In vivo test of PUR/PDGF implants in rat skin excisional wounds

After PDGF release and bioactivity were measured *in vitro*, the PUR/PDGF scaffolds were implanted into excisional wounds on the backs of adult male Sprague-Dawley rats to test biological activity in a wound healing model. The PUR/PDGF delivery system was selected for *in vivo* studies based on several considerations. First, the differences in the shape of the release profiles for the PUR/PDGF and PUR/G-PDGF systems were relatively minor. Second, the *in vitro* bioactivity of the growth factor released from the two delivery systems was comparable; however, the cumulative release of PDGF from the PUR/PDGF system was almost 20% higher than that from the PUR/G-PDGF system, thereby requiring a lower dosage of growth factor. Third, the PDGF powder system was considerably simpler than the granule system and required fewer processing steps. Therefore, the PUR/PDGF system was selected for the *in vivo* studies. The loading of PDGF in the scaffolds was 0 μg (control), 1.8 μg, and 18 μg respectively. Preliminary experiments showed no statistically significant difference in new tissue ingrowth at the 18 μg dose compared to the 1.8 μg loading, so further experiments were performed at the lower dose only. After 3, 7, and 14

days post-implantation, the rats were sacrificed, and the harvested implants were processed for histology.

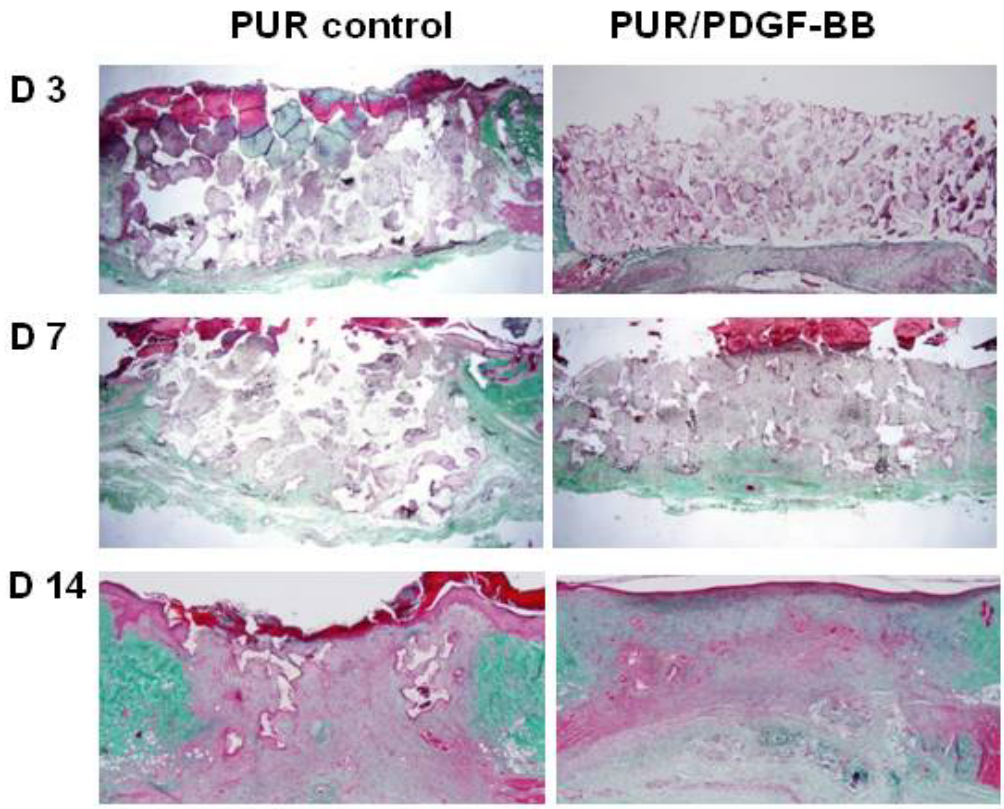

Figure II-7 Thichrome staining and quantitative evaluation of *in vivo* implants. In the representative images, the white, red, and green sections represent the presence of polymer, tissue, and collagen deposition respectively

As shown in Figure II-7 (trichrome stain), PUR/PDGF scaffolds promoted significantly more new granulation tissue formation and polymer resorption compared to the blank PUR control at all time points. As the healing progressed, new extracellular matrix with dense collagen fibers filled the defect. At day 7, a remarkable level of new tissue infiltration and scaffold degradation was observed for the PDGF samples. At day 14, the polymer had almost completely resorbed, being replaced by new tissue accompanied by deposition of collagen. In addition, a complete epithelial layer had formed on the upper surface of the

wound/implant site. The amounts of both remaining polymer and new tissue formation within the scaffold at different time points were analyzed quantitatively based on the area percentage measured from the histological images (Figure II-8, A and B). Statistical analysis between the control and PDGF groups (ANOVA with bonferoni correction, $p \leq 0.05$) showed that the amount of polymer within PDGF samples was significantly ($p \leq 0.05$) lower than the control scaffold, and that the new tissue formation within the PUR/PDGF scaffolds was significantly higher than the control at all time points.

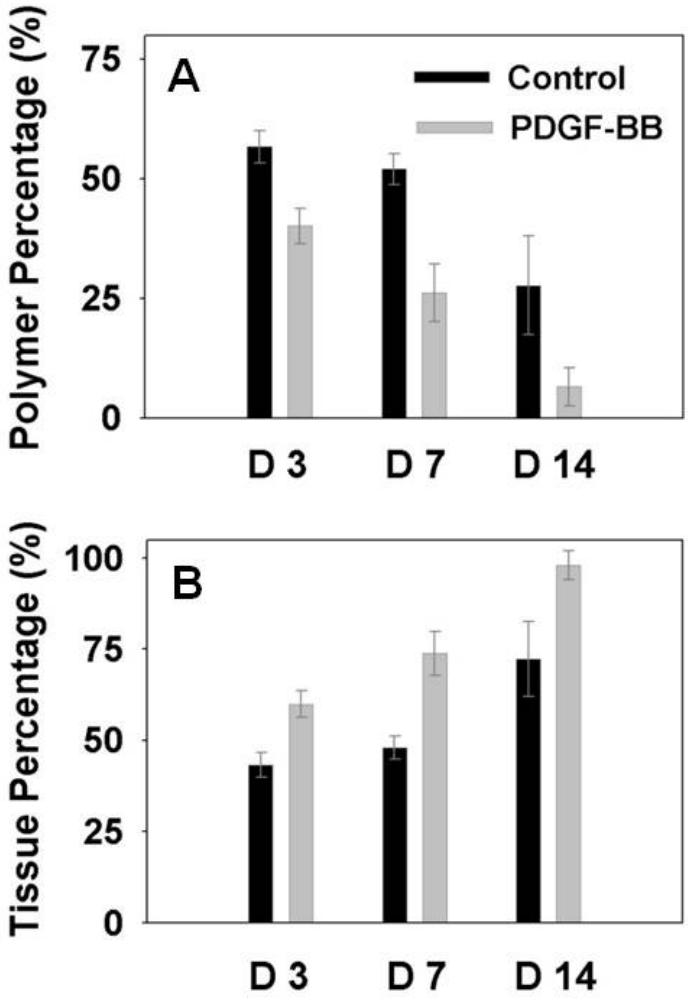

Figure II-8 Histomorphometry analysis with the area percentage of polymer and new granule tissue within the implants are shown in (A) and (B).

H&E staining (Figure II-9) indicated the presence of both inflammatory cells (macrophages and neutrophils) and fibroblasts within the scaffold, and there was no substantial difference between the control and PUR/PDGF scaffolds in the relative proportion of these infiltrating cell populations. There was a typical neutrophil infiltration into the polymer scaffold at day 3 and 7. At day 14, the PDGF sample showed few definitive inflammatory cells while giant cells were observed around the remnant PUR scaffold in the control.

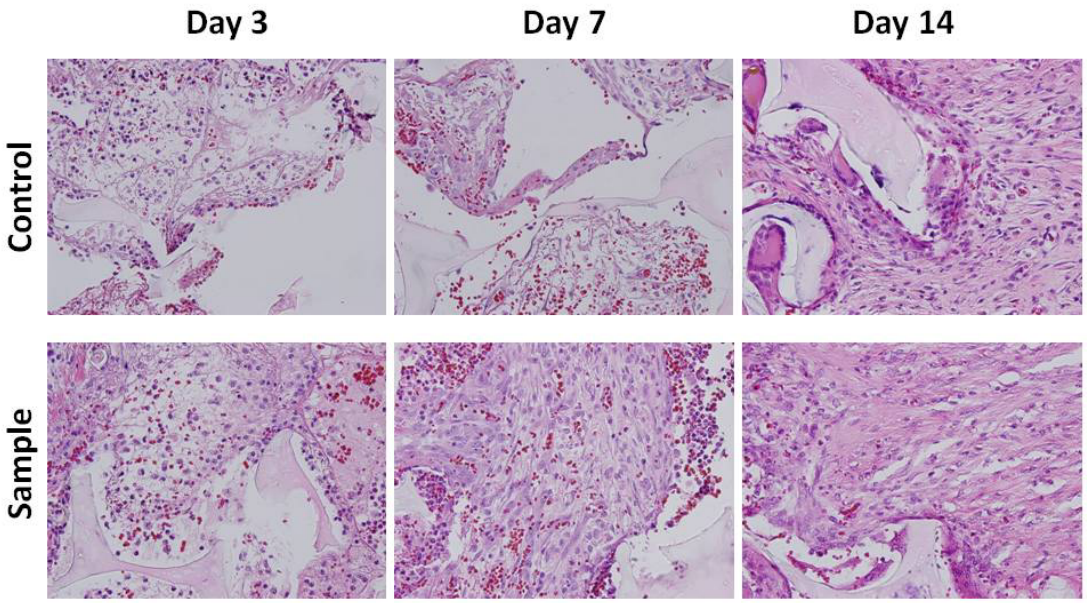

Figure II-9 H&E staining of *in vivo* implants at 40X magnification. Representative tissue sections were photographed from 3, 7, and 14 day excisional wounds containing PUR scaffold alone (control) or scaffold containing 1.8 μg PDGF-BB (sample). The scaffold is visible as a pale, acellular structure. At day 3, the interstices of the scaffold already contain a largely fibrinous matrix and an inflammatory infiltrate with both mononuclear cells and neutrophils. At day 7, the sample exhibits a notably higher proportion of spindle-shaped fibroblasts. At 14 days, both specimens show evidence of interstitial fibrous connective tissue, but it is more apparent and abundant, relative to the cellular component, in the treated group. The scaffold material is associated with giant cells that appear to be attempting to engulf the residual scaffold.

Discussion

The stabilization of therapeutic proteins in delivery systems is a challenging problem, due in part to the need to preserve the three-dimensional conformation of the protein. While proteins have been incorporated into polymer scaffolds to achieve sustained release, there are a limited number of studies investigating release of biologically active molecules from reactive two-component polymers. Ascorbic acid dissolved in glycerol was utilized as a chain extender to form a polyurethane network through reaction with a lysine diisocyanate (LDI) prepolymer. Ascorbic acid released from the polyurethane exhibited linear release kinetics (32). However, the applicability of this approach with proteins is limited, due to the potential that the chemical reaction will covalently bind the protein to the polymer network as evidenced by the low cumulative release of BSA dissolved in water (Figure II-1). However, adding the protein as a powder or coating the protein-loaded microspheres with gelatin protected the protein from reacting with the isocyanate, thus preserving its bioactivity. Addition of a glucose excipient significantly altered the release profile as observed for BSA-FITC (Figure II-1), and an optimal glucose dosage exists that maximizes the cumulative release of BSA. Glucose and heparin were used as excipients when including PDGF powder into polyurethane scaffold. Glucose, which is in the form of solid particles that diffuse through the scaffold, has been proposed to act as a porogen which increases the diffusivity of the protein (33), as evidenced by the less than 10% cumulative release of PDGF in the absence of glucose (data not shown). Heparin is known to bind to several growth factors via electrostatic forces, thus enhancing the bioactivity of the protein (10, 28). PEG 600 (50%), which is a liquid at ambient temperature, was included in the polyol component prior to polymerization with HDIt. The terminal hydroxyl groups on the PEG molecule react with the NCO groups to form urethane linkages, thereby covalently binding the PEG to the polymer

network. Thus it is not likely that PEG acted as an excipient since the urethane bonds hydrolyze over a much longer time scale than that of protein release.

In the present study, I reasoned that sustained release of PDGF could be achieved by binding the protein to heparin-conjugated PLGA microspheres followed by gelatin granulation to protect the protein from reacting with the isocyanate during the formation of the scaffold. Binding of BMP-2 to heparin immobilized on the surface of PLGA scaffolds has yielded a nearly linear release profile for up to 14 days (10), and similar results have been reported for bFGF bound to heparin-conjugated PLGA nanospheres (28). bFGF bound to heparin-conjugated porous PLGA microspheres showed a small burst release on the first day followed by sustained release for about 15 days (34). Although I obtained a reduced burst and higher sustained release for PUR/G-PDGF compared with PUR/PDGF, the burst release was still higher than that reported previously for BMP-2 (10) and bFGF (34). Furthermore, the ELISA assay (Figure II-3B) showed decreased antibody binding activity of the released PDGF compared with the radiolabeling assay (Figure II-3A), suggesting a slight loss in the protein activity during granulation.

In vitro cell proliferation analysis suggested that the released PDGF from PUR/PDGF and PUR/G-PDGF scaffolds had ~20% lower activity than fresh PDGF. Considering that the release profiles for both delivery strategies showed no substantial differences, the PUR/PDGF scaffold was selected for the *in vivo* study on the basis of simpler fabrication. I also reasoned that since PDGF functions in the early stages of cell proliferation (35), release of the growth factor in the first few days of healing would recruit cells to the scaffold and accelerate healing.

In previous studies, we have shown that two-component PUR scaffolds synthesized from aliphatic and lysine-derived polyisocyanates are biocompatible and degrade to non-

cytotoxic decomposition products when implanted subcutaneously (12). When implanted in excisional wounds, the scaffolds supported the ingrowth of cells and new tissue. The presence of PDGF within the implants shown in this report improved excisional wound healing significantly due to accelerated polymer degradation and enhanced new granulation tissue formation. There was little difference between the active and control scaffolds in terms of the inflammatory response at days 3 and 7, but there were significantly more inflammatory cells in the control than the PDGF sample at day 14. The presence of inflammatory cells may release reactive oxygen species in the early stages as well as enzymes such as cholesterol esterase, esterase, and carboxyl esterase (36). Both these effects have been reported to degrade poly(ester urethane)s (37-39). Both inflammatory cells and fibroblasts have been reported to play a role in the acceleration of wound healing by PDGF (40). Considering that PDGF has been reported to attract neutrophils, macrophages, and fibroblasts (41), it is possible that the inflammatory cells attracted to the PUR/PDGF scaffolds accelerated degradation of the polymer through the reactive oxygen and enzymatic mechanisms described above. The enhanced formation of granulation tissue in the PUR/PDGF scaffolds relative to the control likely results from the recruitment of fibroblast cells which resulted in endogenous growth factor production, provisional extracellular matrix synthesis, fibroblast proliferation, and collagen synthesis (40, 42, 43).

Nanofibrous scaffolds incorporating PLGA microspheres encapsulated with PDGF have been shown to achieve nearly linear release kinetics of PDGF with a small burst release *in vitro* (9). These materials have also been reported to promote chemokine expression and tissue neogenesis in mid-sagittal incision model of rat dorsa (8). No significant tissue infiltration was observed at day 3, but significant tissue neogenesis was observed at day 7 and almost complete tissue penetration occurred at day 14 (8). In related experiments, a surface adsorption method for releasing PDGF was also investigated, which did not promote

tissue neogenesis as well as the microsphere approach (8) due to the bolus release of growth factor (i.e., within several hours) (10). These results underscore the importance of sustained release beyond the first few hours to accelerate wound healing. In the nanofiber experiments, two different PDGF dosages (11.9 μg/ml and 119 μg/ml scaffold) and release strategies (fast and slow) were investigated. Formation of new tissue was highest for the fast delivery system at the 119 μg /ml dosage. In contrast, for the PUR scaffolds, we observed no effect of PDGF dosage on new tissue formation at dosages of 11.5 μg /ml and 115 μg /ml scaffold. Furthermore, for the nanofiber scaffolds at the low PDGF dosage (11.9 μg/ml scaffold), new tissue formation was significantly higher for the slow release system (characterized by a burst release < 5% on day 1) compared to the fast release system (a burst release of 30% on day 1). Surprisingly, for the PUR/PDGF delivery system where the burst release on day 1 is 60%, we have observed significant new tissue formation promoted by PDGF as early as day 3, compared to day 7 for the nanofiber scaffolds. While the models used in the nanofiber and PUR studies differ, our data suggest that a burst release in the first few days followed by a lower sustained release may accelerate healing. It is important to note that the accelerated *in vivo* degradation of PUR/PDGF scaffolds is anticipated to substantially modify the release profile as compared to *in vitro* release assays. Stated another way, the observed accelerated degradation of the PUR scaffolds in the presence of PDGF *in vivo* may have a feedback effect, where the release of PDGF stimulates polymer degradation, which further increases the release of PDGF from the scaffold.

Conclusion

When released from a reactive two-component polyurethane scaffold in the first several days of the healing process, PDGF promotes cell proliferation, enhanced granulation tissue formation, and acceleration of scaffold degradation. The bioactivity of the released growth

factor is substantially preserved in the presence of the chemical reaction between the isocyanate and hydroxyl groups. The ability of PUR scaffolds to promote new tissue formation in excisional wounds in rat skin, achieved through local delivery of PDGF, suggests the potential utility of biodegradable polyurethanes both as a supportive scaffold and as a protein delivery system for tissue restoration.

Acknowledgement

This work was funded by the National Institute on Aging (AG-06528), the Department of Veterans Affairs, the Orthopaedic Trauma Research Program (DOD-W81XWH-07-1-0211) and Vanderbilt University School of Engineering.

References

1. Heldin CH, Westermark B. Mechanism of action and *in vivo* role of platelet-derived growth factor. Physiol Rev. 1999 Oct;79(4):1283-316.

2. Centrella M, McCarthy TL, Kusmik WF, Canalis E. Isoform-specific regulation of platelet-derived growth factor activity and binding in osteoblast-enriched cultures from fetal rat bone. J Clin Invest. 1992 Apr;89(4):1076-84.

3. Piche JE, Graves DT. Study of the growth factor requirements of human bone-derived cells: a comparison with human fibroblasts. Bone. 1989;10(2):131-8.

4. Gruber R, Varga F, Fischer MB, Watzek G. Platelets stimulate proliferation of bone cells: involvement of platelet-derived growth factor, microparticles and membranes. Clin Oral Implants Res. 2002 Oct;13(5):529-35.

5. McGill JJ, Strates BS, McGuire MH. Stimulation of Osteogenesis by Platelet Derived Growth-Factor and A Transforming Growth-Factor. Clinical Research. 1991;39(3):A788.

6. Grotendorst GR, Martin GR, Pencev D, Sodek J, Harvey AK. Stimulation of Granulation-Tissue Formation by Platelet-Derived Growth-Factor in Normal and Diabetic Rats. Journal of Clinical Investigation. 1985;76(6):2323-9.

7. Nash TJ, Howlett CR, Martin C, Steele J, Johnson KA, Hicklin DJ. Effect of Platelet-Derived Growth-Factor on Tibial Osteotomies in Rabbits. Bone. 1994;15(2):203-8.

8. Jin Q, Wei G, Lin Z, Sugai JV, Lynch SE, Ma PX, et al. Nanofibrous scaffolds incorporating PDGF-BB microspheres induce chemokine expression and tissue neogenesis *in vivo*. PLoSONE. 2008;3(3):e1729.

9. Wei GB, Jin QM, Giannobile WV, Ma PX. Nano-fibrous scaffold for controlled delivery of recombinant human PDGF-BB. Journal of Controlled Release. 2006;112(1):103-10.

10. Jeon O, Song SJ, Kang SW, Putnam AJ, Kim BS. Enhancement of ectopic bone formation by bone morphogenetic protein-2 released from a heparin-conjugated poly(L-lactic-co-glycolic acid) scaffold. Biomaterials. 2007;28(17):2763-71.

11. Lin Z, Sugai JV, Jin Q, Chandler LA, Giannobile WV. Platelet-derived growth factor-B gene delivery sustains gingival fibroblast signal transduction. J Periodontal Res. 2008 Aug;43(4):440-9.

12. Hafeman AE, Li B, Yoshii T, Zienkiewicz K, Davidson JM, Guelcher SA. Injectable biodegradable polyurethane scaffolds with release of platelet-derived growth factor for tissue repair and regeneration. PharmRes. 2008;25(10):2387-99.

13. Bennett S, Connolly K, Lee DR, Jiang Y, Buck D, Hollinger JO, et al. Initial biocompatibility studies of a novel degradable polymeric bone substitute that hardens in situ. Bone. 1996 Jul;19(1):S101-S7.

14. Zhang JY, Beckman EJ, Hu J, Yang GG, Agarwal S, Hollinger JO. Synthesis, biodegradability, and biocompatibility of lysine diisocyanate-glucose polymers. Tissue Engineering. 2002;8(5):771-85.

15. Zhang JY, Beckman EJ, Piesco NP, Agarwal S. A new peptide-based urethane polymer: synthesis, biodegradation, and potential to support cell growth *in vitro*. Biomaterials. 2000;21(12):1247-58.

16. Guan JJ, Sacks MS, Beckman EJ, Wagner WR. Synthesis, characterization, and cytocompatibility of efastomeric, biodegradable poly(ester-urethane)ureas based on poly(caprolactone) and putrescine. Journal of Biomedical Materials Research. 2002;61(3):493-503.

17. Santerre JP, Woodhouse K, Laroche G, Labow RS. Understanding the biodegradation of polyurethanes: From classical implants to tissue engineering materials. Biomaterials. 2005 Dec;26(35):7457-70.

18. Gorna K, Gogolewski S. Biodegradable polyurethanes for implants. II. *In vitro* degradation and calcification of materials from poly(epsilon-caprolactone)-poly(ethylene oxide) diols and various chain extenders. Journal of Biomedical Materials Research. 2002;60(4):592-606.

19. Gorna K, Gogolewski S. Preparation, degradation, and calcification of biodegradable polyurethane foams for bone graft substitutes. Journal of Biomedical Materials Research Part A. 2003;67A(3):813-27.

20. Guelcher S, Srinivasan A, Hafeman A, Gallagher K, Doctor J, Khetan S, et al. Synthesis, *In vitro* degradation, and mechanical properties of two-component poly(ester

urethane)urea scaffolds: Effects of water and polyol composition. Tissue Engineering. 2007;13(9):2321-33.

21. Guelcher SA. Biodegradable polyurethanes: Synthesis and applications in regenerative medicine. Tissue Engineering Part B-Reviews. 2008;14(1):3-17.

22. Guelcher SA, Patel V, Gallagher KM, Connolly S, Didier JE, Doctor JS, et al. Synthesis and *in vitro* biocompatibility of injectable polyurethane foam scaffolds. Tissue Engineering. 2006;12(5):1247-59.

23. Simmons A, Padsalgikar AD, Ferris LM, Poole-Warren LA. Biostability and biological performance of a PDMS-based polyurethane for controlled drug release. Biomaterials. 2008;29(20):2987-95.

24. Boateng JS, Matthews KH, Stevens HNE, Eccleston GM. Wound healing dressings and drug delivery systems: A review. Journal of Pharmaceutical Sciences. 2008;97(8):2892-923.

25. Guan J, Stankus JJ, Wagner WR. Biodegradable elastomeric scaffolds with basic fibroblast growth factor release. Journal of Controlled Release. 2007;120(1-2):70-8.

26. Hafeman AE, Zienkiewicz KJ, Davidson JM, Guelcher SA. Injectability of Biodegradable, Porous Polyurethane Scaffolds for Tissue Regeneration. TERMIS-NA 2008 Annual Conference, Abstract 2008.

27. Berkland C, Kipper MJ, Narasimhan B, Kim KK, Pack DW. Microsphere size, precipitation kinetics and drug distribution control drug release from biodegradable polyanhydride microspheres. Journal of Controlled Release. 2004;94(1):129-41.

28. Jeon O, Kang SW, Lim HW, Chung JH, Kim BS. Long-term and zero-order release of basic fibroblast growth factor from heparin-conjugated poly(L-lactide-co-glycolide) nanospheres and fibrin gel. Biomaterials. 2006;27(8):1598-607.

29. Lejeune KE, Mesiano AJ, Bower SB, Grimsley JK, Wild JR, Russell AJ. Dramatically stabilized phosphotriesterase-polymers for nerve agent degradation. Biotechnol Bioeng. 1997 Apr 20;54(2):105-14.

30. Guan J, Wagner WR. Synthesis, characterization and cytocompatibility of polyurethaneurea elastomers with designed elastase sensitivity. Biomacromolecules. 2005 Sep-Oct;6(5):2833-42.

31. Taite LJ, Yang P, Jun HW, West JL. Nitric oxide-releasing polyurethane-PEG copolymer containing the YIGSR peptide promotes endothelialization with decreased platelet adhesion. J Biomed Mater Res B Appl Biomater. 2008 Jan;84(1):108-16.

32. Zhang JY, Doll BA, Beckman EJ, Hollinger JO. Three-dimensional biocompatible ascorbic acid-containing scaffold for bone tissue engineering. Tissue Eng. 2003;9(6):1143-57.

33. Park K. Controlled Drug Delivery: Challenges and Strategies: Springer Netherlands; 1997.

34. Chung HJ, Kim HK, Yoon JJ, Park TG. Heparin immobilized porous PLGA microspheres for angiogenic growth factor delivery. Pharmaceutical Research. 2006;23(8):1835-41.

35. Tatsuyama K, Maezawa Y, Baba H, Imamura Y, Fukuda M. Expression of various growth factors for cell proliferation and cytodifferentiation during fracture repair of bone. European Journal of Histochemistry. 2000;44(3):269-78.

36. Salthouse TN. Cellular enzyme activity at the polymer-tissue interface: a review. JBiomedMaterRes. 1976;10(2):197-229.

37. Santerre JP, Labow RS, Adams GA. Enzyme Biomaterial Interactions - Effect of Biosystems on Degradation of Polyurethanes. Journal of Biomedical Materials Research. 1993;27(1):97-109.

38. Labow RS, Duguay DG, Santerre JP. The Enzymatic-Hydrolysis of A Synthetic Biomembrane - A New Substrate for Cholesterol and Carboxyl Esterases. Journal of Biomaterials Science-Polymer Edition. 1994;6(2):169-79.

39. Labow RS, Erfle DJ, Santerre JP. Neutrophil-Mediated Degradation of Segmented Polyurethanes. Biomaterials. 1995;16(1):51-9.

40. Pierce GF, Mustoe TA, Altrock BW, Deuel TF, Thomason A. Role of Platelet-Derived Growth-Factor in Wound-Healing. Journal of Cellular Biochemistry. 1991;45(4):319-26.

41. Chen G, Quinn LS. Partial Characterization of Skeletal Myoblast Mitogens in Mouse Crushed Muscle Extract. Journal of Cellular Physiology. 1992;153(3):563-74.

42. Pierce GF, Mustoe TA, Lingelbach J, Masakowski VR, Griffin GL, Senior RM, et al. Platelet-derived growth factor and transforming growth factor-beta enhance tissue repair activities by unique mechanisms. JCell Biol. 1989;109(1):429-40.

43. Pierce GF, Mustoe TA, Senior RM, Reed J, Griffin GL, Thomason A, et al. *In vivo* incisional wound healing augmented by platelet-derived growth factor and recombinant c-sis gene homodimeric proteins. JExpMed. 1988;167(3):974-87.

CHAPTER III

THE EFFECTS OF RHBMP-2 RELEASED FROM BIODEGRADABLE POLYURETHANE/MICROSPHERE COMPOSITE SCAFFOLDS ON NEW BONE FORMATION IN RAT FEMORA: PLUG DEFECT AND CRITICAL SIZE SEGMENTAL DEFECT

Abstract

Scaffolds prepared from biodegradable polyurethanes (PUR) have been investigated as a supportive matrix and delivery system for skin, cardiovascular, and bone tissue engineering. While previous studies have suggested that PUR scaffolds are biocompatible and moderately osteoconductive, the effects of encapsulated osteoinductive molecules, such as recombinant human bone morphogenetic protein (rhBMP-2), on new bone formation have not been investigated for this class of biomaterials. The objective of this study was to investigate the effects of different rhBMP-2 release strategies on new bone formation in PUR scaffolds implanted in rat femoral defects: both the simple plug model and the more stringent critical size segmental model. In the simplest approach, rhBMP-2 was added as a dry powder prior to the foaming reaction, which resulted in a burst release followed by a sustained release for 21 days. Encapsulation of rhBMP-2 in either 1.3-micron or 113-micron PLGA microspheres prior to the foaming reaction reduced the burst release. In the rat femoral plug defect model, at 4 weeks post-implantation, all rhBMP-2 treatment groups enhanced new bone formation relative to the scaffolds without rhBMP-2. Scaffolds incorporating rhBMP-2 powder promoted the most extensive new bone formation, while scaffolds incorporating rhBMP-2 encapsulated in 1.3-micron microspheres, which exhibited the lowest burst release, promoted the least extensive new bone formation. Thus our

observations suggest that an initial burst release followed by sustained release is better for promoting new bone formation. This conclusion was further confirmed in another more stringent animal model, the rat femoral critical size segmental defect, where we observed better new bone formation promoted by scaffolds incorporated with rhBMP-2 powder than clinically used collagen sponge adsorbed with rhBMP-2 which has a bolus release, but very few amount of new bone formation was promoted by the small particle approach. We reason that the burst release of rhBMP-2 could be responsible in attracting cells into the scaffolds while sustained release function as a morphogen to differentiate cells.

Introduction

Incorporation of signaling molecules, such as growth factors, in a scaffold to support ingrowth of cells and new tissue is an effective approach to regenerating tissue such as bone. Polymer scaffolds have been used extensively in bone tissue engineering. Ideally, the scaffold should support cell attachment and ingrowth of new tissue, as well as biodegrade at a rate matching that of new tissue ingrowth.

Scaffolds synthesized from biodegradable polyurethanes (PUR) have been investigated in skin (1-3), cardiovascular (4-7), and bone (8, 9) tissue engineering applications. In these applications, PUR scaffolds have been reported to support cell in-growth and tissue remodeling, as well as biodegrade to non-cytotoxic decomposition products (3, 4, 10-12). A distinguishing feature of these biomaterials is the potential to inject them as a reactive two-component liquid or paste that cures in situ to form a solid elastomeric scaffold without causing tissue damage or inducing a significant inflammatory response (1, 9, 13, 14). PUR scaffolds have also been investigated as delivery systems for controlled release of growth factors, including bFGF and rhPDGF-BB (2, 13, 15). We have previously demonstrated that rhPDGF-BB released from two-component reactive PUR scaffolds implanted in rat skin

excisional wounds both enhanced new tissue formation and also accelerated polymer degradation, suggesting that the bioactivity of the growth factor was not adversely affected by the chemical reaction (2).

The osteoinductive growth factor bone morphogenetic protein-2 (BMP-2) stimulates osteoblast differentiation and promotes bone formation. Recombinant human (rh) BMP-2 delivered from a collagen sponge (INFUSE® Bone Graft, Medtronic) is an FDA-approved therapy for posterior-lateral spine, tibia, and specific craniofacial applications. The collagen sponge delivery system results in a bolus release of growth factor in the first several hours (16). Unfortunately, there is no conclusive evidence regarding the optimal release kinetics. There is, however, evidence that BMP-2 promotes bone formation via different mechanisms such as osteoblast differentiation, cheomoattraction, angiogensis, and cell signaling at the initiation of fracture healing. A number of studies have suggested that sustained release of rhBMP-2 (17-19) is more effective than a bolus release for promoting new bone formation. For example, delayed percutaneous injection of rhBMP-2 into the fracture site one week after surgery resulted in enhanced fracture healing relative to injection within one day in a primate model (20). The improvement in healing associated with delayed injection was conjectured to result from a larger number of cells at the fracture site. Other studies have suggested that BMP-2 plays an important role at early stages in the healing process. BMP-2 is involved in promoting angiogenesis (21) and migration of human mesenchymal progenitor cells (MPCs) (22). It may also serve as the trigger in the fracture healing cascade as demonstrated by its early maximal expression on day 1 as measured in a mouse tibia fracture model (23). Taken together, these previous studies suggest that both a burst and sustained release of rhBMP-2 are beneficial. A burst release of rhBMP-2 is anticipated to increase cellular migration and promote angiogenesis, while sustained release is anticipated to promote differentiation of the responding cells and thus more new bone formation.

One purpose of the present study was to evaluate the ability of rhBMP-2 delivered from PUR scaffolds to heal bone defects, compared with rhBMP-2 delivered from collagen sponge which is used clinically. Scaffolds fabricated from biodegradable segmented PUR elastomers supported new bone formation when implanted in monocortical defects in the iliac crest of sheep for six months (8, 24), implying that the materials are moderately osteoconductive. Delivery of rhBMP-2 from polymeric scaffolds, such as poly(lactic-co-glycolic acid) (PLGA) and poly(propylene fumarate) (PPF), has been shown to promote new bone formation (25-31), but the effects of rhBMP-2 released from two-component reactive polyurethanes on new bone formation have not been investigated. It has been suggested that the harsh polymerization conditions, such as cross linking and thermal gradients, associated with reactive biomaterials may adversely affect the bioactivity of added growth factors (32). Although we have previously shown that rhPDGF powder encapsulated in reactive PUR scaffolds retained ~80% of its bioactivity (2), these results do not necessarily translate to rhBMP-2. Another objective of this study was to modulate the release kinetics by encapsulating rhBMP-2 in microspheres of varying size prior to embedding in the PUR scaffolds. The burst release from microspheres in the range of 35 – 45 μm reportedly decreased when embedded in PPF/microsphere composite scaffolds (32). However, the effects of particle size on release kinetics and new bone formation have not been previously investigated. In this study, we have investigated the effects of microsphere size on rhBMP-2 release kinetics and new bone formation in two different rat femoral models: the simpler plug defect model, and the more stringent critical size segmental defect model. Both animal tests yielded consistent results which proved our hypothesis that, while sustained release of rhBMP-2 is superior to bolus release of rhBMP-2 in promoting new bone formation, the burst release of rhBMP-2 is also critical in initiating early events of bone regeneration such as cell recruitment and neovascularization.

Materials and methods

Materials

Polyvinyl alcohol (PVA), glycolide, and D,L-lactide were obtained from Polysciences (Warrington, PA). The tertiary amine catalyst TEGOAMIN33, which comprised a solution of 33 wt% triethylene diamine (TEDA) in dirpropylene glycol, was received from Goldschmidt (Hopewell, VA) as a gift. Polyethylene glycol (PEG, 600 Da) was purchased from Alfa Aesar (Ward Hill, MA). Dichloromethane (DCM) and glucose were from Acros Organics (Morris Plains, NJ). Hexamethylene diisocyanate trimer (HDIt, Desmodur N3300A) was received as a gift from Bayer Material Science (Pittsburgh, PA). Lysine triisocyanate (LTI) was purchased from Kyowa Hakko (New York, NY). Stannous octoate catalyst was received from Nusil technology (Overland Park, KS). α-minimal essential medium (α-MEM) was purchased from Fisher Scientific (Pittsburgh, PA). PLGA (50/50, intrinsic viscosity 0.58 dL/g) was purchased from LACTEL (Pelham, AL). Recombinant human bone morphogenetic protein-2 (rhBMP-2) was received as a gift from Professor Jeffrey Hollinger at Carnegie Mellon University. All other reagents were purchased from Sigma-Aldrich (St. Louis, MO).

Poly(lactic-co-glycolic acid) (PLGA) microspheres fabrication

A double emulsion technique was used to fabricate PLGA microspheres (2, 33). PLGA (50/50, 0.58 dL/g) and PEG (4600 Da), at a ratio of 9:1, were dissolved in DCM at polymer concentrations of 10% and 5% for large and small size particles, respectively. A glucose solution of BSA-FITC (fluoroisothiocyanate-labeled bovine serum albumin) or rhBMP-2 was added to the polymer DCM solution, followed by sonication to form the water-in-oil (w/o) emulsion. The w/o emulsion was then added to a PVA solution (0.3% and 5% for large and small size particles, respectively) under intense stirring to form the water-in-oil-in-water (w/o/w) double emulsion. A homogenizer was used for the first 100 s of stirring.

Subsequently, the double emulsion was mixed using a stir bar for another 2.5 h to evaporate the DCM solvent.

The particles were then recovered by centrifugation, washed, and lyophilized. Large microspheres (PLGA-L) were imaged using an Olympus BX60 microscope, and the particle size distribution (PSD) was calculated by sampling ~500 particles. Small microspheres (PLGA-S) were imaged by scanning electron microscopy (Hitachi S-4200 SEM), and the PSD determined by dynamic laser light scattering (Malvern ZetaSizer 3000HS). The loading efficiency of rhBMP-2 into PLGA particles were determined as reported previously (18). Briefly, the microspheres were dissolved in DCM, rhBMP-2 was extracted into PBS over a period of 36 h, and the concentration of rhBMP-2 was then measured by ELISA. The thermal transition of as-received PLGA and PLGA particles were measured using a Thermal Analysis Q2000 Differential Scanning Calorimeter (DSC). Two cycles of cooling and heating in the temperature range of -50 ºC and 150 ºC, at a speed of 10 ºC/min, were recorded for 5 mg samples.

Synthesis and characterization of polyurethane (PUR) scaffolds

Polyester triols (900 Da) were prepared from a glycerol starter and a backbone comprising [60wt% ε-caprolactone, 30wt% glycolide, and 10wt% D,L-lactide] or [70wt% ε-caprolactone, 20wt% glycolide, and 10wt% D,L-lactide] as published previously (10, 12). PUR scaffolds were synthesized by one-shot reactive liquid molding of hexamethylene diisocyanate trimer (HDIt; Desmodur N3300A) or Lysine triisocyanate (LTI) and a hardener comprising 900-Da polyol (or a 50/50 w/w mixture of polyester triol and PEG600), 1.5 parts per hundred parts polyol (pphp) water, 1.5~4.5 pphp TEGOAMIN33 tertiary amine catalyst, 1.5 pphp sulfated castor oil stabilizer, and 4.0 pphp calcium stearate pore opener. The isocyanate was added to the hardener, mixed for 30 s in a Hauschild SpeedMixer™ DAC

150 FVZ-K vortex mixer (FlackTek, Inc., Landrum, SC), and the resulting liquid mixture poured into a cylindrical mold where it cured as a free-rise foam after ~20 minutes (10, 12). The targeted index (the ratio of NCO to OH equivalents × 100) was 100 for PUR scaffolds incorporating small PLGA particles and 115 for all other scaffolds. In order to incorporate protein into PUR scaffold, lyophilized protein powder, PLGA-L-protein, or PLGA-S-protein was added to the hardener component before mixing with the isocyanate to prepare the scaffolds. Specific formulations evaluated are listed in Table III-1. For each delivery strategy, the concentration of rhBMP-2 was controlled at 2.5 μg per scaffold.

Table III-1 Summary of PUR compositions. The formulation of the proteins added to the hardener component is listed for each material.

PUR type	**Additives in the hardener**
PUR, HDIt or LTI	N/A
PUR/BMP-2, HDIt or LTI	BMP-2/heparin (1:20) powder, 2 wt% Glucose
PUR/PLGA-L-BMP-2, HDIt	PLGA-L-BMP-2, 14 wt%
PUR/PLGA-S-BMP-2, HDIt or LTI	PLGA-S-BMP-2, 9 wt%
PUR/BSA-FITC, HDIt	BSA-FITC powder, 2 wt% Glucose
PUR/PLGA-L-BSA-FITC, HDIt	PLGA-L-BSA-FITC, 14 wt%
PUR/PLGA-S-BSA-FITC, HDIt	PLGA-S-BSA-FITC, 9 wt%

Scanning electron microscopy (Hitachi S-4200 SEM, Finchampstead, UK) was utilized to measure the pore size and determine the internal pore morphology of the polyurethane scaffolds. The density and core porosity were calculated as reported previously (2, 10), with three replicates for each PUR type. The thermal transitions of scaffolds were measured

using a Thermal Analysis Q2000 Differential Scanning Calorimeter (DSC). Two cycles of cooling and heating in the temperature range of -50 ºC and 150 ºC, at a speed of 10 ºC/min, were recorded for 5 mg samples. The storage and loss moduli of the scaffolds was also evaluated by dynamic mechanical analysis (DMA) in compression mode with a temperature sweep of -80 ºC to 100 ºC, at a frequency of 1 Hz, 20-μm amplitude, 0.3-% strain, and 0.2-N static force (2, 13). Confocal microscopy was performed using a Zeiss LSM510 confocal microscope to the image distribution of BSA-FITC within the microspheres and scaffolds.

The temperature profiles during foaming of the polyurethane scaffolds were measured to determine the exotherm from the reaction. After the isocyanate and resin components (with or without microspheres) were combined, a thermocouple (Fluke 53II) was inserted into the center of the reactive liquid mixture for the duration of foaming. The temperature was recorded every 15 or 30 seconds.

In vitro release experiment

Three replicate scaffold samples (~50 mg) containing 2.5 μg rhBMP-2 were immersed in 1 ml release medium (α-MEM incorporating 1% BSA) contained in polypropylene vials sealed by O-rings. BSA were included to minimize adsorption of rhBMP-2 onto the scaffolds and vials (2). The medium of PUR samples was refreshed every 24 h to minimize degradation of the growth factor (2), and the medium of collagen samples was refreshed as indicated in the plot. The rhBMP-2 concentration of daily pools as indicated in the cumulative release plot was determined using a Human BMP-2 Quantikine ELISA kit (R&D systems, Minneapolis, MN). The daily release plot was generated from a logarithm curve fit from the raw data. The power law model (34, 35) was used to fit the accumulative release curves in order to elucidate the drug release mechanism.

In vitro alkaline phosphatase (ALP) activity assay

The releasates from the first 9 days from PUR/rhBMP-2 and PUR/PLGA-L-rhBMP-2 separately were combined and examined for ALP activity using MC3T3 osteoprogeniter cells. MC3T3 cells were plated on 48-well plates in α-MEM containing 10% FBS. When the cells reached confluence, the culture medium was changed to α-MEM containing 2.5% FBS with or without 100 ng/ml of rhBMP-2 releasate. Fresh rhBMP-2 was used as a positive control. The cell culture medium was changed every two days. At days 3 and 7, cells were washed with phosphate-buffered saline and lysed with 80 μl of 0.05% Triton X-100. The plates were then subjected to three freeze/thaw cycles. The lysates (20 μl) were added to 100 μl of substrate buffer (2 mg/ml disodium p-nitrophenylphosphate hexahydrate and 0.75M 2-amino-2-methyl-1-propanol). After incubation of the mixtures at 37°C for 30 min, absorbance at 405 nm was measured. ALP activity was determined from a standard curve generated by employing the reaction of a p-nitrophenyl solution. The ALP activity was normalized by the total protein content determined using the BCA assay (Pierce). One way ANOVA with bonferroni correction ($p<0.05$) was used for evaluation of statistical significance.

In vivo evaluation of rhBMP-2 implants in a rat femoral plug defect

All surgical procedures were reviewed and approved by the Institutional Animal Care and Use Committee. Male Sprague-Dawley rats (Harlan Labs) aged 8 weeks (200-250g) were used for this study. A monocortical plug bone defect (3 mm diameter x 5 mm deep) was created in the distal region of the femur diaphysis (36), and a cylindrical PUR scaffold (3×5 mm) was implanted into the defect. Treatment groups included PUR (without rhBMP-2 as a control), PUR/rhBMP-2, PUR/PLGA-L-rhBMP-2, and PUR/PLGA-S-rhBMP-2 (n=6). The dosage of rhBMP-2 within each experimental scaffold was 2 μg (60 μg rhBMP-2/ml

scaffold). After two and four weeks post-implantation, the rats were sacrificed and the femurs removed and fixed in 10% phosphate-buffered formalin.

Quantitative 3D analysis of bone ingrowth in the scaffolds was performed using a μCT40 (SCANCO Medical, Bassersdorf, Switzerland), at a voxel size of 24 mm (isotropic). The X-ray source settings were 55 kVp and 145 mA with an integration time of 300 ms. The region of interest (100 axial slices) was centered over the defect site in the distal femur. After reconstruction, the bone tissue was segmented from air or soft tissue using a threshold of 270 per thousand (or 438.7 mgHA/cm^3), a Gaussian noise filter of 0.8, and support of 2. This threshold was consistent through all specimens. Utilizing the Scanco evaluation software, we quantified the amount of bone ingrowth into the scaffold as the percentage of bone volume (BV) per total volume (TV), in which TV was generated by measuring the contour of the defect site. Because the μCT40 is calibrated to known densities of hydroxyapatite (phantom), the mineral density (mgHA/cm^3) of each voxel was automatically provided for segmented bone. We recorded the mean volumetric bone density of the mineralized tissue (mBMD) in the metaphysis.

Rat bones were then decalcified with 10% ethylenediaminetetraacetic acid (EDTA; Invitrogen), dehydrated, embedded in paraffin, and sectioned at 5 μm thickness. The coronal slice sections were stained with hematoxylin and eosin (H&E). Specimens were examined under light microscopy. The amount of bone ingrowth in the scaffolds was quantified at the center sections of the implants (37). The area of bone ingrowth in the scaffolds was highlighted using adobe photoshiop elements 7.0 and measured using image analysis software (Scion Image, Scion Corp., Frederick, MD), and the ratio of bone ingrowth area per whole implant area was evaluated. One way ANOVA with bonferroni correction

($p<0.05$) was used for evaluation of statistical significance for both μCT imaging and histomorphometry analysis.

In vivo test of rhBMP-2 implants in a critical size rat femoral segmental defect

A previously described rat femur critical sized defect model (38) was used to investigate the difference in bone regeneration between recombinant BMP-2 (rhBMP-2) delivered from a collagen sponge, PUR, and PUR/PLGA-S over a 4 or 8 week time period. The rats were divided into 5 groups with 2 time points (n=10): Collagen sponge and rhBMP-2 (Collagen +BMP), blank Fast Release PUR scaffolds (FR), blank Slow Release PUR/PLGA-S scaffolds (SR), Fast Release PUR scaffolds and rhBMP-2 (FR + BMP), or Slow Release PUR/PLGA-S scaffolds and rhBMP-2 (SR + BMP). The collagen sponge (MedChem Products, Inc., Woburn, MA) was cut down under sterile conditions into 6 x 3 mm implants, each loaded with 2 μg rhBMP-2 (R&D Systems®, Minneapolis, MN) in solution for 15 minutes prior to implantation (as per manufacturer's directive). The scaffolds were prepared as stated earlier. The polyurethane scaffolds were synthesized from lysine-triisocyanate (LTI) and polyester triol comprising 70wt% ε-caprolactone, 20wt% glycolide, and 10wt% D,L-lactide. All implants were 6x3 mm cylindrical pieces; there was a total of 2 μg rhBMP-2 per implant.

In conducting the research described in this report, the investigators adhered to the Guide for the Care and Use of Laboratory Animals by the Institute of Laboratory Animal Resources, National Research Council, in accordance with the stipulations mandated for an AAALAC accredited facility. The methods used for the critical size defect creation and fixation are described previously (39). Briefly, a 6 mm segmental defect was created and stabilized under aseptic conditions in the left femur of each of 100 Sprague-Dawley rats. Using aseptic technique, a longitudinal incision was made over the left anterolateral femur,

and the entire femoral shaft was exposed using blunt dissection. A polyacetyl plate (length 25 mm, width 4 mm and height 4 mm) was fixed to the surface of the femur using 6 K-wires. A 6 mm mid-diaphyseal full-thickness defect was created with a small reciprocating saw blade (MicroAire 1025, MicroAire, Charlottesville, VA) under continuous irrigation with sterile saline. The defects in all animals were implanted either collagen sponge implant or PUR scaffold. The wound was closed in a layered fashion. A high-resolution radiograph of each femur with the stabilized defect was obtained using a Faxitron X-ray system (Faxitron X-ray Corporation, Wheeling, Illinois (Model: MX-20) Image settings Time: 15 Sec KV: 35 Window Level: 3380/1250) at initial surgery to confirm correct placement of the implant. The animals were allowed full activity in their cages postoperatively, administered adequate analgesia (IM buprenorphine) and monitored daily for signs of pain and systemic infection. The animals were euthanized 4 or 8 weeks later with Fatal Plus. The femurs were harvested and immersed in formalin for 48 hours then 70% alcohol for further assessment of regenerated bone volume and histology.

MicroCT: The samples were scanned using micro computed tomography (CT) SkyScan 1076 (Skyscan, Aartselaar, Belgium) at 100 kV source voltage and 100 μA source current with no filter used and at a spatial resolution of 8.77 μm. The reconstructions were performed using NRecon software (Skyscan, Aartselaar, Belgium) and resulted in grayscale images spanning a density range from 1.35 to 5.34 gm/cm^3 corresponding to gray scale values 0 to 255. DataViewer (Skyscan, Aartselaar, Belgium) was used to reslice the CT images along coronal sections which were used to reorient the CT slices to be perpendicular to the axis of the femurs and CT thresholding was performed to include only ossified tissues. The thresholds were selected as the histogram minima between the peaks representing the formalin in which the sample was scanned and the bone volume of the sample. The geometric mean of the threshold for all 100 samples in the study was used to determine the

upper and lower threshold for binarization as 39 and 250, which corresponds to a density span of 1.97 to 5.27 gm/cm^3. The region of interest was chosen by creating a volume that spanned 6 mm from the proximal to the distal interface of the native bone to include the entire defect generated. The total volume of bone ingrowth in this 3D volume was computed using CTAn software (Skyscan, Aartselaar, Belgium). The average bone density of the regenerated bone was determined from the mean grayscale value of the pixels included in the binarized selection. The bone volume was multiplied by this average bone density to calculate regenerated bone mass, which thus effectively accounted for both bone quantity (volume) and quality (density).

Histology: Specimens were fixed in 10% Neutral Buffered Formalin, dehydrated, and embedded in methylmethacrylate. 5 μm thick central sections were cut in the longitudinal plain and stained with Goldner's trichrome to differentiate between bone/soft tissue and polymer: mineralized tissue stained dark green, osteoid and collagen bright orange/red, and soft tissue red or orange. In specimens containing polymer, the polymer appears as unstained white area within the defect. For quantitative analysis of the relative areas of bone, soft tissue, and polymer, high resolution digital images were acquired at 1.25x. The relative areas of bone, soft tissue, and polymer (when present) within the defect were quantified using Metamorph software. The area of interest comprising the bone defect area was defined by drawing a polygon using the ends of the 4 host cortices as points of reference.

Results

Characterization of PLGA microspheres

PLGA microspheres were fabricated using a double emulsion technique. Previous studies have shown that the activity of released rhBMP-2 is not adversely affected by the presence of the DCM solvent used in the double emulsion technique (40), and the NMR spectra indicated that no residual DCM solvent was present in the microspheres (data not shown). Images of PLGA-L (light microscopy) and PLGA-S (SEM) microspheres are shown in Figure III-1A and C. PLGA-L microspheres fit a normal distribution (Figure III-1B), with an average size of 114 ± 40 μm (Table III-2). Interestingly, the PLGA-S microspheres fit a log-normal distribution (Figure III-1D), with an average size of 1.30 ± 0.39 μm (Table III-2). While both formulations incorporated 10% PEG4600 prior to formation of the microspheres, the PLGA-S and PLGA-L microspheres contained varying amounts of PEG due to differences in PEG encapsulation efficiency. As measured by 1H-NMR, PLGA-L microspheres had higher PEG content (6.7 wt%) compared to the PLGA-S (0.11 wt%) (Table III-2).

Table III-2 Summary of properties of PLGA microspheres.

	Average size	Size standard deviation	PEG content (NMR)	Yield	Initial BMP-2 Loading	Encapsulation Efficiency	Tg (DSC)
PLGA-L	114 μm	40	6.7%	79.5%	1.79 ug/ml	78.3%	34.4 °C
PLGA-S	1.30 μm	0.39	0.11%	80.3%	2.77 ug/ml	65.2%	45.9 °C

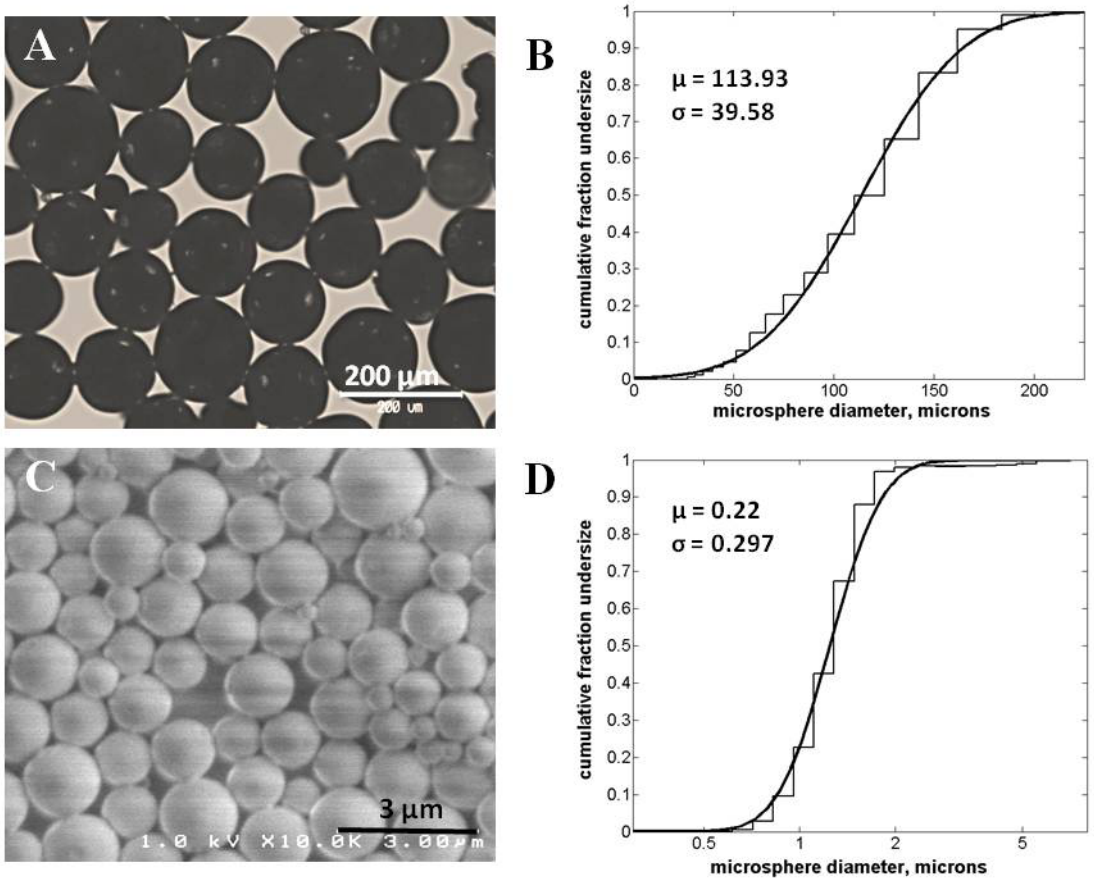

Figure III-1 PLGA particles characterization: imaging and size distribution. (A) imaging of PLGA-L by light microscope, (B) particle size distribution of PLGA-L (light microscopy), (C) imaging of PLGA-S by SEM, and (D) particle size distribution of PLGA-S (Malvern Zetasizer).

The DSC data (Figure III-2) show that the PLGA microspheres undergo a single glass transition temperature, suggesting that the microspheres are phase-mixed. This observation is consistent with a previous study showing that blends of PLGA and PEG (10,000 g/mol) are miscible when solvent-cast from a solution in chloroform (41). Due to the differences in PEG content, the PLGA-L microspheres had a lower Tg (34.4 ºC, Table III-2) compared to the PLGA-S microspheres (45.9 ºC). This observation is consistent with the well-known Fox equation, which predicts the glass transition temperature of polymer blends Tg,B as a function of the weight fraction wi of each component:

$$1/T_{g,B} = w_1/T_{g1} + w_2/T_{g2} \quad (1)$$

Considering that the Tg of the pure PLGA and the pure PEG components were 41.5ºC and -22ºC (42), respectively, the Fox equation predicts Tg values of 41.4 ºC and 34.0 ºC for the PLGA-S and PLGA-L microspheres. The value of Tg = 34.0ºC predicted from the Fox equation is in good agreement with the experimental value of 34.4ºC (Table III-2) for the PLGA-L microspheres. However, for the PLGA-S microspheres, the measured value of Tg (45.9 ºC) exceeds that of the pure PLGA used to fabricate the microspheres. It is conjectured that the increase in Tg of the PLGA-S microspheres results from the incorporation of poly(vinyl alchol) (PVA) stabilizer, which has Tg = 85 ºC (as indicated in the product specification). In order to prepare a stable suspension of ~1 μm microspheres, a higher concentration of PVA stabilizer in the aqueous phase was required for the PLGA-S microspheres. Although the concentration of PVA in the PLGA microspheres could not be determined from the NMR spectra due to overlapping peaks with PEG and PLGA, it is likely that the PVA content was higher in the PLGA-S microspheres due to the higher concentration of PVA in the aqueous phase and larger surface-to-volume ratio.

For both PLGA-L and PLGA-S formulations, the overall yield of microspheres was ~80% as shown in Table III-2. However, the rhBMP-2 encapsulation efficiency for PLGA-L microspheres was significantly higher than that measured for the PLGA-S microspheres (78.3 and 65.2%, respectively). Furthermore, when the concentration of PLGA-S microspheres in the PUR scaffolds exceeded 10 wt%, the materials became unstable, exhibiting large voids. Therefore, to maintain the targeted 2.5 μg rhBMP-2/ scaffold loading, the loading of rhBMP-2 in the PLGA-S microspheres was higher than that of PLGA-L microspheres (Table III-2).

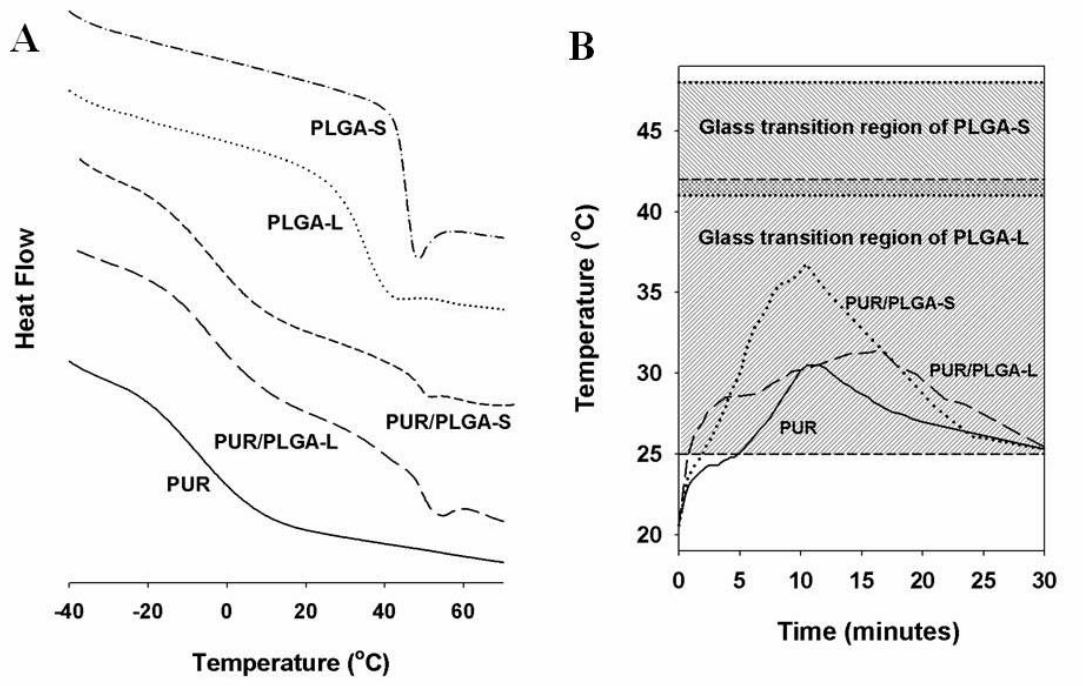

Figure III-2 (A) DSC profiles of PUR scaffolds and PLGA microspheres and (B) temperature profile during the polymerization reaction. The glass transition regions for PLGA-L and PLGA-S microspheres are indicated by the hatched lines on the plot.

Synthesis and characterization of PUR scaffolds

Two-component porous PUR(HDIt) scaffolds synthesized by reactive liquid molding exhibited interconnected pores as evidenced by SEM imaging (Figure III-3A). The pore size was in the range of 200 – 600 μm and the thickness of the pore walls and struts was less than ~100 μm thick. The incorporation of PLGA-S microspheres did not substantially change the pore morphology (Figure III-3, B and C), but the presence of PLGA-L microspheres in the scaffold resulted in more irregular pore shapes. The porosity of the blank PUR(HDIt) scaffolds was calculated from the density to be 92.9%, and although there was a significant reduction in porosity associated with the addition of PLGA microspheres, the decrease in porosity was small, ranging from 2.0 – 2.5% (Table III-3).

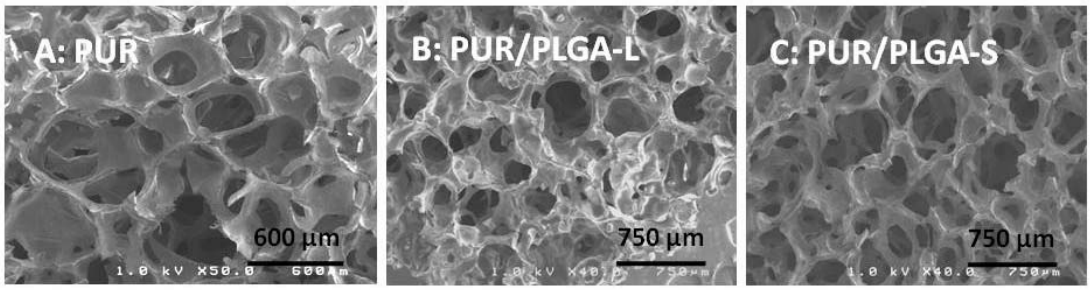

Figure III-3 SEM images of PUR scaffold incorporating FITC-BSA: (A) BSA-FITC added as a lyophilized powder, (B) BSA-FITC microencapsulated in PLGA-L microspheres, and (C) BSA-FITC microencapsulated in PLGA-S microspheres.

Table III-3 Physical and mechanical properties of PUR scaffolds. E' represents the storage modulus measured by DMA.

PUR type (n=3)	Density ($kg \cdot m^{-3}$)	Porosity (vol-%)	T_g (ºC) DSC 1st cycle	T_g (ºC) DSC 2nd cycle	E' at 37 ºC (MPa, DMA)
PUR	86.6±2.7	92.9±0.2	-8.6	-8.6	0.82±0.35
PUR/PLGA-L	116.7±2.7	90.4±0.2	-4.8, 39.5	1.9	2.31±0.28
PUR/PLGA-S	110.2±2.5	90.9±0.2	-5.2, 44.5	-4.8	0.54±0.13

DSC scans for PUR(HDIt), PLGA-S, PLGA-L, PUR(HDIt)/PLGA-S, and PUR(HDIt)/PLGA-L are shown in Figure III-2. The glass transition temperatures (calculated as the midpoint of the glass transition region from the DSC scan) are listed in Table III-3. PUR(HDIt) scaffolds without microspheres exhibited a single Tg of -8.6 ºC, which suggests phase mixing of the isocyanate and polyol components consistent with our previous studies (10, 13). As shown in Figure III-2 and Table III-3, the addition of PLGA microspheres resulted in a phase-separated polymer blend with two Tgs, one corresponding to the PUR component at about -5ºC and one corresponding to the PLGA component at 40 – 45 ºC. Interestingly, when the PUR(HDIt)/PLGA scaffolds were heated to 55 ºC (just above Tg), quenched to -50 ºC, and re-

heated to 55 ºC, the materials exhibited only one Tg that was intermediate between that of the PUR scaffold and PLGA microspheres (Table III-3). This observation suggests that the PLGA and PUR polymers are miscible, which is not surprising considering that the PUR(HDIt) contains a polyester soft segment. The reaction exotherm is plotted in Figure III-2B. When the reaction is initiated at ambient (e.g., 20 – 23 ºC) conditions, the maximum temperature attained for PUR(HDIt)/PLGA-L scaffolds is ~32 ºC and the material cools to ambient temperature after 30 min. Superimposed on the reaction exotherms are the glass transition regions measured for PLGA-S and PLGA-L microspheres. Interestingly, the glass transition region for the PLGA-L microspheres overlaps with the reaction exotherm, suggesting that the PLGA-L microspheres may soften during the reaction, thereby promoting inter-penetration of PUR(HDIt) and PLGA chains at the interface. The modest shift in Tg from -8.6 ºC for the blank PUR(HDIt) scaffold to -4.8 ºC for the PUR(HDIt)/PLGA-L scaffold further suggests that the reaction exotherm promoted softening and mixing near the surface of the PLGA-L microspheres.

DMA temperature sweeps were typical of rubbery elastomers as reported previously (2, 13), exhibiting a glassy region below Tg, a glass transition region, and a rubbery plateau at temperatures above Tg. The storage moduli at 37 ºC were measured to be 0.82 MPa, 2.31 MPa, and 0.54 MPa for PUR(HDIt), PUR(HDIt)/PLGA-L, and PUR(HDIt)/PLGA-S, respectively (Table III-3). The incorporation of PLGA-L microspheres increased the storage modulus significantly, while the presence of PLGA-S microspheres decreased the storage modulus. The effects of PLGA-S microspheres on mechanical properties are consistent with a previous study showing that the compressive modulus of poly(propylene fumarate) (PPF) scaffolds decreased when 35 – 45 μm microspheres were embedded in the scaffold (32).

Distribution of protein in microspheres and PUR scaffolds

Confocal microscopy (32) was used to image the distribution of the model BSA-FITC protein in the microspheres and scaffolds. For both PLGA-L-BSA-FITC and PLGA-S-BSA-FITC microspheres, the protein appeared to be more concentrated near the surface of the microspheres (Figure III-4, B and C). For PUR(HDIt)/BSA-FITC scaffolds, the BSA-FITC powder was distributed uniformly throughout the pore walls of the scaffold (compare Figure III-4D to the blank PUR(HDIt) scaffolds in Figure III-4A). However, the confocal images suggest that the particle size distribution was rather broad, which is conjectured to result from poor dispersion of the hydrophilic lyophilized rhBMP-2/glucose powder in the hydrophobic polymer.

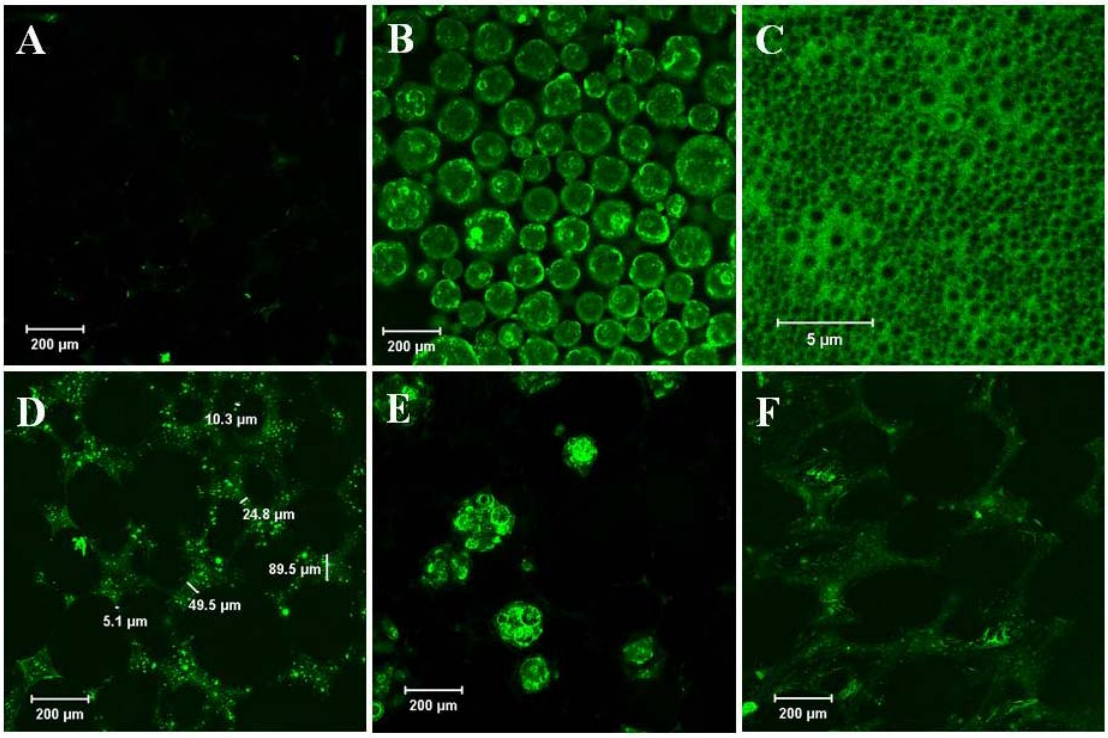

Figure III-4 Confocal microscopy images of PLGA microspheres and PUR scaffolds. (A) Blank PUR, (B) PLGA-L-BSA-FITC, (C) PLGA-S-BSA-FITC, (D) PUR/BSA-FITC, (E) PUR/PLGA-L-BSAFITC,and (F) PUR/PLGA-S-BSA-FITC.

For PUR(HDIt)/PLGA-L-BSA-FITC scaffolds (Figure III-4E), since the wall of the scaffold was in most cases less than ~100 μm thick (Figure III-4D), many of the particles were only partially embedded in the scaffold. In some cases the PLGA-L microspheres appeared to thicken the pore walls and struts, which are conjectured to reinforce the mechanical properties of the PUR(HDIt)/PLGA-L scaffolds. In contrast, due to their smaller size, PLGA-S-BSA-FITC particles were completely embedded and uniformly distributed throughout the pore walls of the scaffold (Figure III-4F). Furthermore, the small particles appeared to be well-dispersed and did not aggregate as extensively as the BSA-FITC powder. The confocal images suggest that PUR(HDIt)/PLGA-S scaffolds presented two barriers to diffusion, the PLGA microspheres and the PUR pore wall, which was anticipated to substantially reduce the burst release (32).

In vitro release profile of rhBMP-2 from PUR(HDIt) scaffolds

Release profiles for rhBMP-2 encapsulated in PUR(HDIt) scaffolds and PLGA microspheres are presented in Figure III-5A. When rhBMP-2 was added to the scaffolds as a lyophilized powder, a burst release of 36% was observed on day 1, followed by a period of sustained release until day 21. As anticipated, microencapsulation of rhBMP-2 in PLGA-L and PLGA-S microspheres substantially decreased the burst release to <15%. However, the burst release surprisingly increased from 8% for PLGA-L-rhBMP-2 microspheres to 25% for the PUR(HDIt)/PLGA-L-rhBMP-2 scaffold. We have observed similar effects for BSA-FITC and tobramycin (unpublished results). As discussed previously, it is conjectured that the reaction exotherm promotes interfacial mixing of PUR(HDIt) and PLGA chains and subsequent diffusion of rhBMP-2 into the PUR(HDIt) phase during cure. These effects may be exacerbated by the observation that the distribution of the hydrophilic drug is weighted toward the surface (33). In contrast to the PLGA-L-rhBMP-2 microspheres, encapsulation of PLGA-S-rhBMP-2 microspheres in PUR scaffolds was observed to reduce the burst release

from 13% to 3%, which supports the hypothesis that embedding of PLGA-S microspheres in the pore walls of the scaffold increases the resistance to mass transfer.

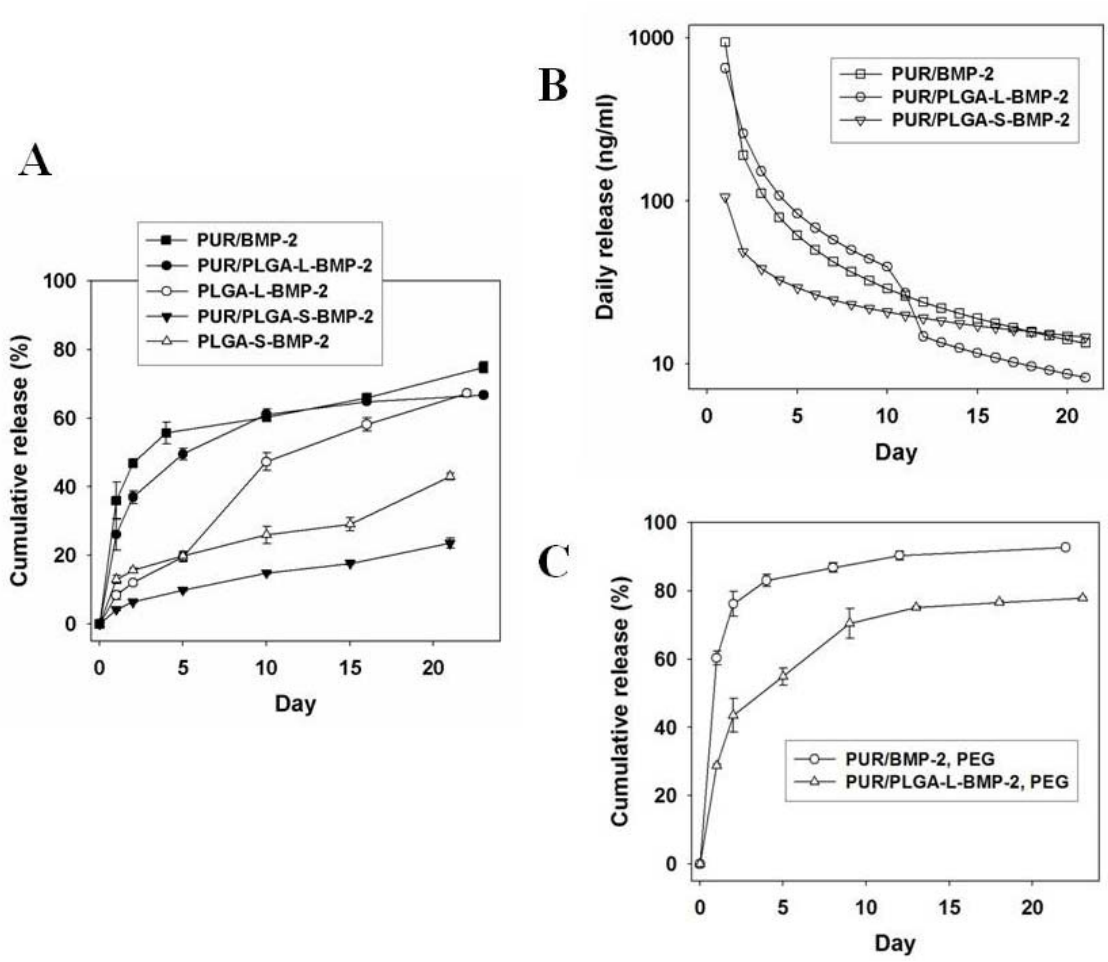

Figure III-5 *In vitro* release profile of BMP-2. (A) Cumulative release from PUR scaffolds and PLGA particles, (B) daily release from PUR scaffolds, and (C) cumulative release from scaffolds incorporating 50% PEG. Release kinetics were measured by ELISA.

The daily release profiles were calculated by fitting the cumulative release profile to a logarithm function as shown in Figure III-5B, where the differences in the amount of rhBMP-2 released in the first 12 days between the three delivery systems are clearly evident. The presence of 50% PEG in the polyester triol before reacting with isocyanate resulted in a higher burst and cumulative release (Figure III-5C), which is conjectured to

result from enhanced diffusivity and/or solubility of the protein within the scaffold due to the hydrophilic PEG component (43).

Cumulative release curves measured for non-PEG containing foams (Figure III-5A) were fit to a power law model (34, 35):

$$M_t/M_0 = A \cdot t^n \quad (2)$$

Fitting parameters are listed in Table III-4. In this model, M_t is the cumulative amount of rhBMP-2 released at time t, M_0 is the total amount of rhBMP-2 released (assumed to be the dose of rhBMP-2 added to the material), A is a constant, and n is the reaction order associated with the release.

Table III-4 Parameters obtained by fitting rhBMP-2 release data to the power law model. M_t/M_0, t, A, and R^2 represent cumulative percentage released (%), time (day), constant, and the coefficient of determination, respectively.

$M_t/M_0 = A \cdot t^n$	n value	A	R^2
PUR/BMP-2	0.21	38.60	0.952
PUR/PLGA-L-BMP-2	0.30	28.57	0.959
PLGA-L-BMP-2	0.72	7.65	0.977
PUR/PLGA-S-BMP-2	0.55	4.24	0.997
PLGA-S-BMP-2	0.33	12.17	0.942

Values of n lower than 0.5 have been reported for porous materials (34), and an n value near 0.5 indicates a Fickian diffusion mechanism (34, 35). For the data shown in Figure III-5, the values of n were determined to be 0.21, 0.72, 0.30, 0.33, and 0.55 for PUR/rhBMP-2, PLGA-L-rhBMP2, PUR/PLGA-L-rhBMP-2, PLGA-S-rhBMP-2 and PUR/PLGA-S-rhBMP-2

materials, respectively. Encapsulation of PLGA-L-rhBMP-2 microspheres in the PUR scaffolds decreased the value of n. However, encapsulation of PLGA-S microspheres in PUR scaffolds increased the value of n from 0.33 to approximately 0.5, suggesting a diffusion-controlled release mechanism. When n = 0.5, Eq (1) reduces to the Higuchi equation (44), where A is defined as follows:

$$A = [C_{sat}D(2C_{load} - C_{sat})]^{1/2} \quad (3)$$

In Eq (3), C_{sat} = saturation concentration of the drug, C_{load} = loading concentration of the drug (e.g., the dose of rhBMP-2 added to the material), and D = the diffusivity of the drug in the polymer. When the PLGA-S-rhBMP-2 microspheres were embedded in the PUR scaffold, the value of A decreased from 12.2 to 4.2, which is consistent with the notion that the diffusivity of rhBMP-2 is lowest in these materials due to the two polymeric barriers (e.g., PLGA and PUR) to mass transfer.

In vitro bioactivity of released rhBMP-2

To verify the bioactivity of released rhBMP-2 from PUR scaffolds, the releasates were tested for ALP activity using MC3T3 cells. Both rhBMP-2 releasates from PUR/rhBMP-2 and PUR/PLGA-L-rhBMP-2 scaffolds significantly enhanced ALP activity at day 3 and day 7, when compared to the negative control (Figure III-6). There is no significant difference between the releasates and the fresh rhBMP-2 in terms of ALP activity. These results suggest that the osteoinductive potential of the rhBMP-2 was preserved during the chemical reaction associated with the foaming process.

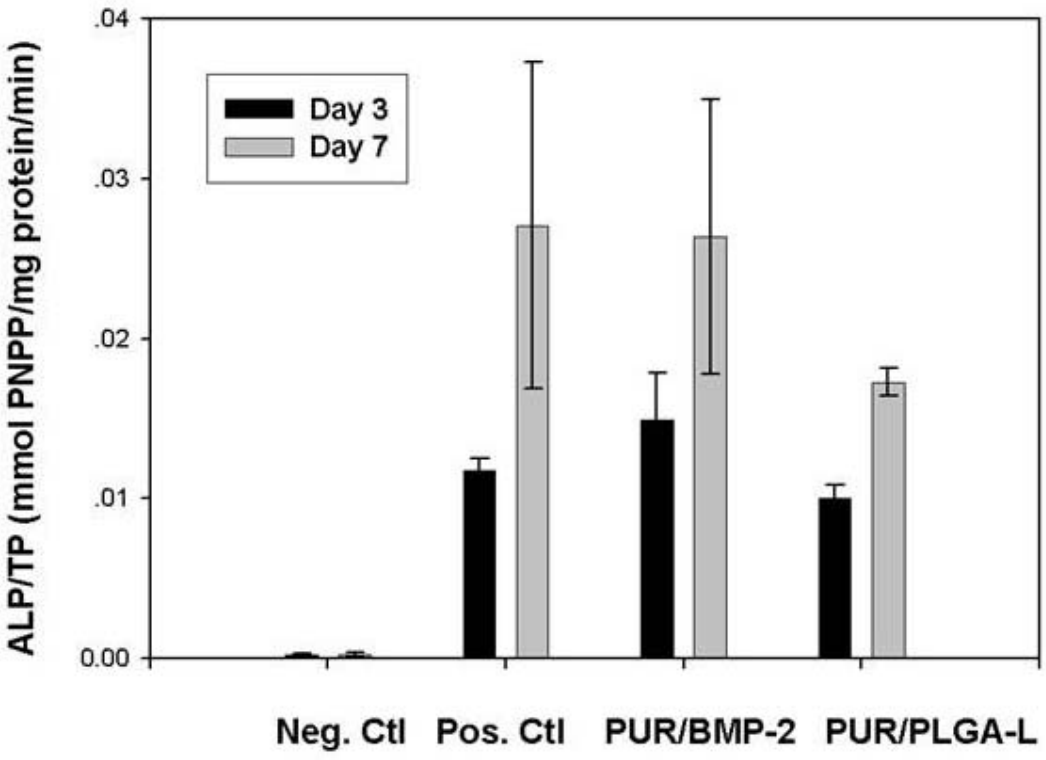

Figure III-6 *In vitro* alkaline phosphatase activity assay of rhBMP-2 releasates from PUR scaffolds. MC3T3 cells were treated with or without 100 ng/ml rhBMP-2 released from PUR scaffolds and ALP activity was measured at days 3 and 7. Fresh rhBMP-2 solution (100 ng/ml) was used as a positive control, and serum media containing no rhBMP-2 was used as the negative control.

In vivo study of rhBMP-2 scaffolds in rat femoral plug defects

To evaluate the *in vivo* osteoinductivity of PUR(HDIt) scaffolds incorporating rhBMP-2, cylindrical PUR scaffolds were implanted into rat femoral plug defects (Figure III-7A). At week 2, μCT analysis showed that both PUR(HDIt)/rhBMP-2 and PUR(HDIt)/PLGA-L-rhBMP-2 materials enhanced bone ingrowth near the bottom surface of the implant compared to the control with no rhBMP-2 (Figure III-7B). Conversely, there was no significant increase in new bone formation in PUR(HDIt)/PLGA-S-rhBMP-2 implants, presumably due to the relatively low cumulative amount of rhBMP-2 released at 2 weeks. At

week 4, substantial new bone formation was visible throughout the entire volume of the implants in all treatment groups (Figure III-7C). The most extensive bone ingrowth was observed in PUR(HDIt)/rhBMP-2 samples, which exhibited formation of new cortex. Although the amount of bone ingrowth in PUR(HDIt)/PLGA-S-rhBMP-2 scaffolds at week 2 was relatively small, there was significantly more new bone formation in these scaffolds relative to the control at week 4, which is conjectured to result from sustained release of rhBMP-2.

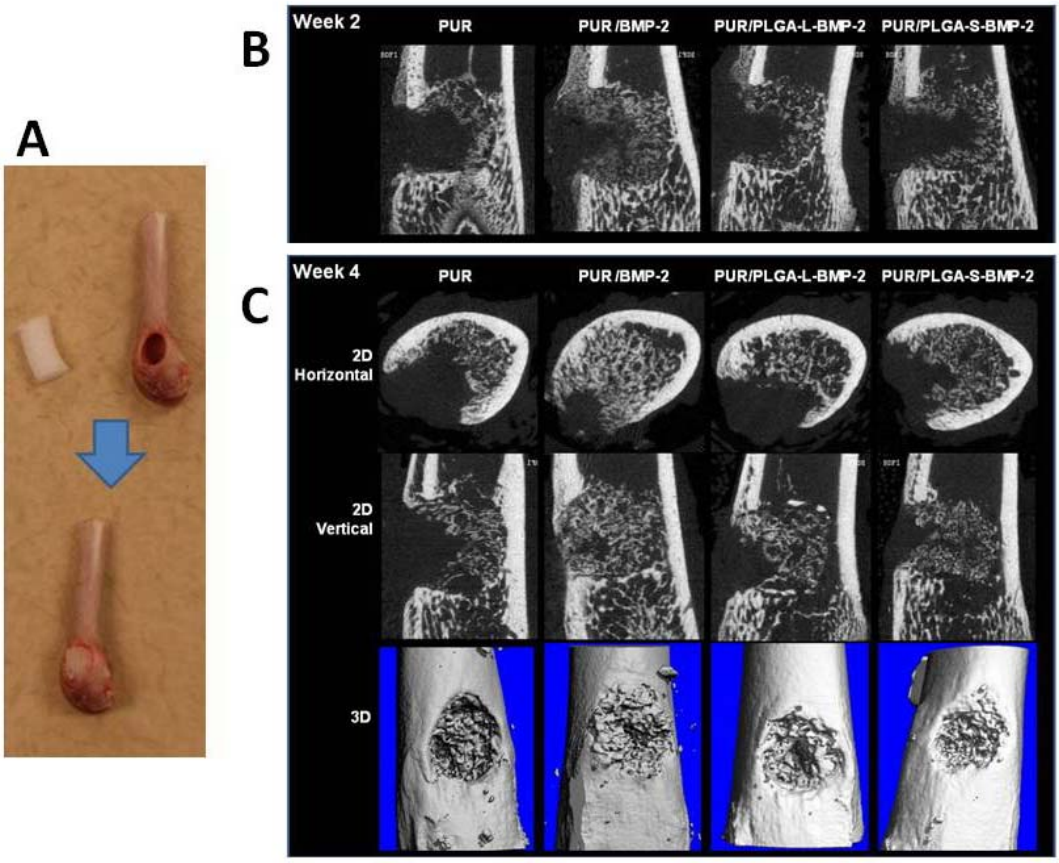

Figure III-7 *In vivo* evaluation of the effects of PUR/rhBMP-2 scaffolds on new bone formation in a rat femoral plug model. Treatment groups included: PUR control (no rhBMP-2), PUR/rhBMP-2, PUR/PLGA-L-rhBMP-2, and PUR/PLGA-S-rhBMP-2. The PUR cylinders (5 mm × 3 mm) were implanted into rat femoral plug defects (A), and harvested for μCT imaging at weeks 2 (B) and 4 (C) respectively.

In the quantitative μCT analysis at week 4 (Figure III-8), the volume of new bone formation per total scaffold volume (BV/TV, %) was significantly higher for all the rhBMP-2 treatment groups than the control ($p<0.05$). Furthermore, new bone formation in the PUR(HDIt)/rhBMP-2 materials was significantly higher than that observed for the PUR(HDIt)/PLGA-rhBMP-2 treatment groups.

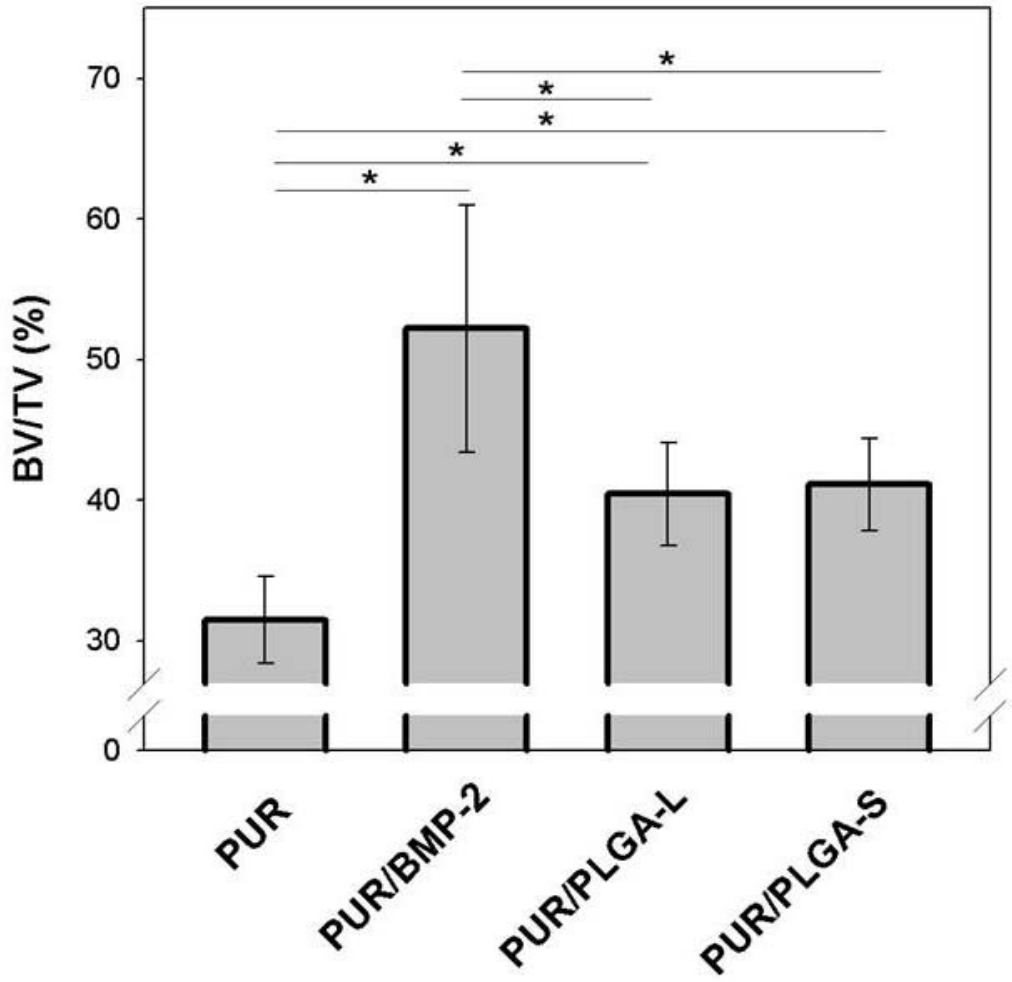

Figure III-8 Quantitative analysis of mineralized new bone formation from μCT images promoted by PUR/rhBMP-2, PUR/PLGA-L-rhBMP-2, and PUR/PLGA-S-rhBMP-2 scaffolds. The percentage of bone volume (BV) relative to total volume (TV) of each implant was assessed from μCT imaging. Stars and lines indicate significance differences between groups ($p<0.05$).

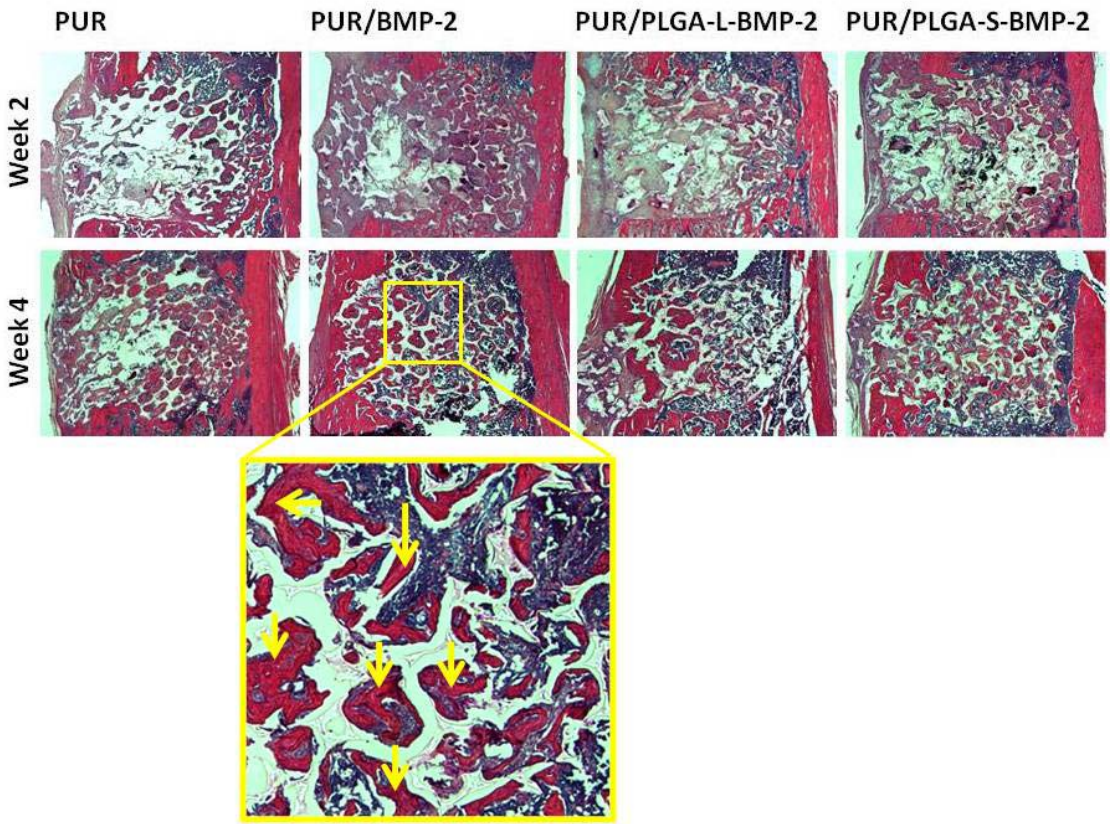

Figure III-9 Histological evaluation of new bone formation promoted by PUR/rhBMP-2, PUR/PLGA-L-rhBMP-2, and PUR/PLGA-S-rhBMP-2 scaffolds. Explanted bones were fixed in formalin, decalcified in EDTA, embedded in paraffin, and processed for H&E staining. The yellow arrows point to areas in the high magnitude images representing new bone formation.

Since μCT images only reveal the presence of mineralized bone (45), histological analysis was performed to give a more detailed analysis on the new bone tissue formation promoted by rhBMP-2 at early stage when the bone cells are not yet mineralized. In the histological analysis at week 2, bone ingrowth (the red areas within implants, highlighted in the high magnitude image with yellow arrows) from the surrounding tissue was enhanced in the rhBMP-2 treatment groups compared to the control (Figure III-9). At week 4, a substantial amount of mature bone formation was observed throughout the entire area of the rhBMP-2 implants, whereas new bone formation was observed only at the peripheral

area in the control group (Figure III-9). New bone formation in the scaffold was most extensive in the PUR(HDIt)/rhBMP-2 materials, which is consistent with the μCT analysis. Histomorphometry data show that the rhBMP-2 treatment groups promoted new bone tissue formation significantly both at week 2 and week 4 (Figure III-10). PUR(HDIt)/rhBMP-2 seems to perform slightly better than the other two treatment groups although no statistically significant differences were observed.

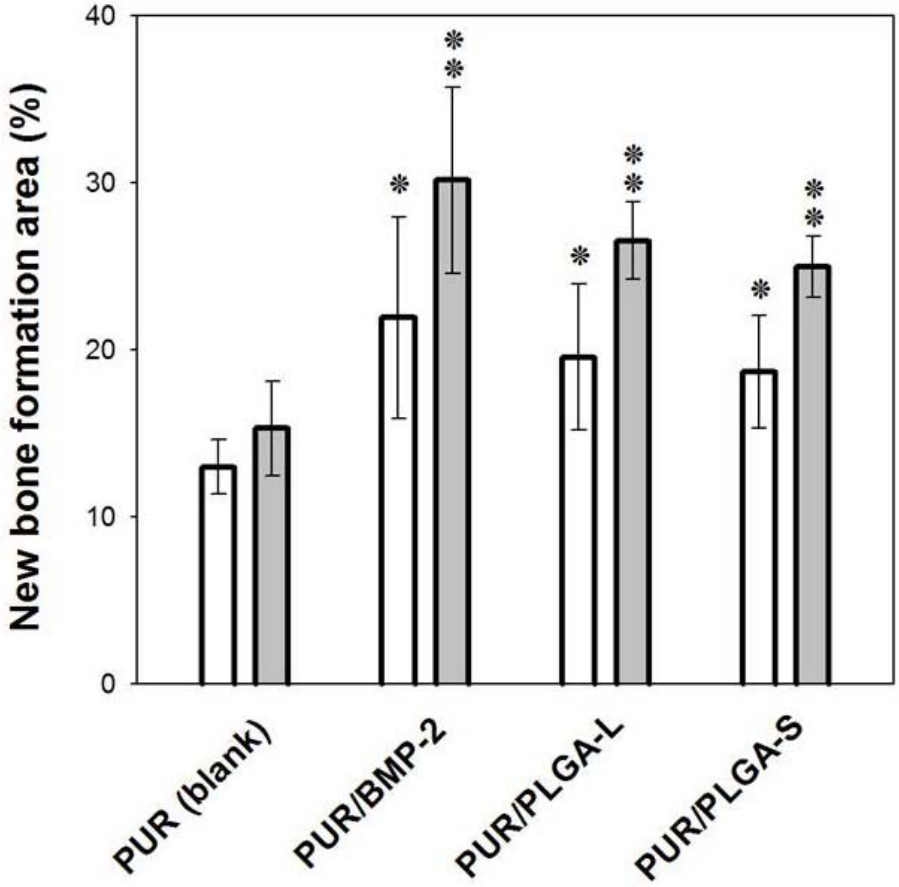

Figure III-10 Histomorphometric analysis of new bone formation promoted by PUR/rhBMP-2, PUR/PLGA-LrhBMP-2, and PUR/PLGA-S-rhBMP-2 scaffolds at weeks 2 (hollow bars) and 4 (filled bars). Areas of new bone formation were highlighted using Photoshop elements 7.0 and then measured using Scion imaging software. Single stars indicate significance differences between treatment groups and the negative control (no rhBMP-2) at week 2, and double stars indicate significance differences between treatment groups and the negative control at week 4 ($p<0.05$).

In vitro release of rhBMP-2 from collagen and PUR(LTI) scaffolds

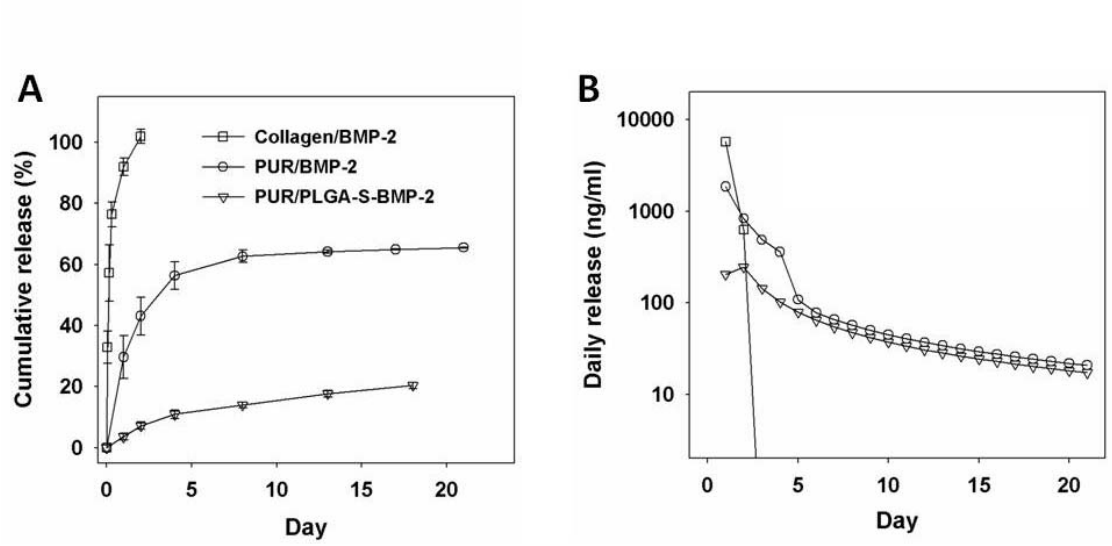

Figure III-11 *In vitro* release profile of BMP-2 from PUR(LTI) and collagen sponge: (A) Cumulative release, and (B) daily release.

Release profiles for rhBMP-2 from the collagen carrier and the PUR scaffolds are presented in Figure III-11A when rhBMP-2 was embedded into the scaffolds as lyophilized powder, a burst release of 36% was observed on day 1, followed by a period of sustained release until day 21. In contrast, the cumulative release of rhBMP-2 from the collagen carrier was 92% on day 1 and reached 100% on day 2. When BMP-2 were encapsulated in PLGA microspheres (1.3 micron) before incorporated in PUR, the burst release was nearly gone, but the sustainable release period is similar to that of the powder approach. The daily release profiles were calculated by fitting the cumulative release profile to a logarithm function as shown in Figure III-11B, where the differences in the amount of rhBMP-2 released in the first 20 days between the three delivery systems are clearly evident. This suggests that PUR FR is a more sustainable release system than collagen sponge, which could potentially enhance the *in vivo* function of BMP-2. The microsphere approach resulted in suppressed daily release for the first few days, followed by comparable daily

concentration release to the powder approach thereafter. Hence, when tested *in vivo*, we would be able to examine the differences in promoting new bone formation as a result of different release profiles, therefore elucidating the roles of bolus release, burst release, and sustained release respectively.

In vivo study of PUR(LTI) and collagen scaffolds with rhBMP-2 in rat critical size femoral segmental defects

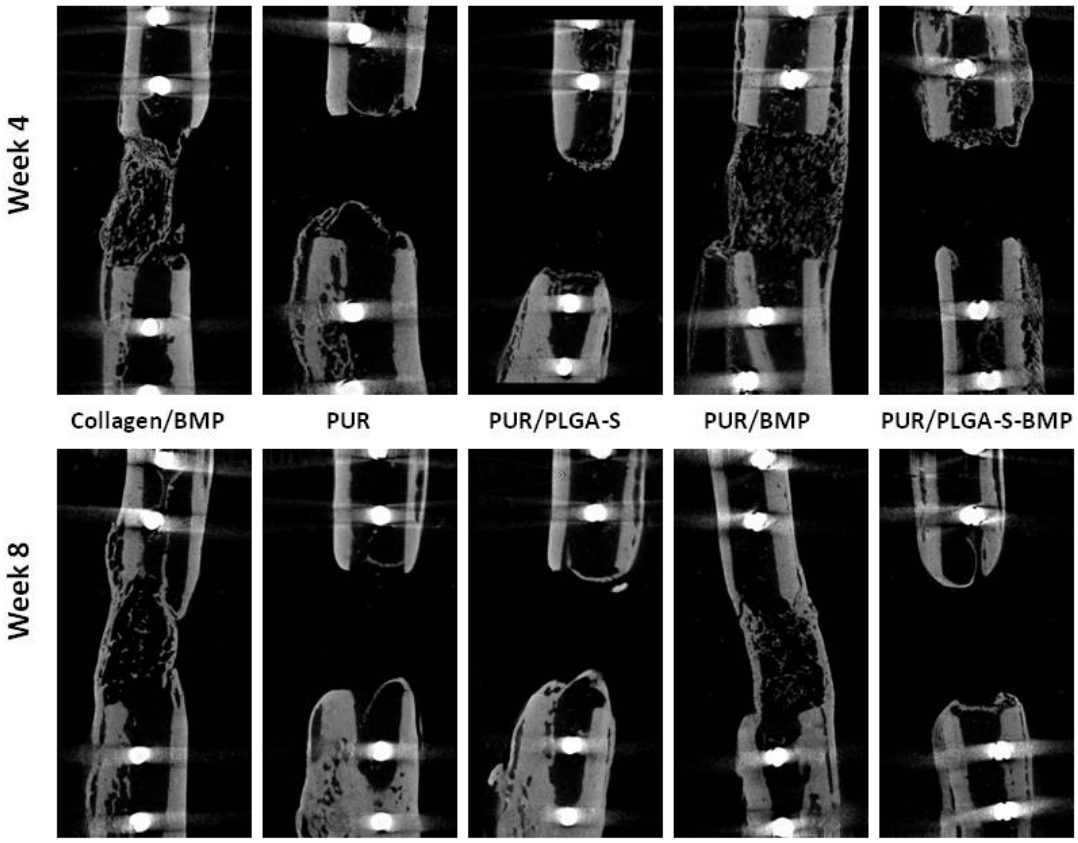

Figure III-12 *In vivo* evaluation of new bone formation by μCT in a rat critical size segmental defect (6 mm), treated with collagen/rhBMP-2, PUR/rhBMP-2, and PUR/PLGA-S-rhBMP-2 respectively.

The PUR (with or without BMP-2, delivered by powder approach or small microspheres encapsulation approach) or collagen scaffolds were implanted in the critical size rat femoral

segmental defect for 4 or 8 weeks, before harvested for new bone examination by both microCT and histomorphometry. μCT scanning images (Figure III-12) showed that more total bone volume in the PUR(LTI)/rhBMP-2 group was regenerated compared to all of the other groups at both weeks 4 and 8. Compared to the blank PURs and the PUR(LTI)/PLGA-S-rhBMP-2 group, more total bone volume was regenerated in the group treated with collagen/rhBMP-2 at both time points. Little bone was generated in the PUR(LTI)/PLGA-S-rhBMP-2 treatment group compared with blank scaffolds.

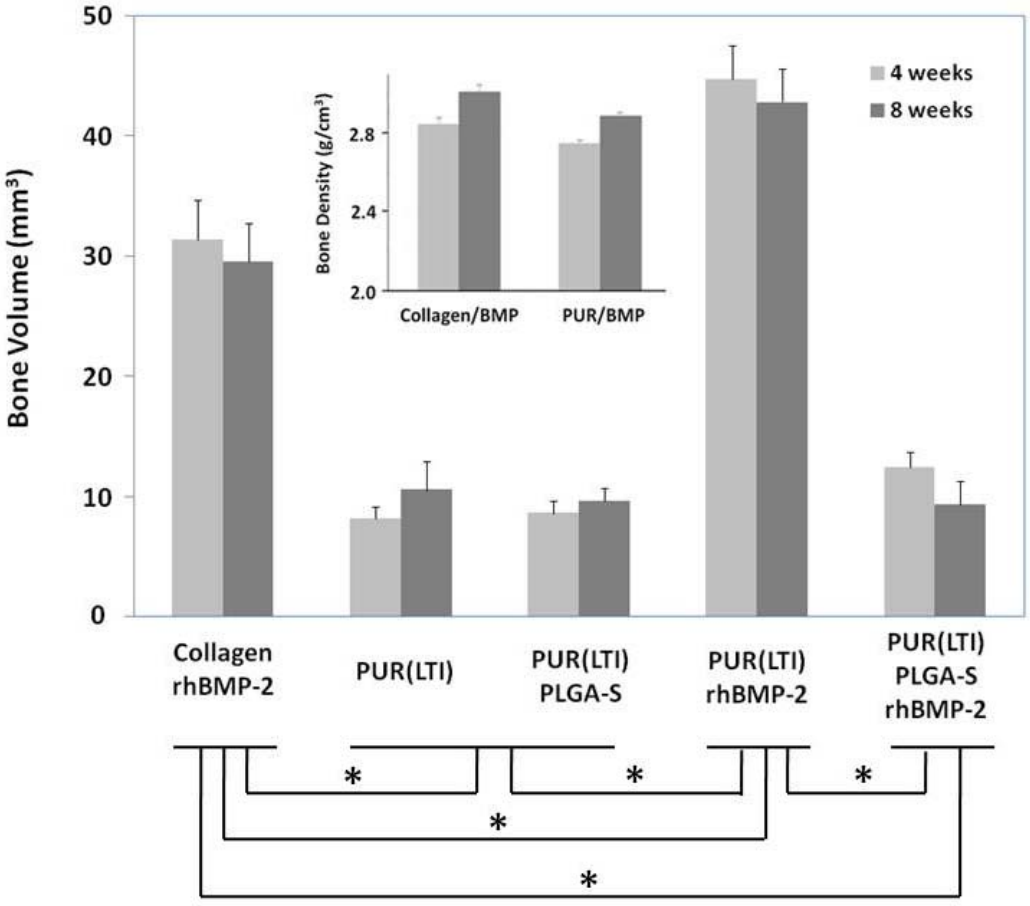

Figure III-13 New bone quantification in the segmental defects based on μCT images, with inlet showing the density of new formed bone in collagen/rhBMP-2 and PUR(LTI)/rhBMP-2 groups at both time points. One way ANOVA with bonferroni correction ($p<0.05$) was used for evaluation of statistical significance, and the significance between groups was depicted as * where existed.

Quantitative μCT analysis (Figure III-13) showed that there were significant differences in terms of amount of new bone formation between PUR(LTI)/rhBMP-2 group and all other treatment groups, and between collagen/rhBMP-2 group and PUR(LTI)/PLGA-S-rhBMP-2 group. There was no significance between blank PURs and PUR(LTI)/PLGA-S-rhBMP-2 group. There were no significant differences in the amount of total bone regenerated at week 4 compared to at week 8 in any treatment group, but if looked at the density of bone regenerated (Figure III-13 inlet), there was a significant increase between weeks 4 and 8 in both the PUR(LTI)/rhBMP-2 group and the collagen/rhBMP-2 group.

Again, histological analysis was performed to give a more detailed analysis on the new bone formation process (Figure III-14). There was osteoid formation in the collagen/rhBMP-2 group within the callus in continuity with the host cortex as well as some marrow infiltration and scattered blood vessels at week 4. The PUR(LTI)/rhBMP-2 group showed osteoid formation within the callus along the longitudinal axis in line with host cortex at week 4, and at higher magnification (Figure III-15), there is a remarkably consistent pore tissue response pattern within the scaffold architecture whereby they are filled with myeloprogenitor cells with a surrounding ring of osteoid and large blood vessels both within and around the perimeter of the pore. At weeks 8, for both collagen/rhBMP-2 and PUR(LTI)/rhBMP-2 treatment groups, the new bone tend to distribute toward the cortex area, indication reorganization occurs between weeks 4 and 8. At both time points, the PUR scaffolds are still visible but the collagen carrier has been resorbed or degraded. The blank PURs and PUR(LTI)/PLGA-S-rhBMP-2 group showed some marrow and soft tissue infiltration into the pores but blunted callus formation at both ends of the defect at both time points.

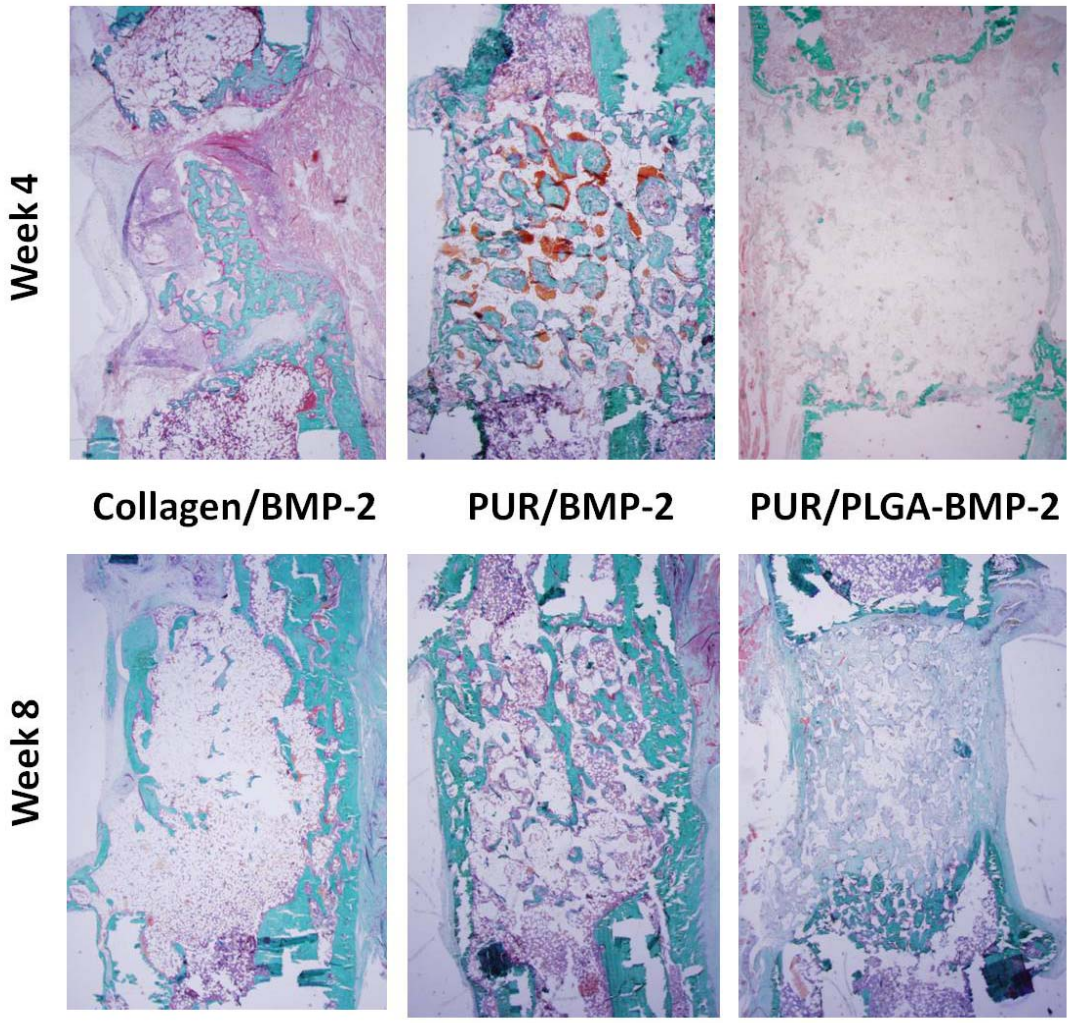

Figure III-14 New bone examination by histological staining in the segmental defects. The green, pink, and red represent bone tissue, soft tissue, and osteoids respectively. The white represents polymer in the PUR groups or soft tissue in the collagen group.

When the amount of new bone formation were quantified by histomorphometry (Figure III-16), PUR(LTI)/rhBMP-2 treatment group has slightly more new bone formation than collagen/rhBMP-2 treatment group at weeks 4, but the amounts of new bone at weeks 8 were comparable for both groups. There was no significant change of bone regeneration between week 4 and 8 for the PUR(LTI)/rhBMP-2 treatment group, but there is a slight increase of new bone for the collagen/rhBMP-2 treatment group.

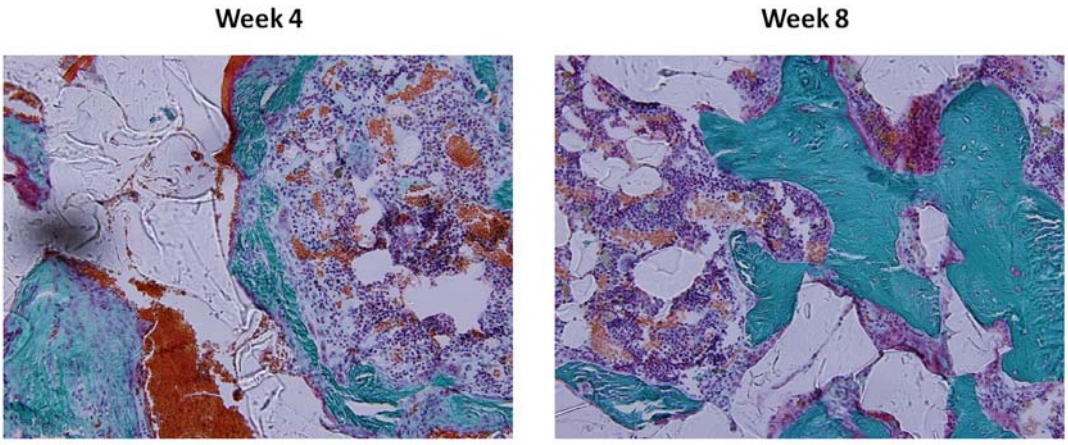

Figure III-15 Histological images of PUR/rhBMP-2 treatment at weeks 4 and 8 showing the presence of different cell types.

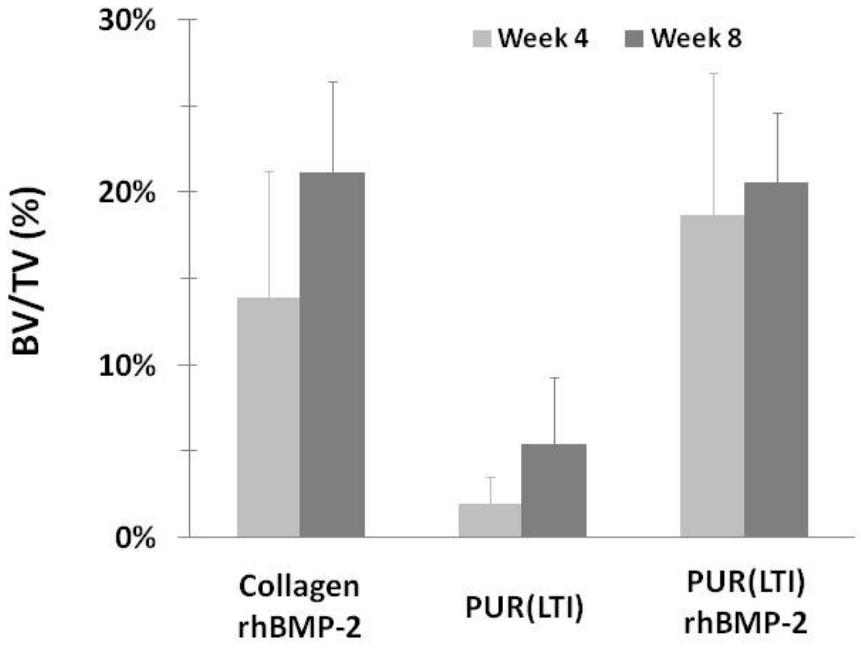

Figure III-16 Histomorphometry analysis of new bone in the segmental defects.

Discussion

Biodegradable polyurethanes have been investigated extensively in tissue engineering as supportive scaffolds for cell attachment, growth, and differentiation. In recent studies, scaffolds fabricated from segmented PUR elastomers comprising hexamethylene diisocyanate (HDI) have been reported to support bone healing in iliac crest defects in sheep at six months (8, 24). In another study, two-component lysine-diisocyanate (LDI)-based biomaterials incorporating 10 wt% β-TCP (5 μm) were implanted and injected into femoral cortical defects in sheep (9). Direct apposition of the biomaterial and bone was observed, as well as ingrowth of new bone into adjacent pores. Similarly, the materials investigated in the present study supported ingrowth of new bone into femoral defects as early as 2 weeks with increased new bone formation at later time points. These results suggest that the two-component PUR scaffolds support bone ingrowth, which is in agreement with previous studies.

Considering the moderate osteoconductivity of PUR scaffolds, as well as their demonstrated ability to delivery biologically active molecules, we reasoned that release of rhBMP-2 would increase new bone formation and accelerate healing *in vivo*. In the present study, we report that the release of rhBMP-2 from PUR scaffolds is tunable by adopting different delivery strategies, and that the release profile affects the extent of cellular infiltration and new bone formation in a rat femoral plug model. In the simplest approach, rhBMP-2 powder was encapsulated in a two-component reactive PUR scaffold to investigate the effects of the chemical reaction on the bioactivity of rhBMP-2. PUR/rhBMP-2 scaffolds exhibited a burst release for the first few days followed by sustained release for approximately 15 days. Addition of PEG600 diol to the polyol component had a significant effect on the burst release. In the absence of PEG, the burst release for rhBMP-2 was only

36% compared to 60% for scaffolds incorporating 50wt% PEG in the polyol component. Covalently bound PEG in the polymer network renders it more hydrophilic, which increases the swelling of the polymer and thus accelerates the release rate (43). Furthermore, the cumulative release of rhBMP-2 from the 50% PEG scaffolds increased from 75% (no PEG) to 95%. In contrast, although the burst release of rhPDGF from PUR scaffolds incorporating PEG was also 60%, the cumulative release at day 21 was only 70% (2). It has been suggested that the unfavorable conditions of the polymerization reaction may adversely affect the bioactivity of unprotected growth factors (e.g., by microencapsulation) (32). However, the bioactivity of the rhBMP-2 powder was preserved, as evidenced by the *in vitro* data (Figure III-6) and the observation that PUR/rhBMP-2 scaffolds promoted a large amount of new bone formation relative to the negative control as early as 2 weeks.

A number of recent studies have shown that sustained release of rhBMP-2 enhances healing relative to a bolus release. Therefore, we sought to reduce the burst release observed for PUR/rhBMP-2 scaffolds by investigating the effects of PLGA microsphere size on rhBMP-2 release kinetics and new bone formation in the rat femoral defects. We reasoned that encapsulation of rhBMP-2 in microspheres would reduce the burst release due to the increased resistance to mass transfer (32), but anticipated that this effect would diminish with increasing size. Our results show that microsphere size significantly affected the *in vitro* release kinetics. The PLGA-S microspheres were completely embedded in the scaffold, and the release of rhBMP-2 was observed to follow diffusion-controlled Fickian mass-transfer kinetics with essentially no burst (34, 35). Furthermore, embedding the PLGA-S microspheres in the PUR scaffolds decreased the release kinetics compared to that from the microspheres alone. These observations are in agreement with previous studies reporting that rhBMP-2 loaded PLGA/Hap particles (19) and PLGA nanospheres embedded in fibrin gels exhibited slower release compared to directly embedding the protein in the

fibrin gel (46). In other studies, incorporation of rhBMP-2-loaded PLGA and poly(propylene fumarate) (PPF) microspheres in reactive PPF scaffolds resulted in a more sustained release with a lower burst phase compared to rhBMP-2 impregnated scaffolds (18, 47). Additionally, Texas red dextran (TRD) encapsulated in PLGA (33 μm) and PPF (43 μm) microspheres that were subsequently encapsulated in PPF scaffolds exhibited a lower burst release relative to that from the microspheres themselves (32).

In contrast, the PLGA-L microspheres were only partially embedded in the scaffolds due to the fact that their size was comparable to the thickness of the pore walls. Furthermore, the Tg data suggest that the reaction exotherm promoted interfacial mixing, so that the burst release of protein actually increased when the PLGA-L microspheres were embedded in the scaffolds. A previous study has shown that the release of TRD from PPF microspheres embedded in PPF scaffolds was significantly slower that that from embedded PLGA microspheres due to crosslinking at the PPF microsphere/PPF scaffold interface (32). These studies suggest that the composition of the interface affects the release kinetics – while interfacial crosslinking presents an additional barrier to mass transfer, interfacial mixing reduces the resistance to mass transfer. Taken together, these observations suggest that the release of rhBMP-2 from microsphere composite scaffolds depends on both the size of the microspheres as well as the compositions of the microspheres and scaffold.

The *in vitro* drug release profile has also been shown to relate to new bone formation *in vivo* (19, 46). In the present study, the release of rhBMP-2 was measured *in vitro* using a perfect sink model (e.g., all the release medium was removed daily) (48) due to the concern that released rhBMP-2 could degrade over time. It has been shown that although the release of rhBMP-2 was accelerated *in vivo* relative to *in vitro* conditions, the differences between treatment groups were similar (18, 47). In the rat femoral plug defect model with the

selected dosage of 2.5 μg rhBMP-2 per implant, the burst release from PUR(HDIt)/rhBMP-2 promoted new mineralized bone formation as early as week 2. The PUR(HDIt)/PLGA-L-rhBMP-2 scaffolds, which exhibited a burst release of 25% (compared to 35% for the PUR(HDIt)/rhBMP-2 formulation), also promoted more new bone formation relative to the control, but the amount of new bone was less than the PUR(HDIt)/rhBMP-2 formulation. The cumulative release from the PUR(HDIt)/rhBMP-2 scaffolds exceeded that from the PUR(HDIt)/PLGA-L-rhBMP-2 scaffolds until day 10, and at day 21 the cumulative release was comparable. This suggests that early release of rhBMP-2 is important for promoting new bone formation, which is in agreement with previous studies. BMP-2 has been reported to recruit human mesenchymal progenitor cells (MPCs) that are essential for bone development, remodeling, and repair (22). In a recent study, rhBMP-2 delivered from Matrigel plugs has been reported to promote angiogenesis in severe combined immunodeficient (SCID) mice via both canonical and noncanonical Wnt pathways (21). The role of BMP-2 in fracture healing has also been investigated. Over a 28-day period of fracture healing in mouse tibias, mRNA expr ession of BMP-2 was highest on day 1 post-fracture, which suggests that BMP-2 may function as the trigger in the fracture healing cascade that regulates the expression of other BMPs (23).

The PUR(HDIt)/PLGA-S-rhBMP-2 treatment group, which yielded no burst release, promoted the least amount of new bone formation compared to the other two rhBMP-2 treatment groups in the plug defect model. However, a significant amount of new bone formation in PUR(HDIt)/PLGA-S-rhBMP-2 scaffolds between weeks 2 and 4 suggests that sustained release is also important to promote new bone formation. This observation is in agreement with a fracture healing study reporting that injection of rhBMP-2 in a calcium phosphate carrier at one week after surgery enhanced healing in a primate osteotomy model relative to percutaneous injection within one day (20). The improvement in healing

observed for the delayed injection treatment group has been attributed to an increased number of cells that respond to the released rhBMP-2. The importance of a sustained release of rhBMP-2 is also underscored by previous studies showing that sustained release of rhBMP-2 protein from polymer scaffolds promoted more bone formation in both orthotopic (19) and ectopic (18, 46) models relative to a bolus release.

The bolus release of rhBMP-2 in the first several hours may contribute to the requirement of high rhBMP-2 dosage in clinical studies when delivered by a collagen sponge (INFUSE® Bone Graft) (49, 50). Due to the fact that BMP-2 is a potent morphogen, there are safety issues associated with administering high levels of the drug (51, 52). Therefore, to mitigate the risk associated with high dosages and reduce the amount of the expensive growth factor that must be delivered to achieve a therapeutic effect, it is desirable to control the release of rhBMP-2 in order to optimize new bone formation. Our findings suggest that both early and sustained release of rhBMP-2 are critical in order to promote optimal bone wound healing, which is consistent with the multiple roles of this growth factor in bone formation. In an alternative approach, dual delivery of rhVEGF and rhBMP-2 synergistically enhanced bone regeneration relative to either factor alone (53, 54), presumably due to enhanced angiogenesis and recruitment of cells to the wound site. It is interesting to note that there was a significant burst release of rhVEGF and minimal burst release of rhBMP-2 in at least one of these studies (53); thus it is likely that the effects of rhBMP-2 on cell recruitment and angiogenesis at the early time points were minimal compared to rhVEGF. Considering the multiple roles of rhBMP-2 in bone healing at both early and late time points, optimizing its release may present compelling opportunities to maximize bone formation with just one growth factor, which is simpler from a regulatory perspective than the dual growth factor approach. Since the femoral plug defect heals

spontaneously within 8 weeks (55), the optimal rhBMP-2 release strategy for healing more challenging defects cannot be identified from the simple model.

Therefore, we investigated the effects of the rhBMP-2 delivery strategy on bone healing in critical-size femoral segmental defects in rats. At the same rhBMP-2 dosage, PUR(LTI)/rhBMP-2 performs better than collagen/rhBMP-2 in promoting angiogenesis and new bone formation due to more sustained release form PUR encapsulation system compared with the bolus release property of collagen adsorption system. PUR(LTI)/PLGA-S-rhBMP-2 yielded little new bone formation due to several reasons. Firstly, this is a critical size model which is more stringent for bone wound to heal. Secondly, the absence of a burst release of rhBMP-2 resulted in limited amount of cells recruitment and angiogenesis which are essential elements for new bone formation, and this further proves the role of rhBMP-2 burst release in triggering bone wound healing process. Overall, the segmental defect study not only revealed the advantage of sustained release of rhBMP-2 from PUR over bolus release from collagen sponge which is currently used in clinical standard care, but also further proved our concept that both a burst followed by sustained release of rhBMP-2 are important for promoting new bone formation.

Conclusion

Biodegradable PUR scaffolds incorporating rhBMP-2 prepared by reactive liquid molding promoted new bone formation in a rat femoral defects: both the simple plug model and the stringent critical size segmental model. The burst release of rhBMP-2 was reduced by encapsulating in PLGA microspheres prior to the foaming reaction, and both microsphere size and composition were observed to affect rhBMP-2 burst release and new bone formation. Our observations suggest that both a burst release within the first several days as well as sustained release is important to enhance formation of new bone tissue.

Acknowledgement

This work was funded by the Orthopaedic Trauma Research Program (DOD-W81XWH-07-1-0211), the Armed Forces Institute of Regenerative Medicine (sub-contract from the Rutgers-Cleveland Clinic Consortium Award DOD-W81XWH-08-2-0034), Vanderbilt University School of Engineering, the Vanderbilt Center for Bone Biology, and the US Army Institute of Surgical Research.

References

1. Bennett S, Connolly K, Lee DR, Jiang Y, Buck D, Hollinger JO, et al. Initial biocompatibility studies of a novel degradable polymeric bone substitute that hardens in situ. Bone. 1996 Jul;19(1):S101-S7.

2. Li B, Davidson JM, Guelcher SA. The effect of the local delivery of platelet-derived growth factor from reactive two-component polyurethane scaffolds on the healing in rat skin excisional wounds. Biomaterials. 2009 Jul;30(20):3486-94.

3. Zhang JY, Beckman EJ, Hu J, Yang GG, Agarwal S, Hollinger JO. Synthesis, biodegradability, and biocompatibility of lysine diisocyanate-glucose polymers. Tissue Engineering. 2002;8(5):771-85.

4. Guan JJ, Sacks MS, Beckman EJ, Wagner WR. Synthesis, characterization, and cytocompatibility of efastomeric, biodegradable poly(ester-urethane)ureas based on poly(caprolactone) and putrescine. Journal of Biomedical Materials Research. 2002;61(3):493-503.

5. Santerre JP, Woodhouse K, Laroche G, Labow RS. Understanding the biodegradation of polyurethanes: From classical implants to tissue engineering materials. Biomaterials. 2005 Dec;26(35):7457-70.

6. Fujimoto KL, Guan J, Oshima H, Sakai T, Wagner WR. *In vivo* evaluation of a porous, elastic, biodegradable patch for reconstructive cardiac procedures. Ann Thorac Surg. 2007 Feb;83(2):648-54.

7. Fujimoto KL, Tobita K, Merryman WD, Guan J, Momoi N, Stolz DB, et al. An elastic, biodegradable cardiac patch induces contractile smooth muscle and improves cardiac remodeling and function in subacute myocardial infarction. J Am Coll Cardiol. 2007 Jun 12;49(23):2292-300.

8. Gorna K, Gogolewski S. Preparation, degradation, and calcification of biodegradable polyurethane foams for bone graft substitutes. Journal of Biomedical Materials Research Part A. 2003;67A(3):813-27.

9. Adhikari R, Gunatillake PA, Griffiths I, Tatai L, Wickramaratna M, Houshyar S, et al. Biodegradable injectable polyurethanes: synthesis and evaluation for orthopaedic applications. Biomaterials. 2008 Oct;29(28):3762-70.

10. Guelcher S, Srinivasan A, Hafeman A, Gallagher K, Doctor J, Khetan S, et al. Synthesis, *In vitro* degradation, and mechanical properties of two-component poly(ester urethane)urea scaffolds: Effects of water and polyol composition. Tissue Engineering. 2007;13(9):2321-33.

11. Guelcher SA. Biodegradable polyurethanes: Synthesis and applications in regenerative medicine. Tissue Engineering Part B-Reviews. 2008;14(1):3-17.

12. Guelcher SA, Patel V, Gallagher KM, Connolly S, Didier JE, Doctor JS, et al. Synthesis and *in vitro* biocompatibility of injectable polyurethane foam scaffolds. Tissue Engineering. 2006;12(5):1247-59.

13. Hafeman AE, Li B, Yoshii T, Zienkiewicz K, Davidson JM, Guelcher SA. Injectable biodegradable polyurethane scaffolds with release of platelet-derived growth factor for tissue repair and regeneration. PharmRes. 2008;25(10):2387-99.

14. Hafeman AE, Zienkiewicz KJ, Davidson JM, Guelcher SA. Injectability of Biodegradable, Porous Polyurethane Scaffolds for Tissue Regeneration. TERMIS-NA 2008 Annual Conference, Abstract 2008.

15. Guan J, Stankus JJ, Wagner WR. Biodegradable elastomeric scaffolds with basic fibroblast growth factor release. Journal of Controlled Release. 2007;120(1-2):70-8.

16. Jeon O, Song SJ, Kang SW, Putnam AJ, Kim BS. Enhancement of ectopic bone formation by bone morphogenetic protein-2 released from a heparin-conjugated poly(L-lactic-co-glycolic acid) scaffold. Biomaterials. 2007;28(17):2763-71.

17. Jeon O, Kang SW, Lim HW, Chung JH, Kim BS. Long-term and zero-order release of basic fibroblast growth factor from heparin-conjugated poly(L-lactide-co-glycolide) nanospheres and fibrin gel. Biomaterials. 2006;27(8):1598-607.

18. Kempen DH, Kruyt MC, Lu L, Wilson CE, Florschutz AV, Creemers LB, et al. Effect of Autologous BMSCs Seeding and BMP-2 Delivery on Ectopic Bone Formation in a Microsphere/Poly(Propylene Fumarate) Composite. Tissue Eng Part A. 2008 Oct 16;15(3):587-94.

19. Kim SS, Gwak SJ, Kim BS. Orthotopic bone formation by implantation of apatite-coated poly(lactide-co-glycolide)/hydroxyapatite composite particulates and bone morphogenetic protein-2. J Biomed Mater Res A. 2008 Oct;87(1):245-53.

20. Seeherman H, Li R, Bouxsein M, Kim H, Li XJ, Smith-Adaline EA, et al. rhBMP-2/calcium phosphate matrix accelerates osteotomy-site healing in a nonhuman primate model at multiple treatment times and concentrations. J Bone Joint Surg Am. 2006 Jan;88(1):144-60.

21. de Jesus Perez VA, Alastalo TP, Wu JC, Axelrod JD, Cooke JP, Amieva M, et al. Bone morphogenetic protein 2 induces pulmonary angiogenesis via Wnt-beta-catenin and Wnt-RhoA-Rac1 pathways. J Cell Biol. 2009 Jan 12;184(1):83-99.

22. Fiedler J, Roderer G, Gunther KP, Brenner RE. BMP-2, BMP-4, and PDGF-bb stimulate chemotactic migration of primary human mesenchymal progenitor cells. J Cell Biochem. 2002;87(3):305-12.

23. Cho TJ, Gerstenfeld LC, Einhorn TA. Differential temporal expression of members of the transforming growth factor beta superfamily during murine fracture healing. J Bone Miner Res. 2002 Mar;17(3):513-20.

24. Gorna K, Gogolewski S. Biodegradable polyurethanes for implants. II. *In vitro* degradation and calcification of materials from poly(epsilon-caprolactone)-poly(ethylene oxide) diols and various chain extenders. Journal of Biomedical Materials Research. 2002;60(4):592-606.

25. Betz MW, Caccamese JF, Coletti DP, Sauk JJ, Fisher JP. Tissue response and orbital floor regeneration using cyclic acetal hydrogels. J Biomed Mater Res A. 2008 Jul 9;99A(3):819-29.

26. Hoshino M, Egi T, Terai H, Namikawa T, Kato M, Hashimoto Y, et al. Repair of long intercalated rib defects in dogs using recombinant human bone morphogenetic protein-2 delivered by a synthetic polymer and beta-tricalcium phosphate. J Biomed Mater Res A. 2008 Jun 18;99A(2):514-21.

27. Kempen DH, Yaszemski MJ, Heijink A, Hefferan TE, Creemers LB, Britson J, et al. Non-invasive monitoring of BMP-2 retention and bone formation in composites for bone tissue engineering using SPECT/CT and scintillation probes. J Control Release. 2008 Dec 3;134(3):169-76.

28. Kim S, Kim SS, Lee SH, Eun Ahn S, Gwak SJ, Song JH, et al. *In vivo* bone formation from human embryonic stem cell-derived osteogenic cells in poly(d,l-lactic-co-glycolic acid)/hydroxyapatite composite scaffolds. Biomaterials. 2008 Mar;29(8):1043-53.

29. Kim SE, Jeon O, Lee JB, Bae MS, Chun HJ, Moon SH, et al. Enhancement of ectopic bone formation by bone morphogenetic protein-2 delivery using heparin-conjugated PLGA nanoparticles with transplantation of bone marrow-derived mesenchymal stem cells. J Biomed Sci. 2008 Nov;15(6):771-7.

30. Kirker-Head C, Karageorgiou V, Hofmann S, Fajardo R, Betz O, Merkle HP, et al. BMP-silk composite matrices heal critically sized femoral defects. Bone. 2007 Aug;41(2):247-55.

31. Takahashi Y, Yamamoto M, Tabata Y. Enhanced osteoinduction by controlled release of bone morphogenetic protein-2 from biodegradable sponge composed of gelatin and beta-tricalcium phosphate. Biomaterials. 2005 Aug;26(23):4856-65.

32. Kempen DH, Lu L, Kim C, Zhu X, Dhert WJ, Currier BL, et al. Controlled drug release from a novel injectable biodegradable microsphere/scaffold composite based on poly(propylene fumarate). J Biomed Mater Res A. 2006 Apr;77(1):103-11.

33. Berkland C, Kipper MJ, Narasimhan B, Kim KK, Pack DW. Microsphere size, precipitation kinetics and drug distribution control drug release from biodegradable polyanhydride microspheres. Journal of Controlled Release. 2004;94(1):129-41.

34. Benita S. Microencapsulation: Methods and Industrial Applications. 2 ed: CRC Press; 2006.

35. Siepmann J, Peppas NA. Modeling of drug release from delivery systems based on hydroxypropyl methylcellulose (HPMC). Adv Drug Deliv Rev. 2001 Jun 11;48(2-3):139-57.

36. Karp JM, Rzeszutek K, Shoichet MS, Davies JE. Fabrication of precise cylindrical three-dimensional tissue engineering scaffolds for *in vitro* and *in vivo* bone engineering applications. J Craniofac Surg. 2003 May;14(3):317-23.

37. Torigoe I, Sotome S, Tsuchiya A, Yoshii T, Maehara H, Sugata Y, et al. Bone Regeneration with Autologous Plasma, Bone Marrow Stromal Cells, and Porous beta-Tricalcium Phosphate in Nonhuman Primates. Tissue Eng Part A. 2009 Feb 3;15(7):1489-99.

38. Chen X, Tsukayama DT, Kidder LS, Bourgeault CA, Schmidt AH, Lew WD. Characterization of a chronic infection in an internally-stabilized segmental defect in the rat femur. J Orthop Res. 2005 Jul;23(4):816-23.

39. Chen X, Kidder LS, Lew WD. Osteogenic protein-1 induced bone formation in an infected segmental defect in the rat femur. J Orthop Res. 2002 Jan;20(1):142-50.

40. Oldham JB, Lu L, Zhu X, Porter BD, Hefferan TE, Larson DR, et al. Biological activity of rhBMP-2 released from PLGA microspheres. J Biomech Eng. 2000 Jun;122(3):289-92.

41. Forcino RG, Jonnalagadda S. The effect of fabrication methods on the mechanical and thermal properties of poly(lactide-co-glycolide) scaffolds. Journal of Applied Polymer Science. 2007 Apr 15;104(2):944-9.

42. www.triton-technology.co.uk/pdf/TTAN_016.pdf.

43. Hafeman AE, Zienkiewicz KJ, Carney E, Litzner B, Stratton C, Wenke JC, et al. Local delivery of tobramycin from injectable biodegradable polyurethane scaffolds. J Biomaterials Science. 2009;DOI:10.1163/156856209X410256.

44. Higuchi T. Rate of release of medicaments from ointment bases containing drugs in suspension. J Pharm Sci. 1961 Oct;50:874-5.

45. Sawyer AA, Song SJ, Susanto E, Chuan P, Lam CX, Woodruff MA, et al. The stimulation of healing within a rat calvarial defect by mPCL-TCP/collagen scaffolds loaded with rhBMP-2. Biomaterials. 2009 Jan 20;30(13):2479-88.

46. Jeon O, Song SJ, Yang HS, Bhang SH, Kang SW, Sung MA, et al. Long-term delivery enhances *in vivo* osteogenic efficacy of bone morphogenetic protein-2 compared to short-term delivery. Biochem Biophys Res Commun. 2008 May 2;369(2):774-80.

47. Kempen DH, Lu L, Hefferan TE, Creemers LB, Maran A, Classic KL, et al. Retention of *in vitro* and *in vivo* BMP-2 bioactivities in sustained delivery vehicles for bone tissue engineering. Biomaterials. 2008 Aug;29(22):3245-52.

48. Saarinen-Savolainen P, Jarvinen T, Taipale H, Urtti A. Method for evaluating drug release from liposomes in sink conditions. International Journal of Pharmaceutics. 1997 Dec 15;159(1):27-33.

49. Boyne PJ, Marx RE, Nevins M, Triplett G, Lazaro E, Lilly LC, et al. A feasibility study evaluating rhBMP-2/absorbable collagen sponge for maxillary sinus floor augmentation. Int J Periodontics Restorative Dent. 1997 Feb;17(1):11-25.

50. Howell TH, Fiorellini J, Jones A, Alder M, Nummikoski P, Lazaro M, et al. A feasibility study evaluating rhBMP-2/absorbable collagen sponge device for local alveolar ridge preservation or augmentation. Int J Periodontics Restorative Dent. 1997 Apr;17(2):124-39.

51. Hoffmann A, Weich HA, Gross G, Hillmann G. Perspectives in the biological function, the technical and therapeutic application of bone morphogenetic proteins. Appl Microbiol Biotechnol. 2001 Oct;57(3):294-308.

52. Hogan BL. Bone morphogenetic proteins: multifunctional regulators of vertebrate development. Genes Dev. 1996 Jul 1;10(13):1580-94.

53. Kempen DH, Lu L, Heijink A, Hefferan TE, Creemers LB, Maran A, et al. Effect of local sequential VEGF and BMP-2 delivery on ectopic and orthotopic bone regeneration. Biomaterials. 2009 Feb 19;30(14):2816-25.

54. Patel ZS, Young S, Tabata Y, Jansen JA, Wong ME, Mikos AG. Dual delivery of an angiogenic and an osteogenic growth factor for bone regeneration in a critical size defect model. Bone. 2008 Nov;43(5):931-40.

55. Nie H, Ho ML, Wang CK, Wang CH, Fu YC. BMP-2 plasmid loaded PLGA/HAp composite scaffolds for treatment of bone defects in nude mice. Biomaterials. 2009 Feb;30(5):892-901.

CHAPTER IV

SUSTAINED RELEASE OF VANCOMYCIN FROM POLYURETHANE SCAFFOLDS INHIBITS INFECTION OF BONE WOUNDS IN A RAT FEMORAL SEGMENTAL DEFECT MODEL

Abstract

Infection is a common complication in open fractures that compromises the healing of bone and can result in loss of limb or life. Currently, the clinical standard of care for treating contaminated open fractures comprises a staged approach, wherein the wound is first treated with non-biodegradable antibiotic-laden poly(methyl methacrylate) (PMMA) beads to control the infection followed by bone grafting. Considering that tissue regeneration is associated with new blood vessel formation, which takes up to 6 weeks in segmental defects, a biodegradable bone graft with sustained release of an antibiotic is desired to prevent the implant from becoming infected, thus allowing the processes of both vascularization and new bone formation to occur unimpeded. In the present study, we utilized biodegradable porous polyurethane (PUR) scaffolds as the delivery vehicle for vancomycin. Hydrophobic vancomycin free base (V-FB) was obtained by precipitating the hydrophilic vancomycin hydrochloride (V-HCl) at pH 8. The decreased solubility of V-FB resulted in an extended vancomycin release profile *in vitro*, as evidenced by the fact that active vancomycin was released for up to 8 weeks at concentrations well above both the minimum inhibitory concentration (MIC) and the minimum bactericidal concentration (MBC). Using PUR prepared from lysine triisocyanate (LTI) (PUR(LTI)), the extended *in vitro* release profile observed for V-FB translated to improved infection control *in vivo* compared to V-HCl in a contaminated critical-sized fat femoral segmental defect. The performance of PUR(LTI)/V-

FB was comparable to PMMA/V-HCl beads *in vivo*. However, compared with PMMA, PUR is a biodegradable system which does not require the extra surgical removal step in clinical use. These results suggest that PUR scaffolds incorporating V-FB could be a potential clinical therapy for treatment of infected bone defects.

Introduction

Infection is a significant factor that compromises the healing of bone fractures (1, 2). A recent retrospective study found that all open type III fractures among combat casualties were infected. The presence of infection had a dramatic effect on patient outcomes, as evidenced by 37% of the patients experiencing delayed union with 14% resulting in amputation (3). Currently, the clinical standard of care for treating contaminated open fractures comprises two steps, wherein the wound is first treated with antibiotics followed by bone grafting. In practice, PMMA beads have been used as the local antibiotic delivery platform, and have been shown to decrease infections in clinical studies (4-6). Compared with systemic parenteral treatment, local antibiotics can achieve substantially higher concentrations at the contaminated site, resulting in more effective treatment of the infection, as well as reduced systemic toxicity concerns (7-9). In a prospective study of patients with infected non-unions, treatment with gentamycin-impregnated PMMA beads resulted in similar rates of infection control and healing of non-unions compared to long-term systemic parenteral delivery of gentamycin (10). Furthermore, a clinical study comparing the efficacy of local and parenteral delivery of antibiotics in patients with infected total hip and knee arthroplasty found that 30% of patients treated with systemic parental gentamycin exhibited recurring infection compared to 15% of patients treated with PMMA-gentamycin beads, although the difference was not statistically significant (8). However, since PMMA does not biodegrade, it must be removed during an additional

surgical step and cannot be allowed to remain in the wound bed during definitive closure. Furthermore, the antibiotic release efficiency is typically low (e.g., <25% cumulative release), the burst release is high (>60% of the released antibiotic is within the first day), and the antibiotics are below therapeutic levels within a week or two (11-14). Resorbable calcium phosphates and sulfates have also been investigated for local antibiotic delivery. Calcium sulfate pellets impregnated with antibiotic (Osteoset T, Wright Medical) have been shown to be effective in treating osteomyelitis in animals and humans (15-17). These biomaterials are biodegradable and osteoconductive, but calcium sulfate has been associated with seromas and drainage problems (18). Additionally, the release of antibiotic is very fast, occurring within the first 2 – 3 days and calcium sulfate dissolves quickly; therefore, it does not possess favorable osteoconductive properties.

While treatment with antibiotic-laden PMMA beads or calcium sulfate pellets effectively controls infection in the wound bed prior to bone grafting, there is a need for a bone graft material that not only enhances bone healing, but also releases an antibiotic that protects the wound from infection during the healing process. Although generally effective at promoting bone growth, the bone graft is essentially a foreign material placed into an avascular and often contaminated defect and could thus possibly function as a nidus for infection. Additionally, blood vessel formation is a prerequisite for bone healing (19, 20), and angiogenesis is known to be essential for bone regeneration in segmental defects (21, 22). It has been shown that vascularization of the fracture callus in sheep progressed during the first three weeks of healing (20), and another study has suggested that complete vascularization of implanted scaffolds may require up to six weeks (22). Therefore, in contaminated bone wounds, it is desirable to maintain a therapeutic level of antibiotic for at least 3 – 6 weeks to control the infection until substantial vascularization occurs in the wound bed.

Biodegradable porous PUR scaffolds have been investigated as supportive scaffolds for cellular infiltration and new bone formation (23-25). Polyurethanes have also been investigated as drug delivery systems. Controlled release of antibiotics has been investigated to develop infection-resistant biomedical PUR implants (26-29), and delivery of biologically active growth factors from PUR scaffolds has been demonstrated (23, 30, 31). In particular, a recent study has shown that controlled release of rhBMP-2 from PUR scaffolds promoted new bone tissue formation in rat femoral plug defects (23). Biodegradable PUR scaffolds have also been shown to release biologically active tobramycin *in vitro* (26). However, the burst release of tobramycin was high (e.g., >50%), and the tobramycin release kinetics was relatively independent of material properties.

Vancomycin, a tricyclic glycopeptide antibiotic, is an effective therapy for treating serious infections caused by gram-positive bacteria such as Staphylococcus aureus (32, 33). Vancomycin has less negative effects on osteoblasts and skeletal cells than other commonly used antibiotics *in vitro* (34, 35), and it does not impede bone growth in fractures *in vivo* (36). Different strategies have been developed for the delivery of vancomycin from polymers, such as poly(trimethylene carbonate)-based surface-eroding delivery systems (37) and nanoparticles presenting vancomycin on the surface (38). Ideally, the delivery system should deliver vancomycin well above the effective antibacterial concentration (i.e., the minimum inhibitory concentration, MIC) in a sustainable manner (2). For treatment of osteomyelitis, it has been suggested that release of antibiotic at concentrations exceeding the MIC for 6 – 8 weeks is desirable (39). Thus one objective of the present study was to synthesize PUR scaffolds incorporating vancomycin with tunable release kinetics, where the release of biologically active vancomycin was extended to 6 – 8 weeks so that the processes of angiogenesis and new bone formation could proceed unimpeded by infection. PUR scaffolds incorporating vancomycin with both fast and slow release kinetics were evaluated

in an infected segmental defect in a rat femur to demonstrate the feasibility of the approach and identify the most effective release strategy.

Materials and Methods

Materials

Glycolide and D,L-lactide were obtained from Polysciences (Warrington, PA). The tertiary amine catalyst TEGOAMIN33, which comprised a 33 wt% solution of triethylene diamine (TEDA) in dipropylene glycol, was received from Goldschmidt (Hopewell, VA) as a gift. Hexamethylene diisocyanate trimer (HDIt, Desmodur N3300A) was received as a gift from Bayer Material Science LLC (Pittsburgh, PA). Lysine triisocyanate (LTI) was purchased from Kyowa Hakko (New York, NY). Stannous octoate catalyst was received from Nusil technology (Overland Park, KS). Vancomycin hydrochloride (V-HCl) was purchased from ACROS organics. Fluorescence-labeled vancomycin (BODIPY@FL conjugate) was purchased from Invitrogen. All other reagents were purchased from Sigma-Aldrich (St. Louis, MO).

Vancomycin hydrochloride (V-HCl) and vancomycin free base (V-FB)

V-HCl was dissolved in water at a concentration of 70 mg/ml, followed by increasing the pH to 8 (where vancomycin has no net charge and the lowest solubility (40)) by adding an appropriate amount of NaOH solution (3N). After incubating for 30 minutes, the precipitated vancomycin free base (V-FB) was filtered, washed with 70% ethanol and methanol separately, dispersed in water, frozen, and lyophilized overnight. The concentration of V-HCl used in the conversion was selected as 70 mg/ml, which is well below the water solubility of 200 mg/ml, in order to avoid V-HCl precipitates in the final V-FB product. For confocal microscopy, V-HCl was mixed with vancomycin BODIPY@FL conjugate at a ratio of 3725:1 in solution, and then lyophilized to obtain fluorescence-

generating V-HCl (FL-V-HCl) or converted to fluorescence-generating V-FB (FL-V-FB) as described above.

Fabrication and characterization of PUR scaffolds

The polyester macrotriol (900 Da) was synthesized from a glycerol starter as published previously (41), with the backbone comprising 70% ε-caprolactone, 20% glycolide, and 10% D,L-lactide for T7C2G1L900 and 60% ε-caprolactone, 30% glycolide, and 10% D,L-lactide for T6C3G1L900. Porous PUR scaffolds were then fabricated using a one-shot two-component reaction between the triisocyanate and the hardener comprising polyester triol, water, TEGOAMIN33 tertiary amine catalyst, sulfated castor oil stabilizer, and calcium stearate pore opener as described previously (41). V-HCl or V-FB was incorporated into the scaffolds by mixing with the hardener component prior to reacting with the triisocyanate. The targeted index (the ratio of NCO to OH equivalents × 100) was 115 for all scaffolds. Two PUR formulations were investigated: (a) PUR(HDIt), a slow-degrading scaffold prepared from HDIt and T6C3G1L900; and (b) PUR(LTI), a fast-degrading scaffold synthesized from LTI and T7C2G1L900. The antibiotic (V-HCl or V-FB) loading was selected as the maximum amount of drug that could be incorporated in the scaffolds without compromising stability and pore morphology, which corresponded to 7 wt% for the PUR(HDIt) materials and 8 wt% for the PUR(LTI) materials. For PUR(LTI) materials, there was no significant difference in V-FB release at 7 and 8 wt% loadings, while the release of V-HCl was ~5% higher at a loading of 8 wt% compared to 7 wt% for days 1 – 15 (data not shown). The amount of water was adjusted for the antibiotic-containing PUR(LTI) scaffolds in order to achieve porosities similar to blank scaffolds. The porosities of the scaffolds were calculated based on the volume and weight (23, 30), and the distribution of FL-V-HCl or FL-V-FB within the PUR(LTI) scaffolds was analyzed by confocal microscopy

with an excitation wavelength of 488 nm, performed on a Zeiss LSM510 confocal microscope in VUMC Cell Imaging Shared Resource (23).

Fabrication of PMMA/vancomycin beads

As described previously (26), the PMMA beads (3 mm in size) were hand-made using an Osteoset® kit (Wright Medical Technology, Arlington, TN). Two grams V-HCl was added to one packet (40 g powder (poly(methyl acrylate, methyl methacrylate), zirconium dioxide, hydrous benzoyl peroxide) and mixed with 20 ml monomer cement (methyl methacrylate, N,N-dimethyl-ptoluidine). The resulting PMMA beads contained 3.33% wt vancomycin for the *in vitro* release and *in vivo* animal studies, and 0.90% wt vancomycin for the KB tests of the scaffolds.

In vitro release of vancomycin

Three replicate PUR scaffold samples (~40 mg, 0.4 ml) or PMMA beads (~60 mg, 0.15 ml) were immersed in 1 ml PBS in polypropylene vials sealed by O-rings. The volume of release medium (1 ml) was selected on the basis that the scaffold was completely immersed in the release medium, and that even if 100% of the vancomycin were released instantaneously, the concentration of the drug in solution would be at least a factor of 6 times less than its solubility. The observation that no significant difference in release profile was observed when the medium volume was increased to 10 ml further suggests that the release was performed under sink conditions. At days 1, 2, 4, 8, 14, 21, 28, 35, 42, 49, and 56, the medium was recovered by squeezing the scaffolds, followed by the addition of 1 ml fresh medium (26). The concentration of vancomycin released at each time point was determined by measuring the absorbance at 280 nm, from which the concentration was calculated using a standard calibration curve (42, 43). The actual mass of drug released was calculated based on the measured concentration and actual collected sample volumes. The

cumulative percentage release was calculated as the ratio of the mass released at each time point to the total amount of vancomycin embedded in the scaffolds. The cumulative release data were fitted to a logarithmic function, which was differentiated with respect to time in order to calculate the daily percentage release. (23) The mass of drug released per day per unit volume of scaffold was calculated from the daily percentage release and the loading of the drug in the scaffold. The Weibull function (44-46) was used to fit the cumulative release curves in order to elucidate the drug release mechanism.

Antibiotic activity assay

The Kirby-Bauer assay was applied to evaluate the biological activity of: (a) the PUR scaffolds and and PMMA beads, and (b) the *in vitro* releasates from the PUR scaffolds and PMMA beads. The objective of the Kirby-Bauer test was to validate that the vancomycin was still active after incorporation in the PUR scaffolds. Methicillin-susceptible Staphylococcus aureus (S. aureus) from the American Type Culture Collection (ATCC 25923) was chosen for the assay (26). The bacteria were suspended in trypticase soy broth at a turbidity that matched a 0.5 MacFarland standard and then spread onto Mueller–Hinton agar plates. PMMA impregnated with V-HCl (0.9 wt%) and PUR scaffolds with V-HCl (8 wt%) or V-FB (8 wt%) were cut into discs (6 mm diameter by 1 mm thick) and placed on the agar plates. All the three treatment groups incorporated the same mass (320 μg) of vancomycin. BBL SensiDiscs incorporating 30-μg vancomycin (BD, Franklin Lakes, NJ, USA) were used as a laboratory positive control. Blank PUR was used as negative control. After incubating the agar plates at 37 ºC for 24 hours, the zones of inhibition (ZI) were measured for each disc. In order to evaluate the bioactivity of vancomycin released from scaffolds and PMMA beads, the releasates from day 1 and weeks 2, 4, 6, and 8 were lyophilized and reconstituted in water to a concentration of 1.5 mg/ml. A mass of 15 μg (dissolved in a 10 μl solution) released vancomycin was subsequently loaded onto blank SensiDiscs. The positive control

was SensiDiscs with 15 μg fresh vancomycin. The discs were placed on agar plates, and ZIs were measured for each disc after incubating the agar plates at 37 ºC for 24 hours. One way ANOVA with Bonferroni correction ($p<0.05$) was used for evaluation of statistical significance.

In vivo animal study

The animal study was approved by the Animal Care and Use Committee at the US Army Institute of Surgical Research. A previously described contaminated critical size defect (CSD) was created in the rat (Sprague-Dawley) femurs (47). Briefly, a 6 mm segmental defect was created and stabilized under aseptic conditions in 40 rats. Using aseptic technique, a longitudinal incision was made over the left anterolateral femur, and the entire femoral shaft was exposed using blunt dissection. A polyacetyl plate (length 25 mm, width 4 mm and height 4 mm) was fixed to the surface of the femur using 6 threaded K-wires. A 6 mm mid-diaphyseal full-thickness defect was created with a small reciprocating saw blade (MicroAire 1025, MicroAire, Charlottesville, VA) under continuous irrigation with sterile saline. The defects in all animals were implanted with 30 mg of type I bovine collagen (Stryker Biotech, Hopkinton, MA, USA) that was ethanol sterilized and subsequently wetted with 105 of colony forming units (CFUs) of Staphylococcus aureus lux (Xenogen 36, Caliper Life Science, Hopkinton, MA) suspended in 0.1 ml of sterile normal saline. This isolate was transgenically modified to emit photons and was sensitive to vancomycin. The contaminated collagen was packed into the defect, and the wound closed in a layered fashion. A high-resolution radiograph of each femur with stabilized defect was obtained using a Faxitron X-ray system (Faxitron X-ray Corporation, Wheeling, Illinois (Model: MX-20, Image settings Time: 10 Sec, KV: 35, Window Level: 3380/1250) at initial surgery to confirm appropriate placement of the implant and adequate creation of the defect.

Treatment: Six hours after contamination, the wounds were debrided and irrigated with 60 ml of saline (47). This time period was chosen because it is clinically relevant (48). Model development work demonstrated that a 6-hr delay was the ideal time for treatment with local antibiotics (49). The wounds in the control group were re-closed with no further treatment. For the experimental groups, PUR scaffolds (PUR(LTI)/V-HCl or PUR(LTI)/V-FB containing 8% wt vancomycin, (340 μg vancomycin) or four 3 mm PMMA/V-HCl beads (clinical control containing 3.33% wt vancomycin, or 2800 μg vancomycin per defect) were then packed into the defects (n = 10) prior to wound closure. To be consistent with clinical practice, two beads were placed in the bony defect and two were placed in the soft tissue. In the present study, we aimed to test our hypothesis that the PUR+vancomycin scaffolds would perform comparably to, or better than, PMMA+vancomycin beads. The cement beads were selected as the clinical control on the basis that they are an established, clinically effective treatment (4, 5). The vancomycin dosage in the PUR scaffolds was selected on the basis that it was the maximum concentration of vancomycin that could be incorporated in the PUR scaffolds while maintaining porosity and dimensional stability. The animals were allowed full activity in their cages postoperatively, and were monitored daily for signs of pain and systemic infection. Following 4 weeks of recovery, the rats were euthanized by Fatal Plus.

Photon Counts: Immediately after euthanasia, the wound site was exposed to allow bacteria quantification using a photon counting camera (Xenogen IVIS® Imaging System 100 Series using the Living Image 2.6.2. (Software Igor Pro 4.09A)). The disarticulated extremities were placed in the Xenogen machine, and a black and white photograph was first taken of the wound followed by a luminescent image with a 2.5 second exposure time. The Region of Interest (ROI) was determined with elliptical ROIs positioned over the

wound to include the entire femur and polyacetyl plate. This method assessed the amount of surface bacteria within the entire wound.

Quantitative Cultures: The femur with defect was harvested from the animals and used for quantitative assessment (47). The plate, K-wires, and all soft tissues were removed. Each femur was weighed, snap-frozen in liquid nitrogen, and ground to a fine powder under sterile conditions. The resulting bone powder was serially diluted in normal saline. Aliquots (100 µl) of each dilution were plated onto the surface of tryptic soy agar, and incubated at 37 °C for 48 hours. The plates were examined for purity and colony morphology. Four to eight dilutions were typically required to obtain a minimum dilution level where the CFUs of bacteria were countable on the culture plate; the actual numbers of recovered CFUs of bacteria were obtained by correcting for the magnitude of the dilution used to obtain them and reported in CFUs per gram of bone tissue.

Results

Properties of vancomycin (V-HCl and V-FB)

Vancomycin contains six functional groups which exhibit dissociable hydrogen atoms at specific pH values (Figure IV-1), including a carboxyl group with a pKa of 2.18, a primary amino group with a pKa of 7.75, a secondary amino group with a pKa of 8.89, and three phenol groups with pKa values of 9.59, 10.40, and 12.0 respectively (40). Therefore, V-HCl has one net positive charge in solution (Figure IV-1A), and has solubility in water equal to 200 mg/ml. V-FB was obtained through precipitation of vancomycin at pH 8. V-FB contains no net charge (Figure IV-1B) and has a water solubility of less than 20 mg/ml, which is substantially lower than that of V-HCl.

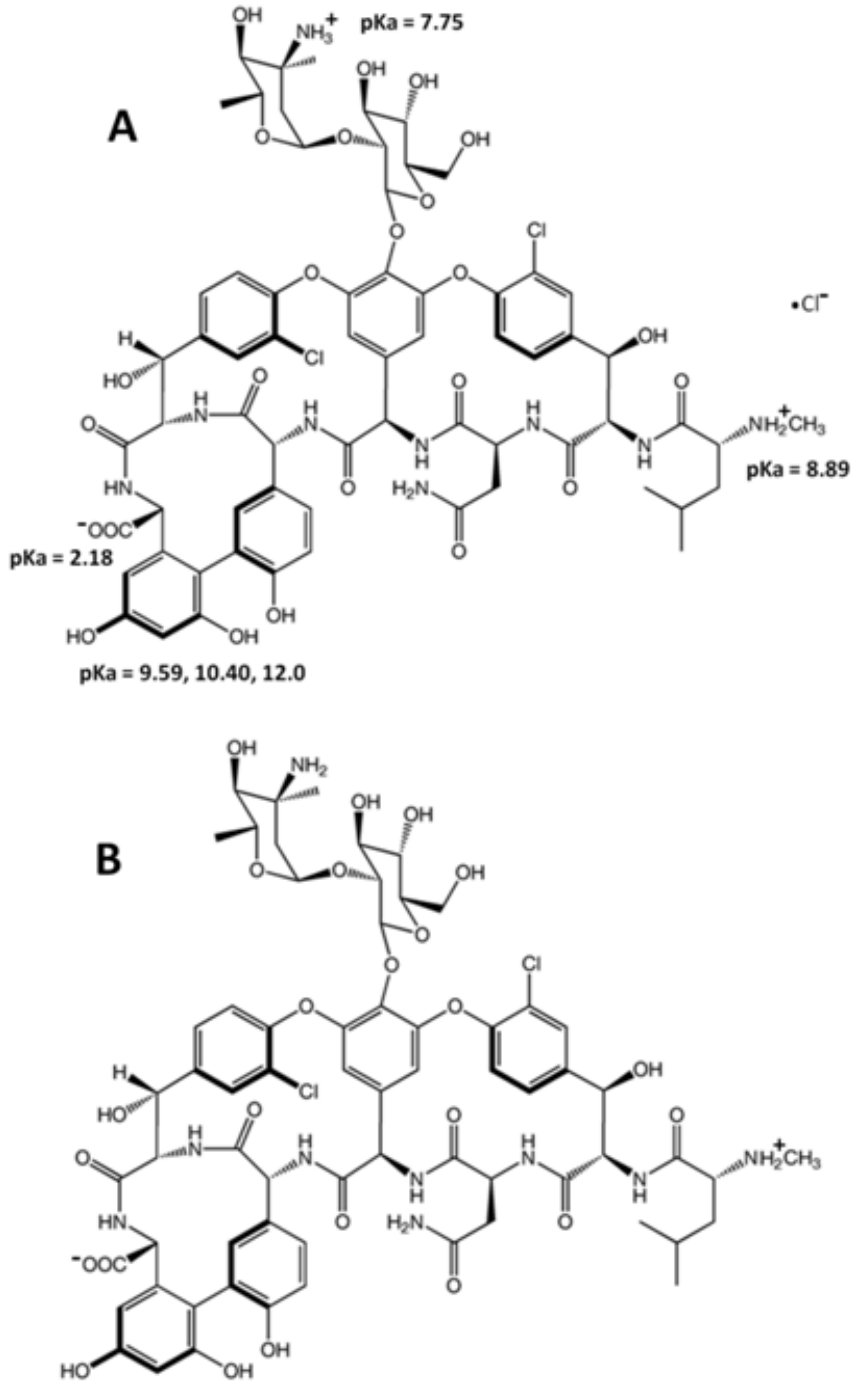

Figure IV-1 The molecular structure of vancomycin hydrochloride (V-HCl, A) and free base (V-FB, B) with pKa values and charges indicated.

Fabrication and activity of PUR scaffolds with vancomycin

Two types of PUR scaffolds were fabricated: PUR(LTI), a fast-degrading material (100% mass loss after 36 weeks *in vitro*) synthesized from LTI and T7C2G1L900, and PUR(HDIt), a slow-degrading material (32% mass loss after 36 weeks *in vitro*, unpublished data) synthesized from HDIt and T6C3G1L900 (26). Two forms of vancomycin were separately incorporated into different PUR scaffolds by mixing with the polyester triol prior to reacting with the triisocyanate. The loadings of antibiotic within the PUR(LTI) and PUR(HDIt) scaffolds were 8 wt% and 7 wt%, respectively. As shown in Table IV-1, all PUR scaffolds exhibited porosity of ~89 - 93%, while PMMA beads were only 24% porous.

Table IV-1 Vancomycin treatment groups. V-HCl denotes the hydrochloride form of vancomycin, while V-FB denotes the free base form of vancomycin. PUR(LTI) scaffolds were synthesized from LTI and T7C2G1L900 polyester triols, while PUR(HDIt) scaffolds were synthesized from HDIt and T6C3G1L900 polyester triols. Vancomycin loading is specified in both wt% and μg/cm^3 scaffold.

Treatment Group	V form	V loading		Porosity
		(wt%)	(μg/cm^3)	
PUR(LTI)/V-HCl	V-HCl	8 wt%	7.90×10^3	91.87%
PUR(LTI)/V-FB	V-FB	8 wt%	7.40×10^3	92.40%
PUR(LTI)	N/A	N/A	N/A	91.45%
PUR(HDIt)/V-HCl	V-HCl	7 wt%	8.93×10^3	89.46%
PUR(HDIt)/V-FB	V-FB	7 wt%	9.10×10^3	89.26%
PUR(HDIt)	N/A	N/A	N/A	92.9% (23)
PMMA/V-HCl	V-HCl	3.33 wt%	2.91×10^4	24.06%

In order to investigate the distribution of vancomycin within the scaffolds, vancomycin BODIPY@FL conjugate was mixed with V-HCl in order to obtain fluorescence-labeled V-HCl

(FL-V-HCl). A portion of FL-V-HCL was then converted to FL-V-FB using the same method of converting V-HCl to V-FB. When incorporated in PUR scaffolds, as evidenced by confocal fluorescence microscopy images (Figure IV-2), both V-HCl and V-FB were distributed uniformly throughout the PUR scaffold walls. The V-HCl particles appeared to have a more needle-like (e.g., high aspect ratio) morphology relative to the V-FB particles.

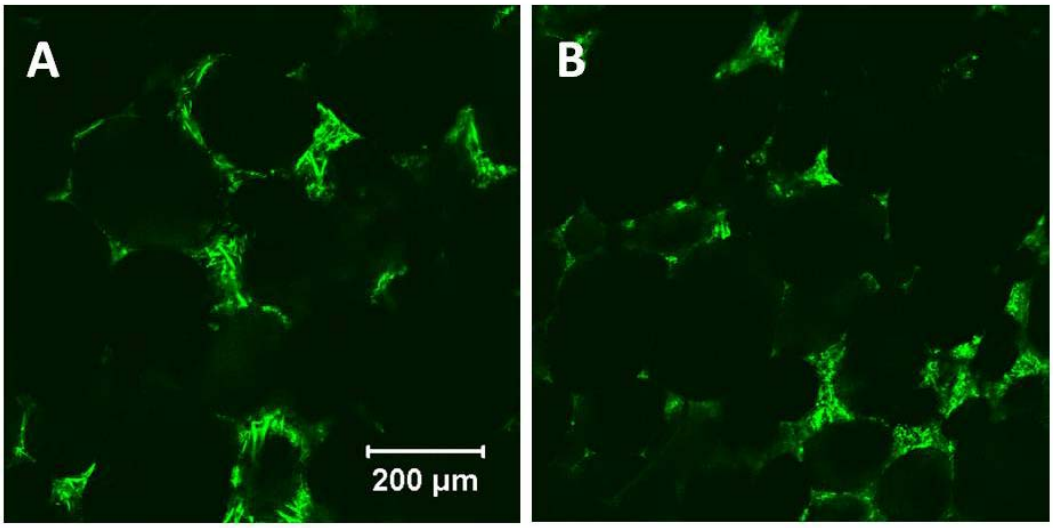

Figure IV-2 Distribution of FL-V-HCl (A) and FL-V-FB (B) in PUR(LTI). Vancomycin BODIPY@FL conjugate was mixed with V-HCl to obtain FL-V-HCl and then converted to FL-V-FB. The loading of either type of FL-V in PUR(LTI) was 8 wt%. The fluorescence images were taken using a confocal microscope with an excitation wavelength of 488 nm.

The bioactivity of both PUR(LTI) and PUR(HDIt) scaffolds incorporating vancomycin (6 mm diameter by 1 mm thick discs) was measured using the Kirby-Bauer diffusion test. The positive laboratory control, comprising BBL SensiDiscs used in clinical pathology laboratories containing 30 µg vancomycin, showed a ZI of 19.5 mm, and the negative control, blank PUR scaffolds, showed a ZI of 0 mm (data not shown). These controls demonstrate that the KB test was performing properly.

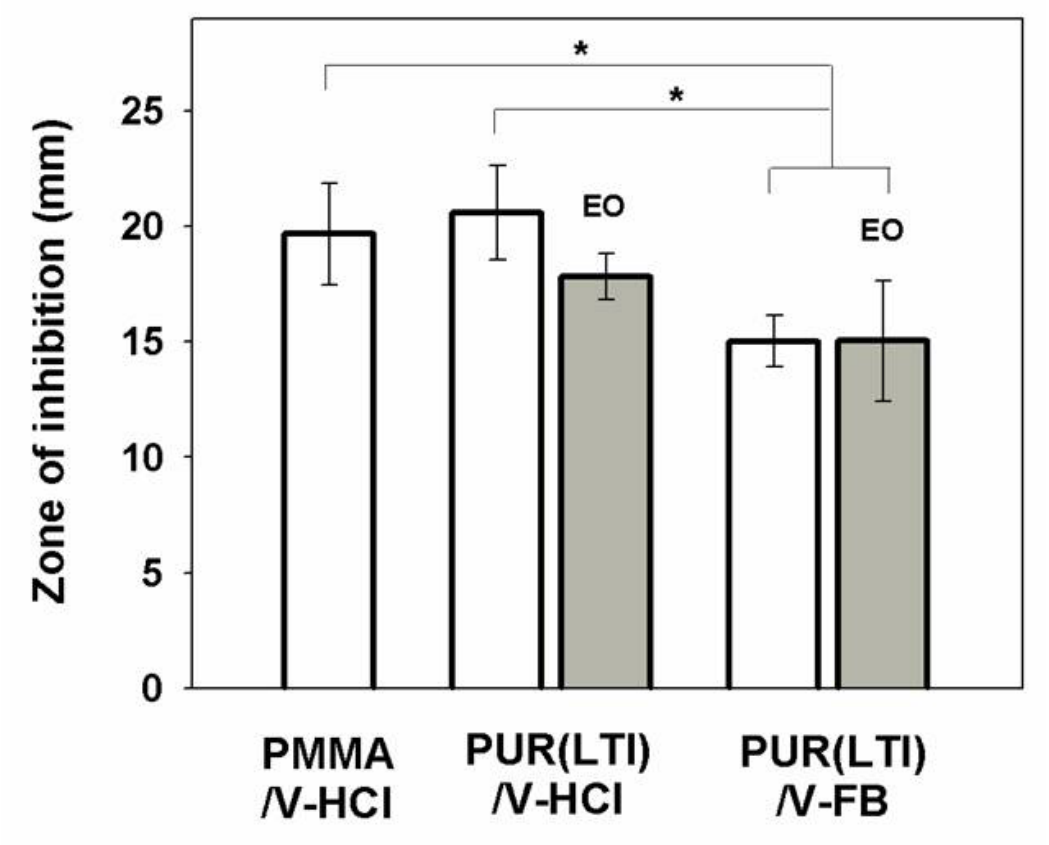

Figure IV-3 Zones of inhibition measured for PUR(LTI)/V-HCl, PUR(LTI)/V-FB, and PMMA/V-HCl materials. Staphylococcus aureus (ATCC 25923) were spread onto Mueller–Hinton agar plates. PUR scaffolds and PMMA beads (6 mm x 1 mm discs) were placed on the agar plates. BBL SensiDiscs incorporating 30 ug V-HCl were used as a laboratory control. After incubating the agar plates at 37 ºC for 24 hours, the zones of inhibition (ZI) were measured for each disc. One way ANOVA with bonferroni correction ($p<0.05$) was used for evaluation of statistical significance, and the significance between groups was depicted as * where existed.

As shown in Figure IV-3, PUR(LTI) discs incorporating V-HCl (PUR(LTI)/V-HCl) demonstrated ZIs comparable to PMMA/V-HCl at the same volume concentration, while PUR(LTI) discs loaded with vancomycin free base (PUR(LTI)/V-FB) showed 25% lower activity than the PUR(LTI)/V-HCl material. It is also interesting to note that sterilization by ethylene oxide (EO) resulted in no significant loss in biological activity of either V-HCl or V-FB. As shown in Figure IV-4, similar to PUR(LTI) materials, the PUR(HDIt) discs

incorporating V-HCl (PUR(HDIt)/V-HCl) showed comparable ZIs PMMA/V-HCl, while PUR(HDIt) discs loaded with V-FB (PUR(HDIt)/V-FB) showed decreased (statistically significant) bioactivity compared with both PUR(HDIt/V-HCl). The lower ZIs observed for PUR discs incorporating V-FB are conjectured to result from the lower water solubility of V-FB relative to V-HCl, resulting in slower release of the drug into the agar gel.

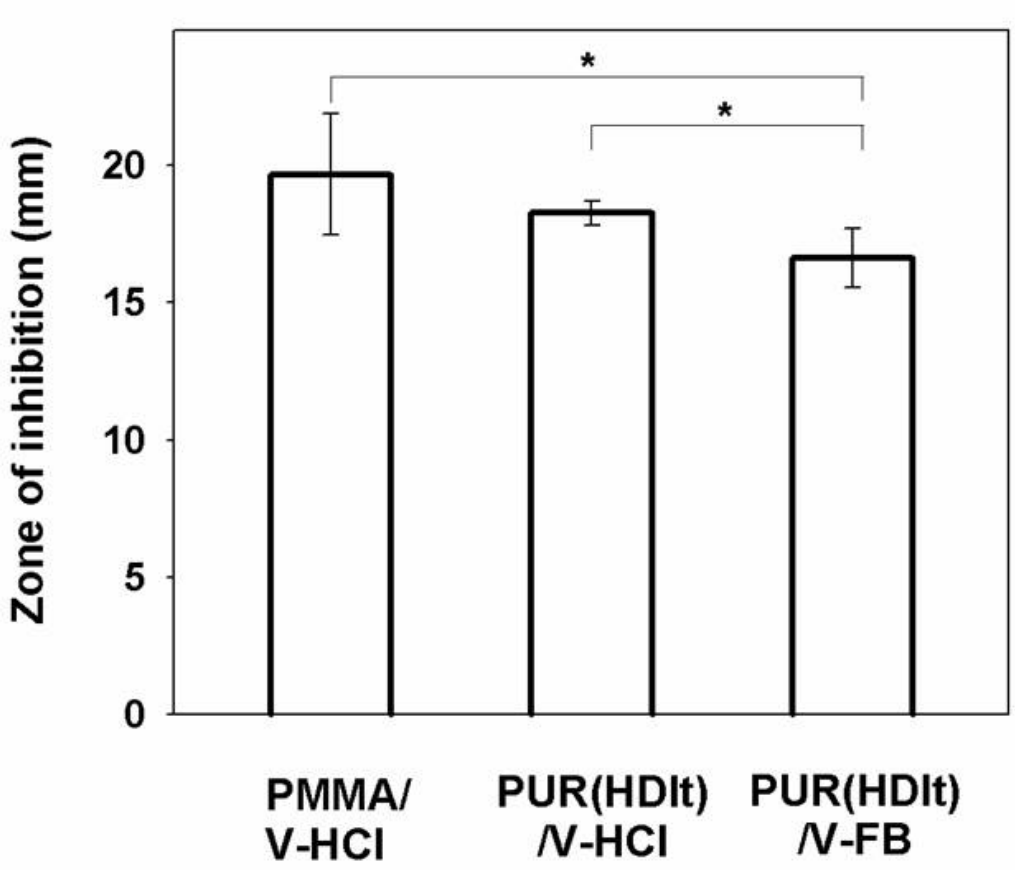

Figure IV-4 Zones of inhibition measured for PUR(HDIt)/V-HCl and PUR(HDIt)/V-FB. Staphylococcus aureus (ATCC 25923) were spread onto Mueller–Hinton agar plates. PUR scaffolds and PMMA beads (6 mm x 1 mm discs) were placed on the agar plates. BBL SensiDiscs incorporating 30 ug V-HCl were used as a laboratory control. After incubating the agar plates at 37 ºC for 24 hours, the zones of inhibition (ZI) were measured for each disc. One way ANOVA with bonferroni correction ($p<0.05$) was used for evaluation of statistical significance, and the significance between groups was depicted as * where existed.

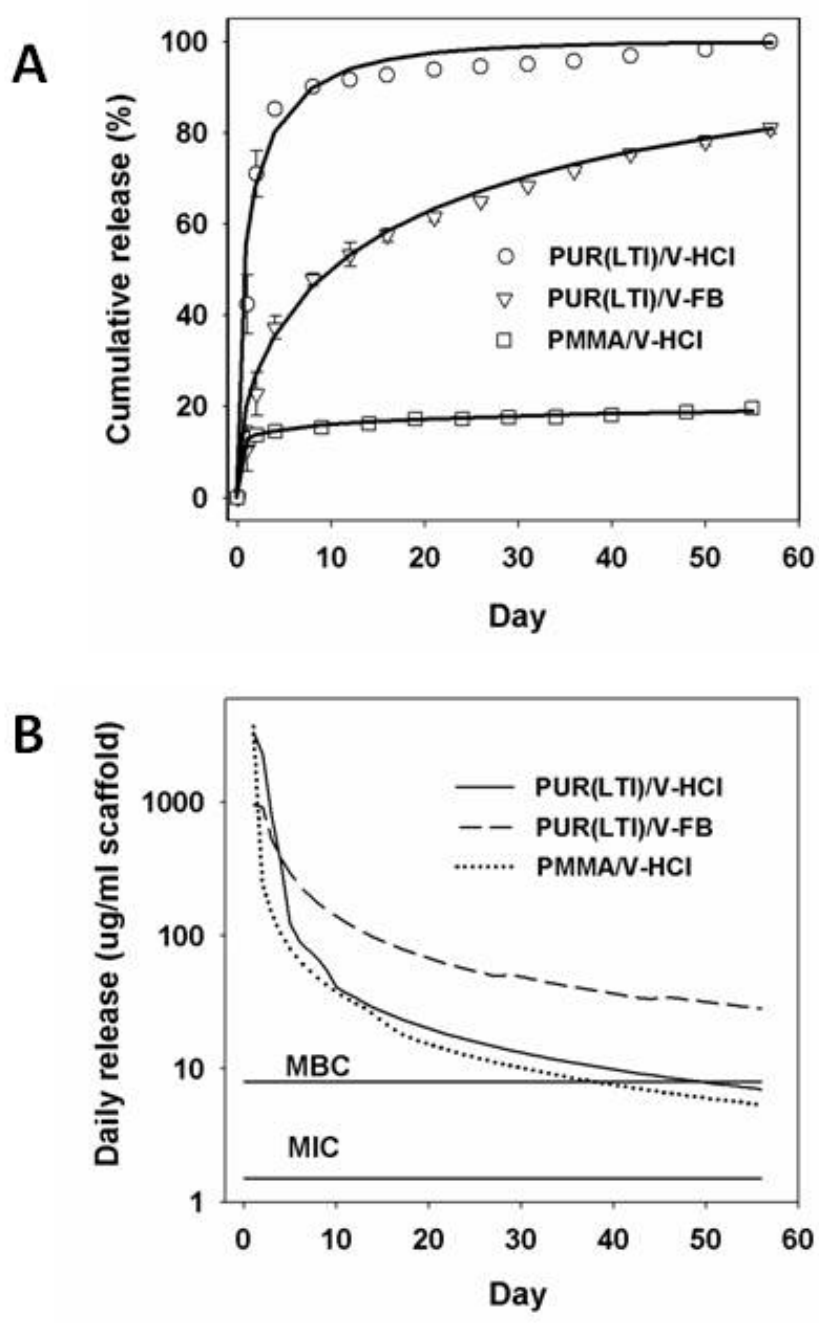

Figure IV-5 Vancomycin release kinetics from PUR(LTI)/V-HCl, PUR(LTI)/V-FB, and PMMA/V-HCl materials. (A) Cumulative release (%, symbols) and simulation by empirical Weibull model (solid lines), and (B) Daily release (μg/cm^3 scaffold). PUR scaffolds (~40 mg, n = 3) or PMMA beads (~60 mg, n = 3) were immersed in 1 ml PBS in polypropylene vials sealed by O-rings. The medium was refreshed as indicated in the methods. The amount of vancomycin released at each time point was determined by measuring the absorbance at 280 nm.

In vitro release of vancomycin from PUR scaffolds and PMMA beads

The *in vitro* release kinetics of vancomycin from PUR(LTI)/V-HCl, PUR(LTI)/V-FB, and PMMA/V-HCl (3.23 wt% V-HCl, the clinical control) were measured in PBS. The PUR(LTI)/V-HCl materials showed a burst release of 42% and 28% on days 1 and 2, respectively, and the cumulative release was 90% at day 8. After day 8, the release was slow (i.e., 0.80%/day at day 8 and 0.09%/day release at day 56) (Figure IV-5, A and B). When vancomycin was transformed from V-HCl to V-FB and embedded in PUR(LTI), the lower solubility was expected to slow the release of vancomycin. This hypothesis is supported by the observation that the release on day 1 of PUR(LTI)/V-FB was only about 11%, compared to 42% observed for PUR(LTI)/V-HCl. Furthermore, as shown in Figure IV-5B, the V-FB exhibited a more sustained release profile from day 8 to day 56 (i.e., 2.42% /day at day 8 and 0.36%/day at day 56) which is 3-fold greater than the corresponding release rates for the V-HCl formulation. Due to the lower burst and more sustained release of V-FB, the concentration of vancomycin remained well above the minimum inhibitory concentration (MIC, 0.75∼2 μg/ml) and minimum bactericidal concentration (MBC, 8 μg/ml) (50, 51) for at least 8 weeks (Figure IV-5B). In contrast, PMMA beads exhibited a burst release of 10% on day 1 followed by a small sustained release on days 8 – 56 (i.e., 0.16%/day at day 8 and 0.02%/day at day 56). The sustained release from PMMA beads is less than that observed for the PUR treatment groups, although the loading of vancomycin per volume PMMA is 4 fold that of PUR scaffolds as shown in Table IV-1.

The release profiles of vancomycin from PUR(HDIt) scaffolds were similar to those observed for PUR(LTI) scaffolds. PUR(HDIt)/V-HCl materials exhibited a burst release for days 1 – 4 followed by a period of slower release from days 8 – 56 (Figure IV-6). The PUR(HDIt)/V-FB materials showed a minimal burst release followed by a sustained release for a period of 6 weeks. The cumulative release of vancomycin was generally less from HDIt

scaffolds compared to LTI scaffolds. For example, on day 42, the cumulative release of V-HCl was 95% for the LTI materials compared to 85% for the HDIt materials. Similarly, on day 42, the cumulative release of V-FB was 70% for the LTI materials compared to 52% for the HDIt materials. The PUR(HDIt)/V-(HCl+FB) materials, which were loaded with 3.5 wt% V-HCl and 3.5 wt% V-FB, resulted in a release profile intermediate to that of the PUR(HDIt)/V-HCl and PUR(HDIt)/V-FB materials, suggesting the possibility of tuning the release profile of vancomycin for different applications by blending V-HCl and V-FB.

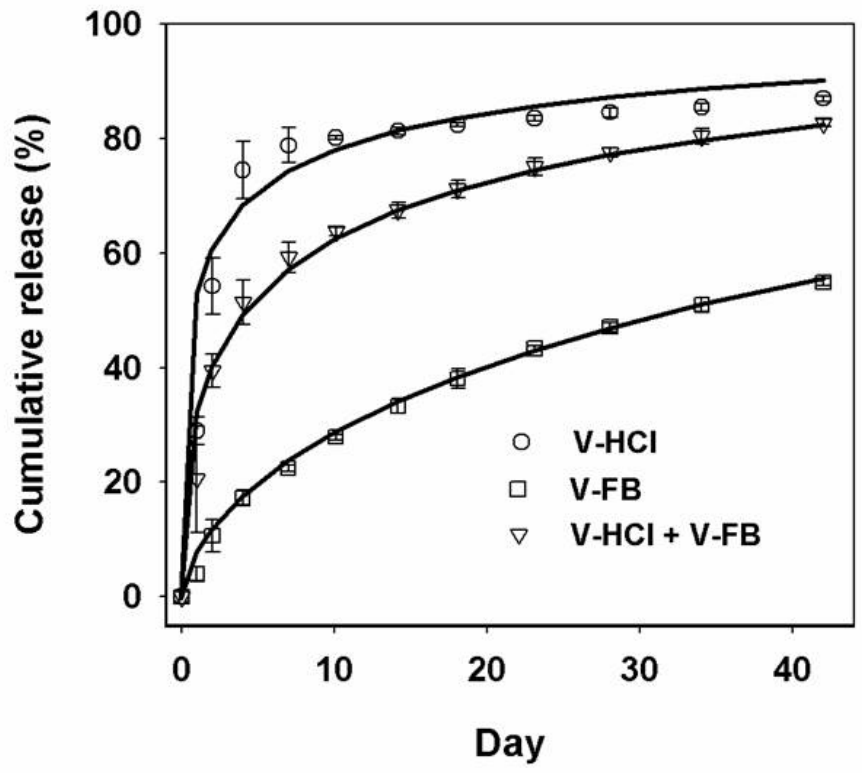

Figure IV-6 Vancomycin release kinetics form PUR(HDIt)/V-HCl, PUR(HDIt)/V-FB, and PUR(HDIt)/V-FB+V-HCl scaffolds: Cumulative release (%, symbols) and simulation by empirical Weibull model (solid lines). PUR scaffolds (~40 mg, n = 3) were immersed in 1 ml PBS in polypropylene vials sealed by O-rings. The medium was refreshed as indicated in the methods. The amount of vancomycin released at each time point was determined by measuring the absorbance at 280 nm.

In vitro vancomycin release mechanism

There are several empirical models available for simulating drug release from polymer scaffolds. Although the power law model has been extensively used, it is most accurate for short time periods or <60% cumulative release of the drug (46). In the present study, the release of vancomycin was measured for up to 56 days and nearly 100% cumulative release for some of the treatment groups. While the power law model was observed to fit the first 4 – 7 days of release, the quality of the fit was poor at longer time points where the cumulative release exceeded ~50%. Therefore, the vancomycin release data from PUR scaffolds and PMMA beads were fit to the Weibull function, another empirical equation which has been used to model drug release for more extended periods of time(44, 46):

$$\frac{M_t}{M_\infty} = 1 - \exp\left(-a \cdot t^b\right) \quad (1)$$

where M_t = the mass of drug released at time t, M_∞ = the mass of drug released at infinite time (assumed equal to the amount of drug added), and a and b are constants (45). A value of b < 0.75 suggests a Fickian diffusion release mechanism (44, 46). The fitting parameters determined from the vancomycin release data are listed in Table IV-2. The values of b calculated for PUR(LTI) scaffolds were found to be approximately 0.50 for both V-HCl and V-FB. Similarly, the values of b determined for PUR(HDIt) materials were found to be 0.30, 0.40, and 0.61 for V-HCl, V-HCl+V-FB, and V-FB respectively. For all treatment groups, b < 0.75 which suggests that the release of either type of vancomycin from PUR scaffolds is diffusion limited. For PUR(LTI), the values of a were found to be 0.81 and 0.22 for V-HCl and V-FB, respectively. Similar trends were observed for the PUR(HDIt) materials, with values of a equal to 0.76, 0.39, and 0.08 for V-HCl, V-HCl+V-FB, and V-FB respectively, thus suggesting a faster release rate for V-HCl as a result of its higher water solubility relative to V-FB. The parameter $\tau = a^{-b}$, defined as the time at which 63.2% of the drug has been

delivered (45), was calculated from the Weibull fitting parameters. The values of τ were calculated to be 1.5 and 20.8 days for V-HCl and V-FB released from PUR(LTI) scaffolds; and 2.5, 10.5, and 58.8 days for V-HCl, V-HCl+V-FB, and V-FB released from PUR(HDIt) scaffolds. These values of τ are consistent with the experimentally observed times required for 63.2% cumulative release of vancomycin (Figure IV-5A and Figure IV-6). The a and b values for V-HCl release from PMMA were 0.14 and 0.11 respectively, which are significantly lower than those from PUR(LTI) scaffolds. The differences in the Weibull model parameters are attributed to the fact that the majority (e.g., <80%) of the antibiotic is sequestered in the PMMA beads, with only the drug trapped near the surface being released (52, 53).

Table IV-2 Simulation of *in vitro* release to the empirical Weibull model. M_t/M_0, t, and R^2 represent cumulative percentage released (%), time (day), and the coefficient of determination respectively. Both a and b are constants.

$\frac{M_t}{M_\infty} = 1 - \exp\left(-a \cdot t^b\right)$		***a***	***b***	***R²***
PUR(LTI)	V-HCl	0.81	0.50	0.978
	V-FB	0.22	0.50	0.990
PUR(HDIt)	V-HCl	0.76	0.30	0.923
	V-HCl + V-FB	0.39	0.40	0.982
	V-FB	0.08	0.61	0.997
PMMA	V-HCl	0.14	0.11	0.996

Bioactivity of released vancomycin

The vancomycin released from PUR(LTI)/V-HCl, PUR(LTI)/V-FB, and PMMA/V-HCl materials up to specified time points were lyophilized and reconstituted to the same concentration (1.5 mg/ml) to evaluate the bioactivity of the released vancomycin at the same concentration of antibiotic. Using fresh vancomycin as a positive control, 15 μg of

released vancomycin was loaded onto SensiDiscs and the zones of inhibition measured using the Kirby-Bauer test.

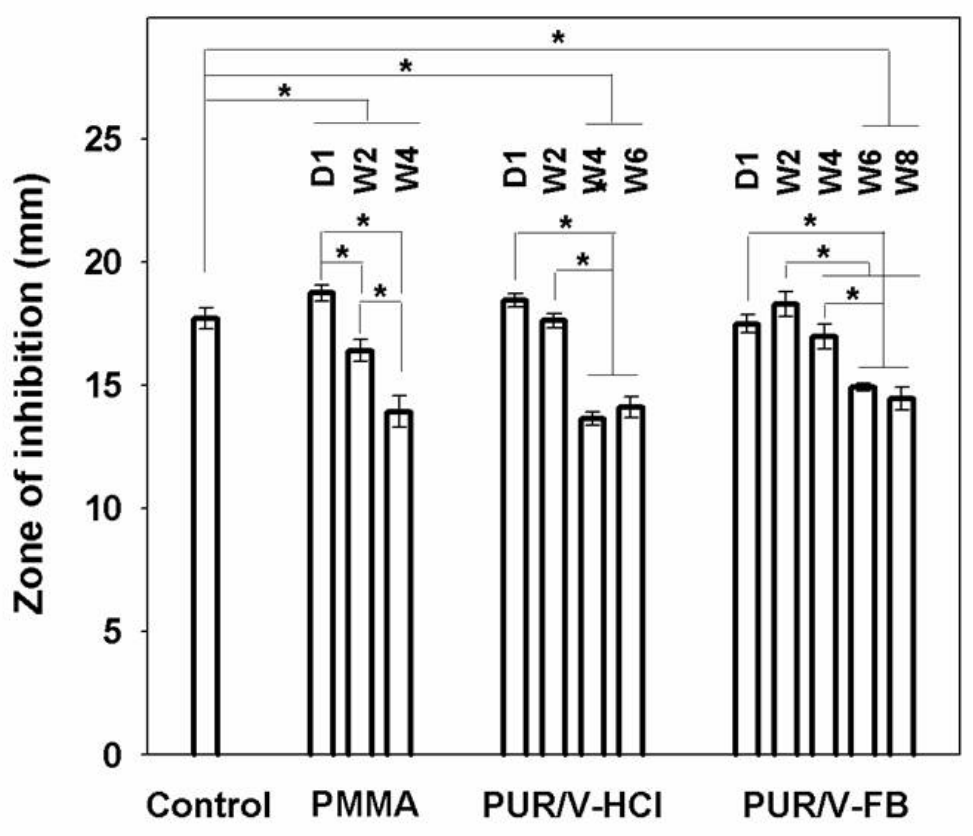

Figure IV-7 Zones of inhibition measured for vancomycin released from PUR(LTI)/V-HCl, PUR(LTI)/V-FB, and PMMA/V-HCl materials for up to 8 weeks. Releasates from day 1 and weeks 2, 4, 6, and 8 were lyophilized and reconstituted to a concentration of 1.5 mg/ml. A mass of 15 µg (dissolved in a 10 µl solution) released vancomycin was subsequently loaded onto blank SensiDiscs. The positive control was SensiDiscs with 15 µg fresh vancomycin. The discs were placed on agar plates, and ZIs were measured for each disc after incubating the agar plates at 37 ºC for 24 hours. One way ANOVA with bonferroni correction ($p<0.05$) was used for evaluation of statistical significance, and the significance between treatment groups and the positive control or different time points within each treatment group was depicted as * where existed.

As shown in Figure IV-7, the released vancomycin from each treatment group at each time period was verified to be bioactive, and the bioactivity decreased with time. For PMMA/V-HCl, the bioactivity of released vancomycin decreased as early as week 2, while

the bioactivity of released vancomycin from the PUR(LTI)/V-HCl materials decreased at week 4. The bioactivity of released antibiotic was highest for the PUR(LTI)/V-FB materials, where the bioactivity did not decrease until week 6. Due to the more sustained release of vancomycin from these materials, biologically active antibiotic was released up to week 8 with a significant but modest (~15%) reduction in bioactivity.

Infection inhibition by PUR scaffolds *in vivo*

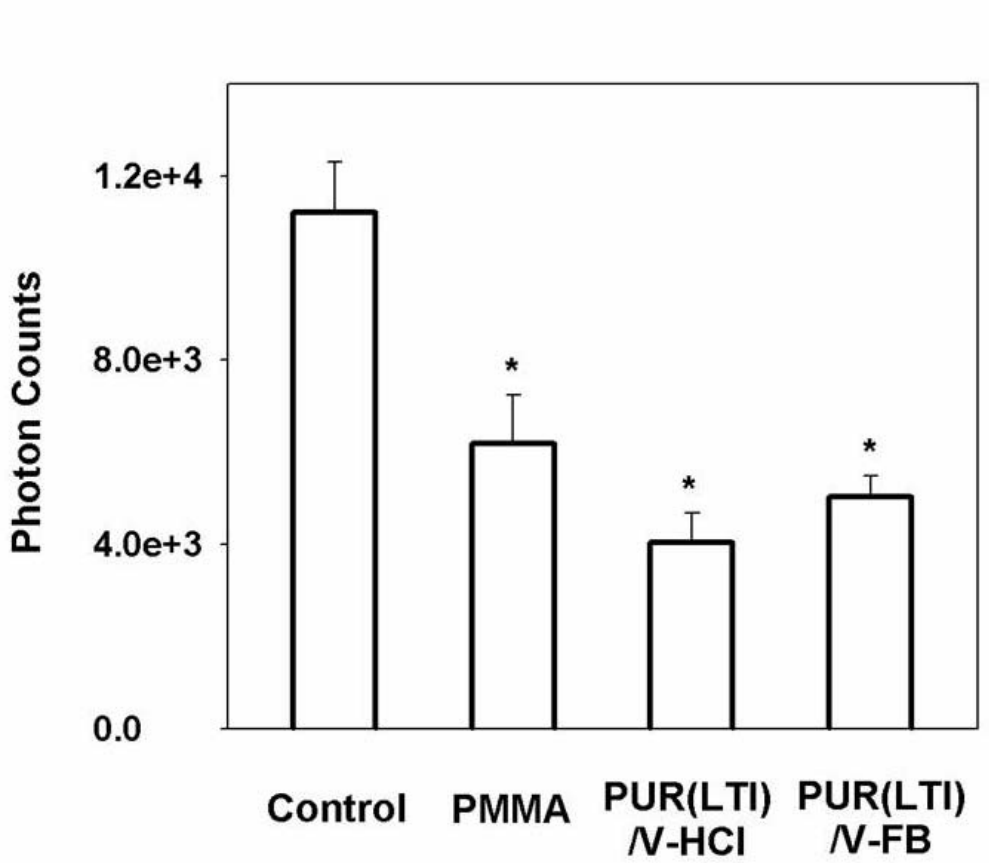

Figure IV-8 Photon counts measured for PUR(LTI)/V-HCl, PUR(LTI)/V-FB, and PMMA/V-HCl materials after 4 weeks implantation time. At 4 weeks, the rats were euthanized, tissue around and within the defects was harvested, and quantitative cultures performed. A photon-counting camera was used to capture the quantitative and spatial distribution of the bacteria within the wound following euthanasia and harvesting of the femur. One way ANOVA with bonferroni correction ($p<0.05$) was used for evaluation of statistical significance, and the significance between vancomycin treatment groups and the negative control was depicted as * where existed.

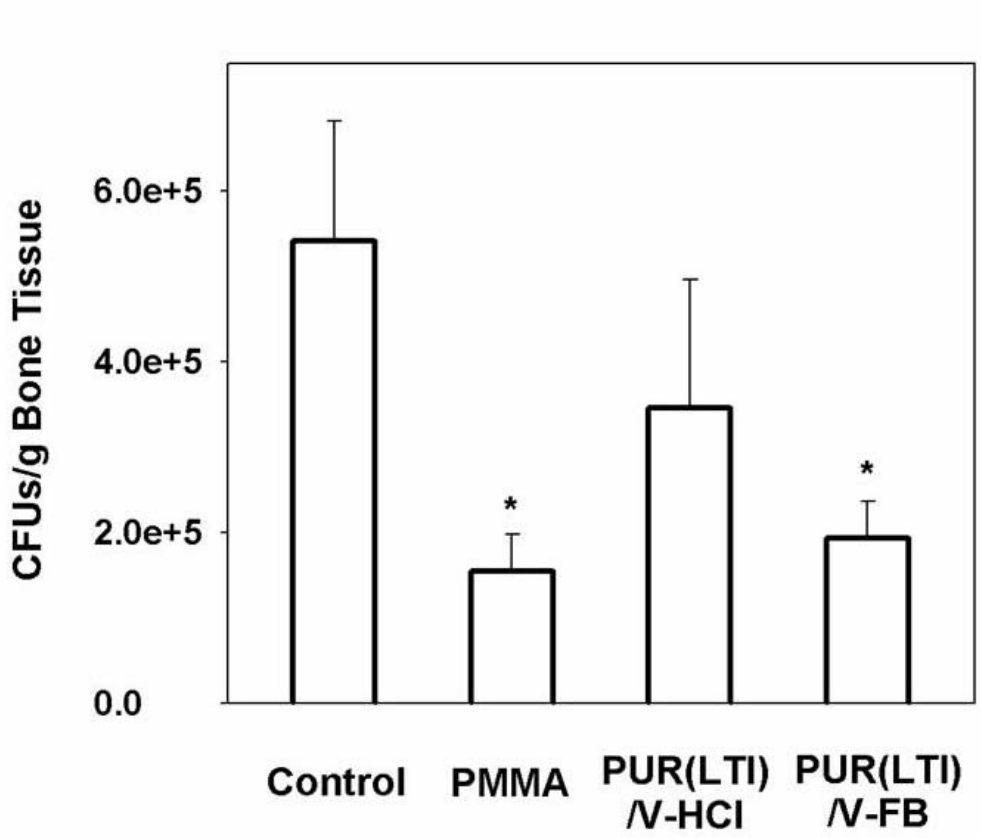

Figure IV-9 CFU counts measured for PUR(LTI)/V-HCl, PUR(LTI)/V-FB, and PMMA/V-HCl materials after 4 weeks implantation time. Each femur was weighed, snap-frozen in liquid nitrogen, and ground to a fine powder under sterile conditions. The resulting bone powder was serially diluted in normal saline. Aliquots (100 µl) of each dilution were plated onto the surface of tryptic soy agar, and incubated at 37 °C for 48 h in 5% CO_2. All CFU counts were normalized to counts/g bone tissue. One way ANOVA with bonferroni correction ($p<0.05$) was used for evaluation of statistical significance, and the significance between vancomycin treatment groups and the negative control was depicted as * where existed.

The PUR(LTI) materials were sterilized by EO treatment at room temperature overnight, which was shown to have a negligible effect on the biological activity of the scaffolds (Figure IV-3). PUR(LTI)/V-HCl, PUR(LTI)/V-FB and PMMA/V-HCl beads were implanted in the contaminated rat femoral segmental defect and the femurs harvested after 4 weeks. The spatial distribution of the bacteria within the wound, detected by photon imaging, shows that all the vancomycin treatment groups inhibited bacteria growth in the soft tissue

significantly compared with the untreated negative control (Figure IV-8). No significant differences were observed between any vancomycin treatment groups for the soft tissue bacteria counts. The femurs were then frozen, ground to a fine powder, and cultured for counting of CFUs per unit weight of bone. The CFU data (Figure IV-9) indicate that all the vancomycin treatment groups inhibited bacteria growth in bone tissue, but only PUR(LTI)/V-FB and PMMA/V-HCl showed significant inhibition effects compared with the untreated control. No significant differences existed between the performance of PMMA/V-HCl beads and the PUR(LTI) treatment groups. Consistent with the definition of a CSD, no significant new bone formation was observed when PUR scaffolds were implanted in rat femoral CSDs in the absence of an osteoinductive factor such as rhBMP2 (unpublished data).

Discussion

Vancomycin is an important antibiotic due to its potential in preventing infections caused by gram positive bacteria such as methicillin resistant S. aureus (MRSA) (1, 32). In previous studies, delivery of vancomycin hydrochloride resulted in low release efficiency when delivered using non-biodegradable materials such as PMMA (11-14). Furthermore, a high burst with minimal sustained release resulted due to the high water solubility of V-HCl in PMMA and other materials (37, 42, 43). In the present study, PMMA beads impregnated with V-HCl resulted in maximum daily release on day 1 followed by slow release thereafter, with only 20% cumulative release of V-HCl. A similar release profile has been reported for tobramycin incorporated within PMMA (26). When incorporated in a porous biodegradable PUR, the release efficiency was significantly enhanced as evidenced by the nearly 100% cumulative release of V-HCl from PUR(LTI) scaffolds at week 8. Additionally, the sustained release is extended to longer time periods relative to PMMA (Figure IV-4). By incorporating

the more hydrophobic, less soluble free base form of vancomycin (V-FB), the burst release was decreased and the sustained release increased. Release profiles of V-HCl and V-FB were fit to the Weibull equation, resulting in value of the exponent b ranging from 0.4 – 0.6, which suggests that the release of vancomycin was diffusion-controlled. The model calculations also showed that by decreasing the water solubility of the drug, the diffusion rate from PUR scaffolds was decreased, which resulted in a more sustained release profile for the hydrophobic V-FB relative to hydrophilic V-HCl. The daily release concentration of V-FB released from PUR(LTI)/V-FB was well above the MIC and MBC up to week 8, and the released V-FB was verified to be bioactive in the Kirby-Bauer bacteria inhibition test. Furthermore, confocal microscopy images revealed that the vancomycin was distributed uniformly throughout the pore walls, which is consistent with our previous results reported for bovine serum albumin (23). PUR(LTI) scaffolds exhibit interconnected pores and undergo hydrolytic degradation with resorption times varying from 26 – 36 weeks *in vitro* (54). In a previous study, we reported that ~75% of the tobramycin incorporated in PUR scaffolds was released after 1 week incubation time *in vitro*, resulting in a 20 – 30% reduction in compressive strength (26). This reduction in strength is attributed to the additional channels and pores created within the scaffold resulting from diffusion of the drug from the polymer into the solution (55).

PUR(LTI) scaffolds incorporating vancomycin were evaluated in an infected rat femoral segmental defect to verify the activity of the released antibiotic *in vivo*, as well as identify the preferred formulation. At week 4, compared with the untreated group, both PUR(LTI)/V-HCl and PUR(LTI)/V-FB treatment groups reduced the number of bacteria counts in soft tissue significantly, and PUR(LTI)/V-FB performed similarly to PMMA/V-HCl in reducing the number of bacteria counts significantly within bone tissue. Taken together, these observations suggest that the PUR(LTI)/V-FB implants exhibited superior infection

control relative to the PUR(LTI)/V-HCl implants at 4 weeks. Furthermore, the *in vivo* data show the PUR(LTI)/V-FB implants performed comparably to the PMMA/V-HCl clinical control. Due to processing constraints associated with the PUR scaffolds, the maximum achievable vancomycin loading was 8 wt%. Due to the high porosity of the PUR scaffolds (~90%), the density of the scaffolds was much lower than that of the PMMA beads; thus the loading of vancomycin in the defects (3mm × 6mm) was substantially less for animals treated with PUR scaffolds (340 μg) compared to those treated with PMMA beads (2800 μg). Since the efficiency of release of vancomycin was considerably higher for PUR scaffolds, the daily release (in units of $\mu g \cdot cm^{-3}$ implant) was comparable for the PUR(LTI)/V-HCl and PMMA/V-HCl treatment groups at all time points (Figure IV-5). However, it is important to note that four beads were placed in the femoral CSDs, two in the bone defect and two in soft tissue, which is consistent with clinical practice. Therefore the volume of the PMMA implants was approximately twice that of the PUR scaffolds (which were only placed in the bone defect), so that the total mass of antibiotic released from the PMMA implants is estimated to be twice that released from the PUR scaffolds based on the *in vitro* release data (Figure IV-5). The observation that the PUR(LTI)/V-HCl implants inhibited the infection in bone to a lesser extent than the PMMA/V-HCl control at 4 weeks is thus attributed to the larger mass of V-HCl released from the PMMA beads compared to the PUR(LTI)/V-HCl scaffolds. The data in Figure IV-5B indicated that at 28 days the daily release exceeded the MIC for all treatment groups, although after day 2 the daily release from the PUR(LTI)/V-FB scaffolds exceeded that from the other treatment groups. Thus the observation that PUR(LTI)/V-FB scaffolds performed comparably to PMMA beads is conjectured to result from the more sustained release achieved with the PUR(LTI)/V-FB scaffolds. While the PUR(LTI)/V-FB implant performed comparably to the PMMA/V-HCl control at 4 weeks, it is anticipated that the more sustained release profile achieved with the PUR(LTI)/V-FB

scaffolds would significantly reduce the infection burden relative to PMMA/V-HCl at longer time points (e.g., 8 weeks) where the release from PUR(LTI)/V-FB continued to exceed the MIC.

The objective of the present study was to compare the performance of biodegradable PUR + vancomycin implants to that of PMMA beads incorporating vancomycin which is the current clinical standard of care for local delivery of antibiotics. Thus no direct comparisons can be made between local delivery of vancomycin from PUR(LTI)/V-FB scaffolds and systemic delivery due to the lack of an additional clinical control comprising an empty scaffold with systemic parenteral delivery of vancomycin. However, previous studies have shown that local delivery of antibiotics can achieve higher concentrations at the contaminated site compared to systemic parenteral treatment (7-9), resulting in potentially more effective management of the infection and reduced systemic toxicity risks. Local delivery of gentamycin from PMMA beads performed comparably to long-term systemic parenteral delivery of gentamycin in the treatment of infected non-unions (10). Additionally, local delivery of antibiotics was reported to reduce the risk of infection for total hip and knee arthoplasties relative to systemic delivery, although the difference was not statistically significant (8). Taken together, these previous studies suggest that local delivery of antibiotics using PMMA beads is at least as effective at controlling infections as systemic delivery. Considering that the PUR(LTI)/V-FB therapy performed comparably to the PMMA/V-HCl beads in the infected rat segmental defect model at 4 weeks, it is anticipated that the PUR(LTI)/V-FB therapy would also perform at least comparably to the systemic delivery approach.

Beads or spacers made from antibiotic-laden bone cements have been clinically adopted for treating infection associated with hip anthroplasty (56, 57). Simplex P, a PMMA bone

cement with tobramycin, has been approved by FDA for second stage revision of total joint replacement, where the antibiotic is claimed to protect the PMMA from infection. PMMA bone cements incorporating antibiotics have also been used to treat chronic osteomyelitis (58-60), and the two-stage procedure comprising treatment with antibiotics to control the infection followed by grafting to heal the defect is the current clinical standard of care for treating contaminated bone wounds (56, 61-63). Nevertheless, cases of secondary infectious complications have been reported (64), which have been attributed to insufficient sustained release of the antibiotic. Furthermore, too low a concentration of antibiotic may induce antibiotic resistance of bacteria (65). Local sustained delivery of antibiotics from the bone graft implanted after the stabilization of the wound bed is anticipated to protect the graft from infection and reduce the frequency of secondary complications. Bone wound healing is dependent on angiogenesis and vascularization (19-22), and previous reports have suggested that a period of up to 6 weeks may be required for full vascularization of scaffolds implanted in segmental defects to occur (22). Another study has shown that at least 6 weeks of effective antibiotic treatment are required in order to control infection for total hip and knee arthroplasties (66). Therefore, sustained release of antibiotic exceeding the MIC for at least 6 weeks post-implantation is anticipated to be necessary for protecting the bone graft from infection and enabling the processes of vasculogenesis and wound healing to proceed. The biodegradable (PUR(LTI)/V-FB) delivery system developed in this study, which is a single-stage approach, presents a potentially significant innovation in the clinical use of antibiotics. By protecting the graft from contamination, infection control and tissue regeneration are allowed to occur simultaneously.

Recent studies have shown that sustained release of recombinant growth factors, such as rhPDGF-BB (30) and rhBMP-2 (23), from PUR scaffolds accelerates cellular infiltration

and ingrowth of new tissue *in vivo*. However, infection is known to inhibit new bone formation, even in the presence of an osteogenic factor (67). While systemic delivery of antibiotics and local delivery of rhBMP-7 from a collagen carrier have been observed to enhance bone formation relative to local delivery of rhBMP-7 alone (68), the effects of local delivery of antibiotics and an osteoinductive factor on new bone formation in infected wounds have not been investigated. Therefore co-delivery of V-FB and rhBMP-2 from a biodegradable PUR scaffold could be a potentially promising approach for healing contaminated bone defects: the vancomycin is anticipated to control the infection so that the osteoinductive effects of the rhBMP-2 are not impeded. If successful, the dual-delivery approach could accelerate healing by protecting the scaffold from bacterial contamination, which could substantially reduce the frequency of secondary infectious complications.

Conclusions

Porous biodegradable PUR scaffolds have been shown to support tunable, sustained release of vancomycin *in vitro*. When implanted in infected segmental defects in rats, PUR/V-FB scaffolds significantly reduced the infection relative to the untreated control and performed comparably to PMMA bone cements after 4 weeks. The release profile of vancomycin from PUR was extended to at least 8 weeks when hydrophilic V-HCl was converted to hydrophobic V-FB. Therefore, PUR scaffolds incorporating V-FB could be a potential clinical therapy for treatment of contaminated bone defects.

Acknowledgments

This work was funded by the Orthopaedic Extremity Trauma Research Program (DOD-W81XWH-07-1-0211) and the US Army Institute of Surgical Research.

References

1. Ginebra MP, Traykova T, Planell JA. Calcium phosphate cements as bone drug delivery systems: a review. J Control Release. 2006 Jun 28;113(2):102-10.

2. Zilberman M, Elsner JJ. Antibiotic-eluting medical devices for various applications. J Control Release. 2008 Sep 24;130(3):202-15.

3. Johnson EN, Burns TC, Hayda RA, Hospenthal DR, Murray CK. Infectious complications of open type III tibial fractures among combat casualties. Clin Infect Dis. 2007 Aug 15;45(4):409-15.

4. Ostermann PA, Seligson D, Henry SL. Local antibiotic therapy for severe open fractures. A review of 1085 consecutive cases. J Bone Joint Surg Br. 1995 Jan;77(1):93-7.

5. Ristiniemi J, Lakovaara M, Flinkkila T, Jalovaara P. Staged method using antibiotic beads and subsequent autografting for large traumatic tibial bone loss: 22 of 23 fractures healed after 5-20 months. Acta Orthop. 2007 Aug;78(4):520-7.

6. Moehring HD, Gravel C, Chapman MW, Olson SA. Comparison of antibiotic beads and intravenous antibiotics in open fractures. Clin Orthop Relat Res. 2000 Mar(372):254-61.

7. Duncan CP, Masri BA. The role of antibiotic-loaded cement in the treatment of an infection after a hip replacement. Instr Course Lect. 1995;44:305-13.

8. Nelson CL, Evans RP, Blaha JD, Calhoun J, Henry SL, Patzakis MJ. A comparison of gentamicin-impregnated polymethylmethacrylate bead implantation to conventional parenteral antibiotic therapy in infected total hip and knee arthroplasty. Clin Orthop Relat Res. 1993 Oct(295):96-101.

9. Hanssen AD, Spangehl MJ. Practical applications of antibiotic-loaded bone cement for treatment of infected joint replacements. Clin Orthop Relat Res. 2004 Oct(427):79-85.

10. Calhoun JH, Henry SL, Anger DM, Cobos JA, Mader JT. The treatment of infected nonunions with gentamicin-polymethylmethacrylate antibiotic beads. Clin Orthop Relat Res. 1993 Oct(295):23-7.

11. Adams K, Couch L, Cierny G, Calhoun J, Mader JT. *In vitro* and *in vivo* evaluation of antibiotic diffusion from antibiotic-impregnated polymethylmethacrylate beads. Clin Orthop Relat Res. 1992 May(278):244-52.

12. Kuechle DK, Landon GC, Musher DM, Noble PC. Elution of vancomycin, daptomycin, and amikacin from acrylic bone cement. Clin Orthop Relat Res. 1991 Mar(264):302-8.

13. Mader JT, Calhoun J, Cobos J. *In vitro* evaluation of antibiotic diffusion from antibiotic-impregnated biodegradable beads and polymethylmethacrylate beads. Antimicrob Agents Chemother. 1997 Feb;41(2):415-8.

14. Nelson CL, Griffin FM, Harrison BH, Cooper RE. *In vitro* elution characteristics of commercially and noncommercially prepared antibiotic PMMA beads. Clin Orthop Relat Res. 1992 Nov(284):303-9.

15. Beardmore AA, Brooks DE, Wenke JC, Thomas DB. Effectiveness of local antibiotic delivery with an osteoinductive and osteoconductive bone-graft substitute. J Bone Joint Surg Am. 2005 Jan;87(1):107-12.

16. Gitelis S, Brebach GT. The treatment of chronic osteomyelitis with a biodegradable antibiotic-impregnated implant. J Orthop Surg (Hong Kong). 2002 Jun;10(1):53-60.

17. McKee MD, Wild LM, Schemitsch EH, Waddell JP. The use of an antibiotic-impregnated, osteoconductive, bioabsorbable bone substitute in the treatment of infected long bone defects: early results of a prospective trial. J Orthop Trauma. 2002 Oct;16(9):622-7.

18. McLaren AC. Alternative materials to acrylic bone cement for delivery of depot antibiotics in orthopaedic infections. Clin Orthop Relat Res. 2004 Oct(427):101-6.

19. Gung YW, Cheng CK, Su CY. A stereomorphologic study of bone matrix apposition in HA-implanted cavities observed with SEM, being prepared by a microvascular cast and freeze-fracture method. Med Eng Phys. 2003 Sep;25(7):565-71.

20. Lienau J, Schmidt-Bleek K, Peters A, Haschke F, Duda GN, Perka C, et al. Differential regulation of blood vessel formation between standard and delayed bone healing. J Orthop Res. 2009 Sep;27(9):1133-40.

21. Li R, Stewart DJ, von Schroeder HP, Mackinnon ES, Schemitsch EH. Effect of cell-based VEGF gene therapy on healing of a segmental bone defect. J Orthop Res. 2009 Jan;27(1):8-14.

22. Geiger F, Bertram H, Berger I, Lorenz H, Wall O, Eckhardt C, et al. Vascular endothelial growth factor gene-activated matrix (VEGF165-GAM) enhances osteogenesis and angiogenesis in large segmental bone defects. J Bone Miner Res. 2005 Nov;20(11):2028-35.

23. Li B, Yoshii T, Hafeman AE, Nyman JS, Wenke JC, Guelcher SA. The effects of rhBMP-2 released from biodegradable polyurethane/microsphere composite scaffolds on new bone formation in rat femora. Biomaterials. 2009 Dec;30(35):6768-79.

24. Adhikari R, Gunatillake PA, Griffiths I, Tatai L, Wickramaratna M, Houshyar S, et al. Biodegradable injectable polyurethanes: synthesis and evaluation for orthopaedic applications. Biomaterials. 2008 Oct;29(28):3762-70.

25. Gorna K, Gogolewski S. Preparation, degradation, and calcification of biodegradable polyurethane foams for bone graft substitutes. Journal of Biomedical Materials Research Part A. 2003;67A(3):813-27.

26. Hafeman AE, Zienkiewicz KJ, Carney E, Litzner B, Stratton C, Wenke JC, et al. Local delivery of tobramycin from injectable biodegradable polyurethane scaffolds. J Biomaterials Science. 2009;DOI:10.1163/156856209X410256.

27. Kwok CS, Wan C, Hendricks S, Bryers JD, Horbett TA, Ratner BD. Design of infection-resistant antibiotic-releasing polymers: I. Fabrication and formulation. J Control Release. 1999 Dec 6;62(3):289-99.

28. Schierholz JM, Steinhauser H, Rump AF, Berkels R, Pulverer G. Controlled release of antibiotics from biomedical polyurethanes: morphological and structural features. Biomaterials. 1997 Jun;18(12):839-44.

29. Ruggeri V, Francolini I, Donelli G, Piozzi A. Synthesis, characterization, and *in vitro* activity of antibiotic releasing polyurethanes to prevent bacterial resistance. J Biomed Mater Res A. 2007 May;81(2):287-98.

30. Li B, Davidson JM, Guelcher SA. The effect of the local delivery of platelet-derived growth factor from reactive two-component polyurethane scaffolds on the healing in rat skin excisional wounds. Biomaterials. 2009 Jul;30(20):3486-94.

31. Guan J, Stankus JJ, Wagner WR. Biodegradable elastomeric scaffolds with basic fibroblast growth factor release. Journal of Controlled Release. 2007;120(1-2):70-8.

32. Lee SH, Lee JE, Baek WY, Lim JO. Regional delivery of vancomycin using pluronic F-127 to inhibit methicillin resistant Staphylococcus aureus (MRSA) growth in chronic otitis media *in vitro* and *in vivo*. J Control Release. 2004 Apr 16;96(1):1-7.

33. Stigter M, Bezemer J, de Groot K, Layrolle P. Incorporation of different antibiotics into carbonated hydroxyapatite coatings on titanium implants, release and antibiotic efficacy. J Control Release. 2004 Sep 14;99(1):127-37.

34. Edin ML, Miclau T, Lester GE, Lindsey RW, Dahners LE. Effect of cefazolin and vancomycin on osteoblasts *in vitro*. Clin Orthop Relat Res. 1996 Dec(333):245-51.

35. Antoci V, Jr., Adams CS, Hickok NJ, Shapiro IM, Parvizi J. Antibiotics for local delivery systems cause skeletal cell toxicity *in vitro*. Clin Orthop Relat Res. 2007 Sep;462:200-6.

36. Haleem AA, Rouse MS, Lewallen DG, Hanssen AD, Steckelberg JM, Patel R. Gentamicin and vancomycin do not impair experimental fracture healing. Clinical Orthopaedics and Related Research. 2004 Oct(427):22-4.

37. Kluin OS, van der Mei HC, Busscher HJ, Neut D. A surface-eroding antibiotic delivery system based on poly(trimethylene carbonate). Biomaterials. 2009 Jun 3.

38. Kell AJ, Stewart G, Ryan S, Peytavi R, Boissinot M, Huletsky A, et al. Vancomycin-modified nanoparticles for efficient targeting and preconcentration of Gram-positive and Gram-negative bacteria. ACS Nano. 2008 Sep 23;2(9):1777-88.

39. Ambrose CG, Gogola GR, Clyburn TA, Raymond AK, Peng AS, Mikos AG. Antibiotic microspheres: preliminary testing for potential treatment of osteomyelitis. Clin Orthop Relat Res. 2003 Oct(415):279-85.

40. Takacsnovak K, Noszal B, Tokeskovesdi M, Szasz G. Acid-Base Properties and Proton-Speciation of Vancomycin. International Journal of Pharmaceutics. 1993 Feb 5;89(3):261-3.

41. Guelcher SA, Srinivasan A, Hafeman AE, Gallagher KM, Doctor JS, Khetan S, et al. Synthesis, *in vitro* degradation, and mechanical properties of two-component poly(ester urethane)urea scaffolds: effects of water and polyol composition. Tissue Eng. 2007;13(9):2321-33.

42. Ruiz JC, Alvarez-Lorenzo C, Taboada P, Burillo G, Bucio E, De Prijck K, et al. Polypropylene grafted with smart polymers (PNIPAAm/PAAc) for loading and controlled release of vancomycin. Eur J Pharm Biopharm. 2008 Oct;70(2):467-77.

43. Adams CS, Antoci V, Jr., Harrison G, Patal P, Freeman TA, Shapiro IM, et al. Controlled release of vancomycin from thin sol-gel films on implant surfaces successfully controls osteomyelitis. J Orthop Res. 2009 Jun;27(6):701-9.

44. Gbureck U, Vorndran E, Barralet JE. Modeling vancomycin release kinetics from microporous calcium phosphate ceramics comparing static and dynamic immersion conditions. Acta Biomater. 2008 Sep;4(5):1480-6.

45. Jørgensen K, Jacobsen L. Factorial design used for ruggedness testing of flow through cell dissolution method by means of Weibull transformed drug release profiles. Int J Pharm. 1992;88(1-3):23-9.

46. Papadopoulou V, Kosmidis K, Vlachou M, Macheras P. On the use of the Weibull function for the discernment of drug release mechanisms. Int J Pharm. 2006 Feb 17;309(1-2):44-50.

47. Chen X, Tsukayama DT, Kidder LS, Bourgeault CA, Schmidt AH, Lew WD. Characterization of a chronic infection in an internally-stabilized segmental defect in the rat femur. J Orthop Res. 2005 Jul;23(4):816-23.

48. Anglen JO. Comparison of soap and antibiotic solutions for irrigation of lower-limb open fracture wounds. A prospective, randomized study. J Bone Joint Surg Am. 2005 Jul;87(7):1415-22.

49. Brown KV, Walker JA, Cortez DS, Murray CK, Wenke JC. Earlier Debridement and Antibiotic Administration Decreases Infection. Journal of Surgical Orthopaedic Advances. 2009, Accepted.

50. Mason EO, Lamberth LB, Hammerman WA, Hulten KG, Versalovic J, Kaplan SL. Vancomycin MICs for Staphylococcus aureus vary by detection method and have subtly increased in a pediatric population since 2005. J Clin Microbiol. 2009 Jun;47(6):1628-30.

51. Coudron PE, Johnston JL, Archer GL. In-vitro activity of LY146032 against Staphylococcus aureus and S. epidermidis. J Antimicrob Chemother. 1987 Oct;20(4):505-11.

52. Xie Z, Liu X, Jia W, Zhang C, Huang W, Wang J. Treatment of osteomyelitis and repair of bone defect by degradable bioactive borate glass releasing vancomycin. J Control Release. 2009 Jun 21.

53. Gbureck U, Vorndran E, Muller FA, Barralet JE. Low temperature direct 3D printed bioceramics and biocomposites as drug release matrices. J Control Release. 2007 Sep 26;122(2):173-80.

54. Hafeman AE, Li B, Yoshii T, Zienkiewicz K, Davidson JM, Guelcher SA. Injectable biodegradable polyurethane scaffolds with release of platelet-derived growth factor for tissue repair and regeneration. PharmRes. 2008;25(10):2387-99.

55. Loo Y, Leong KW. Biomaterials for Drug and Gene Delivery. In An Introduction to Biomaterials, J.O. Hollinger and S.A. Guelcher, eds. Boca Raton, CRC Press 2005.

56. Hsieh PH, Shih CH, Chang YH, Lee MS, Shih HN, Yang WE. Two-stage revision hip arthroplasty for infection: comparison between the interim use of antibiotic-loaded cement beads and a spacer prosthesis. J Bone Joint Surg Am. 2004 Sep;86-A(9):1989-97.

57. Anagnostakos K, Furst O, Kelm J. Antibiotic-impregnated PMMA hip spacers: Current status. Acta Orthop. 2006 Aug;77(4):628-37.

58. Efstathopoulos N, Giamarellos-Bourboulis E, Kanellakopoulou K, Lazarettos I, Giannoudis P, Frangia K, et al. Treatment of experimental osteomyelitis by methicillin resistant Staphylococcus aureus with bone cement system releasing grepafloxacin. Injury. 2008 Dec;39(12):1384-90.

59. Niikura T, Tsujimoto K, Yoshiya S, Tadokoro K, Kurosaka M, Shiba R. Vancomycin-impregnated calcium phosphate cement for methicillin-resistant Staphylococcus aureus femoral osteomyelitis. Orthopedics. 2007 Apr;30(4):320-1.

60. Tuzuner T, Sencan I, Ozdemir D, Alper M, Duman S, Yavuz T, et al. *In vivo* evaluation of teicoplanin- and calcium sulfate-loaded PMMA bone cement in preventing implant-related osteomyelitis in rats. J Chemother. 2006 Dec;18(6):628-33.

61. Magnan B, Regis D, Biscaglia R, Bartolozzi P. Preformed acrylic bone cement spacer loaded with antibiotics: use of two-stage procedure in 10 patients because of infected hips after total replacement. Acta Orthop Scand. 2001 Dec;72(6):591-4.

62. Hsieh PH, Chang YH, Chen SH, Ueng SW, Shih CH. High concentration and bioactivity of vancomycin and aztreonam eluted from Simplex cement spacers in two-stage revision of infected hip implants: a study of 46 patients at an average follow-up of 107 days. J Orthop Res. 2006 Aug;24(8):1615-21.

63. Cui Q, Mihalko WM, Shields JS, Ries M, Saleh KJ. Antibiotic-impregnated cement spacers for the treatment of infection associated with total hip or knee arthroplasty. J Bone Joint Surg Am. 2007 Apr;89(4):871-82.

64. Malchau H, Herberts P, Eisler T, Garellick G, Soderman P. The Swedish Total Hip Replacement Register. J Bone Joint Surg Am. 2002;84-A Suppl 2:2-20.

65. Thomes B, Murray P, Bouchier-Hayes D. Development of resistant strains of Staphylococcus epidermidis on gentamicin-loaded bone cement *in vivo*. J Bone Joint Surg Br. 2002 Jul;84(5):758-60.

66. Masri BA, Duncan CP, Beauchamp CP. Long-term elution of antibiotics from bone-cement: an *in vivo* study using the prosthesis of antibiotic-loaded acrylic cement (PROSTALAC) system. J Arthroplasty. 1998 Apr;13(3):331-8.

67. Chen X, Kidder LS, Lew WD. Osteogenic protein-1 induced bone formation in an infected segmental defect in the rat femur. J Orthop Res. 2002 Jan;20(1):142-50.

68. Chen X, Schmidt AH, Tsukayama DT, Bourgeault CA, Lew WD. Recombinant human osteogenic protein-1 induces bone formation in a chronically infected, internally stabilized segmental defect in the rat femur. J Bone Joint Surg Am. 2006 Jul;88(7):1510-23.

CHAPTER V

INFECTED BONE WOUND HEALING PROMOTED BY DUAL DELIVERY OF VANCOMYCIN FREE BASE AND BONE MORPHOGENETIC PROTEIN FROM BIODEGRADABLE POLYURETHANE SCAFFOLD IMPLANTS

Abstract

Infection is the most common factor compromising bone wound healing. The present standard care is a two-stage approach comprising infection control followed by bone grafting. While complications may also arise from the wound healing process, it is critical to control infection in the graft as well. In previous studies, we have developed bioactive porous polyurethane (PUR) scaffolds for delivery of growth factor and antibiotic individually. The objective of present study is to combine both drugs in the same PUR composite, thereby enabling both infection control and wound healing to take place simultaneously. Bone morphogenetic protein (rhBMP-2) was incorporated in the composite to achieve a release profile containing an initial burst followed by sustained release. Vancomycin free base (V-FB) was incorporated in the composite with sustained release kinetics as demonstrated previously. PUR/rhBMP-2/V-FB was first tested in a non-infected critical size rat femoral segmental defect, and was found to perform slightly better than PUR/rhBMP-2 due to the fact the leaching of V-FB created more space in the scaffold which allowed more cells recruitment. Then we tested PUR/rhBMP-2/V-FB in the infected critical size rat femoral segmental defect, which performed significantly better than both PUR/rhBMP-2 and collagen/rhBMP-2 due to the introduction of infection control during the bone wound healing process. This strategy of protecting the graft from infection during

wound healing eliminates an extra surgical removal step in current clinical standard care, thereby presenting a potentially significant innovation in the clinical treatment of infected bone wounds.

Introduction

Complications resulting from wound infection are detrimental to bone tissue healing. In severe high energy bone wounds with large surface areas of tissue exposed, infection is the most important cause of morbidity and it can lead to undesirable consequences such as delay of union, non-union, and even amputation (1).

Currently, the clinical standard of care for treating contaminated open fractures comprises two steps, wherein the wound is first treated with antibiotics, for example, through non-degradable PMMA cement beads which have to be surgically removed afterward, followed by bone grafting. Growth factors are frequently added to the graft to facilitate cell immigration and new bone formation. In practice, poly(methyl methacrylate) (PMMA) cement beads have been used as the local antibiotic delivery platform, which has been shown to decrease infection in a number of clinical studies (2-4). However, since PMMA does not biodegrade, it must be removed during an additional surgical step and cannot be allowed to remain in the wound bed during definitive closure. Furthermore, the antibiotic release efficiency is typically low and the antibiotics are below therapeutic levels within a week or two (5-8). When the infection under control, the PMMA beads are surgically removed, and the wound is treated with bone graft materials such as natural or synthetic scaffolds. Clinically rhBMP-2 delivered from a collage sponge (INFUSE® Bone Graft) is an FDA-approved therapy for posterior-lateral spine, lower leg (tibia), and certain dental applications. However, the collagen delivery system results in a bolus release of

growth factor in the first several hours (9), which may contribute to the requirement of high rhBMP-2 dosage (10, 11) and results in epitomic bone formation (12, 13).

While treatment with antibiotic-laden PMMA beads may effectively control infection in the wound bed prior to bone grafting, cases of secondary infectious complications have been reported (14) due to the absence of the antibiotic. Furthermore, although effective at promoting bone growth, the foreign bone graft material could potentially function as a nidus for infection due to lack of vascularity. Therefore, it is critical to provide infection control during the bone regeneration process. Since angiogenesis which takes up to six weeks (15, 16) is a prerequisite for bone ingrowth in the graft material, it is desirable to introduce effective antibiotic release in the scaffolds within that period in order to allow bone wounds to heal normally.

Biodegradable PUR scaffolds facilitate the tuning polymer structure to achieve the desired properties for a variety of tissue engineering applications (17-22). Porous PUR scaffolds support cell ingrowth (19, 23-25) and function as drug delivery system (26-28). We previously showed that a modest burst release of rhBMP-2 followed by sustained release is essential for bone regeneration in rat femoral defects (28). The initial release of growth factor was responsible for recruiting cells while the sustained release promoted differentiation of osteoprogenitor cells into osteoblasts. Sustained release of vancomycin was also achieved by converting vancomycin hydrochloride (V-HCl) into less soluble vancomycin free base (V-FB) which translated to better *in vivo* performance for infection control (26).

The hypothesis of this study is that the biodegradable composite PUR incorporating with both the growth factor rhBMP-2 and the antibiotic vancomycin (PUR/rhBMP-2/V-FB)

wound provide control infection and enhance bone regeneration simultaneously for the treatment of infected bone wounds. The scaffolds would biodegrade *in vivo* to non-cytotoxic products, eliminating the secondary removal surgical procedure required in the current clinical standard care.

Materials and methods

Materials

Glycolide and D,L-lactide were obtained from Polysciences (Warrington, PA). The tertiary amine catalyst TEGOAMIN33, which comprised a 33 wt% solution of triethylene diamine (TEDA) in dipropylene glycol, was received from Goldschmidt (Hopewell, VA) as a gift. Lysine triisocyanate (LTI) was purchased from Kyowa Hakko (New York, NY). Stannous octoate catalyst was received from Nusil technology (Overland Park, KS). Glucose were from Acros Organics (Morris Plains, NJ). Vancomycin hydrochloride (V-HCl) was purchased from ACROS organics. Recombinant human bone morphogenetic protein-2 (rhBMP-2) was purchased from R&D systems (Minneapolis, MN). All other reagents were purchased from Sigma-Aldrich (St. Louis, MO).

Synthesis of polyester triol and PUR scaffolds

Polyester triols (900 Da) were prepared from a glycerol starter and a backbone comprising [70wt% ε-caprolactone, 20wt% glycolide, and 10wt% D,L-lactide] as published previously (17, 19). PUR scaffolds were synthesized by one-shot reactive liquid molding of lysine triisocyanate (LTI) and a hardener comprising 900-Da polyol, 1.5~2.0 parts per hundred parts polyol (pphp) water, 4.5 pphp TEGOAMIN33 tertiary amine catalyst, 1.5 pphp sulfated castor oil stabilizer, and 4.0 pphp calcium stearate pore opener. The isocyanate was added to the hardener, mixed for 30 s in a Hauschild SpeedMixer™ DAC 150

FVZ-K vortex mixer (FlackTek, Inc., Landrum, SC), and the resulting liquid mixture poured into a cylindrical mold where it cured as a free-rise foam after ~20 minutes (17, 19). The targeted index (the ratio of NCO to OH equivalents × 100) was 115 for all scaffolds. In order to incorporate drugs into PUR scaffolds, lyophilized rhBMP-2 powder (in presence of heparin and glucose) and V-FB powder were added to the hardener component before mixing with the isocyanate as indicated in specific formulations (Table V-1). Two dosages of rhBMP-2 were chosen: 2.5 μg per implant (low, 60 μg per ml scaffold) as used in previous studies (28), and 25 μg per implant (high, 600 μg per ml scaffold) since infection might compromise outcome of rhBMP-2.

Table V-1 Summary of scaffold formulations for dual delivery studies.

Scaffold formulation	**Description**
PUR + rhBMP2 (Low)	2.5 μg rhBMP-2 per implant embedded in PUR
PUR + rhBMP2 (High)	25 μg rhBMP-2 per implant embedded in PUR
PUR + V-FB + rhBMP2 (Low)	2.5 μg rhBMP-2 and 340 μg V-FB per implant embedded in PUR
PUR + V-FB + rhBMP2 (High)	25 μg rhBMP-2 and 340 μg V-FB per implant embedded in PUR
Collagen + rhBMP2 (Low)	2.5 μg rhBMP-2 per implant, adsorbed on collagen surface
Collagen + rhBMP2 (High)	25 μg rhBMP-2 per implant, adsorbed on collagen surface

In vitro release of rhBMP-2

Three replicate scaffold samples (~50 mg) containing 2.5 μg rhBMP-2 were immersed in 1 ml release medium (α-MEM incorporating 1% BSA) contained in polypropylene vials sealed by O-rings. BSA were included to minimize adsorption of rhBMP-2 onto the scaffolds and vials (27). The medium of PUR samples was refreshed every 24 h to minimize

degradation of the growth factor (27), and the medium of collagen samples was refreshed as indicated in the plot. The rhBMP-2 concentration of daily pools as indicated in the cumulative release plot was determined using a Human BMP-2 Quantikine ELISA kit (R&D systems, Minneapolis, MN).

In vitro release of V-FB

Three replicate PUR scaffold samples (~40 mg, 0.4 ml) were immersed in 1 ml PBS in polypropylene vials sealed by O-rings. At days indicated in the release curve, the medium was recovered by gently squeezing the scaffolds, followed by the addition of 1 ml fresh medium(29). The concentration of vancomycin released at each time point was determined by measuring the absorbance at 280 nm, from which the concentration was calculated using a standard calibration curve (30, 31).

In vivo test in non-infected critical size rat femoral segmental defect

Table V-2 Treatment groups in non-infected segmental defect for dual delivery studies.

Scaffold formulation	**Description**
PUR + rhBMP2 (Low)	2.5 μg rhBMP-2 per implant (60 μg per ml)
PUR + rhBMP2 (High)	25 μg rhBMP-2 per implant (600 μg per ml)
PUR + V-FB + rhBMP2 (Low)	2.5 μg rhBMP-2, 340 μg V-FB per implant
PUR + V-FB + rhBMP2 (High)	25 μg rhBMP-2, 340 μg V-FB per implant

A previously described rat femur critical sized defect model (32) was used to investigate the difference in bone regeneration between recombinant BMP-2 (rhBMP-2) delivered from PUR, with or without V-FB. The treatment groups are listed below (Table V-2). In

conducting the research described in this report, the investigators adhered to the Guide for the Care and Use of Laboratory Animals by the Institute of Laboratory Animal Resources, National Research Council, in accordance with the stipulations mandated for an AAALAC accredited facility. The methods used for the critical size defect creation and fixation are described previously (33). Briefly, a 6 mm segmental defect was created and stabilized under aseptic conditions in the left femur of rats. Using aseptic technique, a longitudinal incision was made over the left anterolateral femur, and the entire femoral shaft was exposed using blunt dissection. A polyacetyl plate (length 25 mm, width 4 mm and height 4 mm) was fixed to the surface of the femur using 6 K-wires. A 6 mm mid-diaphyseal full-thickness defect was created with a small reciprocating saw blade (MicroAire 1025, MicroAire, Charlottesville, VA) under continuous irrigation with sterile saline. The defects in all animals were implanted either collagen sponge implant or PUR scaffold (6×3 mm). The wound was closed in a layered fashion. A high-resolution radiograph of each femur with the stabilized defect was obtained using a Faxitron X-ray system (Faxitron X-ray Corporation, Wheeling, Illinois (Model: MX-20) Image settings Time: 15 Sec KV: 35 Window Level: 3380/1250) at initial surgery to confirm correct placement of the implant. The animals were allowed full activity in their cages postoperatively, administered adequate analgesia (IM buprenorphine) and monitored daily for signs of pain and systemic infection. The animals were euthanized 4 weeks later with Fatal Plus. The femurs were harvested and immersed in formalin for 48 hours then 70% alcohol for further assessment of regenerated bone volume and histology.

The samples were scanned using micro computed tomography (CT) SkyScan 1076 (Skyscan, Aartselaar, Belgium) at 100 kV source voltage and 100 μA source current with no filter used and at a spatial resolution of 8.77 μm. The reconstructions were performed using NRecon software (Skyscan, Aartselaar, Belgium) and resulted in grayscale images spanning

a density range from 1.35 to 5.34 gm/cm^3 corresponding to gray scale values 0 to 255. DataViewer (Skyscan, Aartselaar, Belgium) was used to reslice the CT images along coronal sections which were used to reorient the CT slices to be perpendicular to the axis of the femurs and CT thresholding was performed to include only ossified tissues. The thresholds were selected as the histogram minima between the peaks representing the formalin in which the sample was scanned and the bone volume of the sample. The geometric mean of the threshold for all 100 samples in the study was used to determine the upper and lower threshold for binarization as 39 and 250, which corresponds to a density span of 1.97 to 5.27 gm/cm^3. The region of interest was chosen by creating a volume that spanned 6 mm from the proximal to the distal interface of the native bone to include the entire defect generated. The total volume of bone ingrowth in this 3D volume was computed using CTAn software (Skyscan, Aartselaar, Belgium). The average bone density of the regenerated bone was determined from the mean grayscale value of the pixels included in the binarized selection. The bone volume was multiplied by this average bone density to calculate regenerated bone mass, which thus effectively accounted for both bone quantity (volume) and quality (density).

In vivo test in infected critical size rat femoral segmental defect

The animal study was approved by the Animal Care and Use Committee at the US Army Institute of Surgical Research. A previously described contaminated critical size defect (CSD) was created in the rat (Sprague-Dawley) femurs (32). Briefly, a 6 mm segmental defect was created and stabilized under aseptic conditions the rats as described above. The defects in all animals were then implanted with 30 mg of type I bovine collagen (Stryker Biotech, Hopkinton, MA, USA) that was ethanol sterilized and subsequently wetted with 105 of colony forming units (CFUs) of Staphylococcus aureus lux (Xenogen 36, Caliper Life Science, Hopkinton, MA) suspended in 0.1 ml of sterile normal saline. This isolate was transgenically

modified to emit photons and was sensitive to vancomycin. The contaminated collagen was packed into the defect, and the wound closed in a layered fashion. A high-resolution radiograph of each femur with stabilized defect was obtained using a Faxitron X-ray system (Faxitron X-ray Corporation, Wheeling, Illinois (Model: MX-20, Image settings Time: 10 Sec, KV: 35, Window Level: 3380/1250) at initial surgery to confirm appropriate placement of the implant and adequate creation of the defect.

Six hours after contamination, the wounds were debrided and irrigated with 60 ml of saline (32). This time period was chosen because it is clinically relevant (34). Model development work demonstrated that a 6-hr delay was the ideal time for treatment with local antibiotics (35). The wounds were treated with collagen or PUR as described in Table V-1. The collagen sponge (MedChem Products, Inc., Woburn, MA) was cut under sterile conditions into 6 x 3 mm implants, each loaded with the appropriate dose rhBMP-2 (R&D Systems, Minneapolis, MN) in solution for 15 minutes prior to implantation (as per manufacturer's directive). The animals were allowed full activity in their cages postoperatively, and were monitored daily for signs of pain and systemic infection. Following 8 weeks of recovery, the rats were euthanized by Fatal Plus.

The samples were scanned using μCT as described above. The percent of animals with clinical sign of infection was examined.

Results

In vitro dual release of V-FB and rhBMP-2 from PUR

Both the antibiotic and growth factor were incorporated in PUR scaffolds by mixing with the hardener component before reacting with isocyanate. The release profiles of both V-FB and rhBMP-2 were similar to those when each drug was incorporated in PUR

individually (Figure V-1). There is a burst release of rhBMP-2 within the first few days followed by sustained gradual release for up to 20 days tested. This is important as we have previously demonstrated that both burst release and sustained release of rhBMP-2 are essential for bone tissue regeneration, due to the fact that burst release of rhBMP-2 participates in both early cellular events including cell recruitment and angiogenesis and later stage to differentiate stem cells into osteoblasts (28). The release of V-FB is characterized by a small burst release followed by sustained release for 3 weeks, which is consistent with previous report that effective concentration release of V-FB can be extended for up to 8 weeks (36).

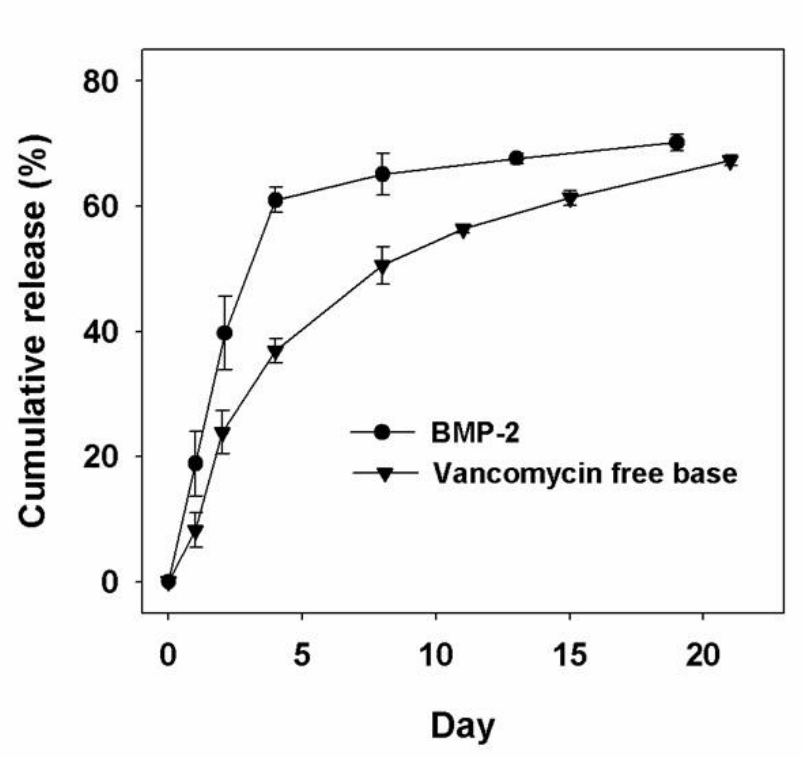

Figure V-1 *In vitro* release of rhBMP-2 and V-FB from PUR/rhBMP-2/V-FB separately. The release experiment was carried out in α-MEM and PBS for rhBMP-2 and V-FB respectively, with medium refreshed every 24 h for rhBMP-2 and as indicated for V-FB.

Test of PUR scaffolds in a non-infected rat femoral segmental defect

Using PUR/rhBMP-2 as control, the PUR/rhBMP-2/V-FB implants were tested in the non-infected rat femoral segmental defect, to evaluate whether the presence of antibiotic would compromise the osteogenic effect of rhBMP-2. Since the presence of antibiotic in the scaffold could compromise the effect of growth factor (37, 38), we tested two rhBMP-2 dosages in this study: 60 μg per ml (low dosage, used in previous studies (28)) and 600 μg per ml (high dosage).

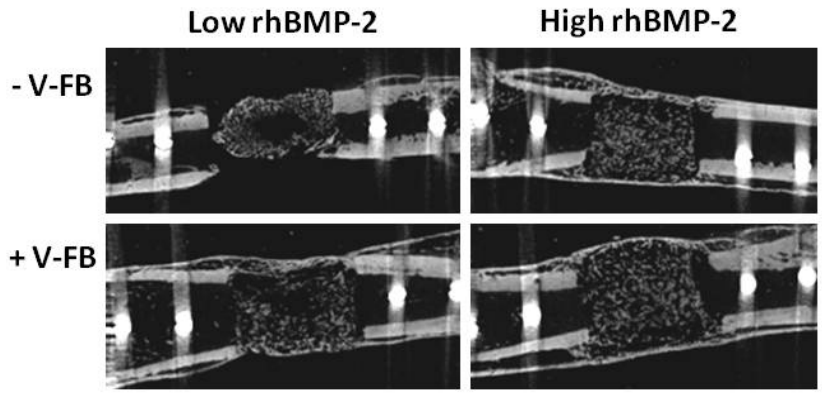

Figure V-2 Representative μCT images at week 4 from the non-infected segmental defect study. PUR implants with both rhBMP-2 dosages were tested, with or without the presence of V-FB.

At 4 weeks, the defects were harvested and both X-ray and μCT images were acquired to examine the amount of new bone formation within the scaffolds. Both representative μCT images (Figure V-2) and quantitative analysis (Figure V-3) shows an rhBMP-2 dosage dependant effect on new bone formation and significant differences exist between two rhBMP-2 dosages with or without V-FB. The presence of V-FB does not compromise the morphogenetic function of rhBMP-2 in promoting new bone formation. In fact, V-FB increases the amount of new bone in the defects especially at low dosage of rhBMP-2, although there is no significant difference exists between treatment groups with or without V-FB at either rhBMP-2 dosage.

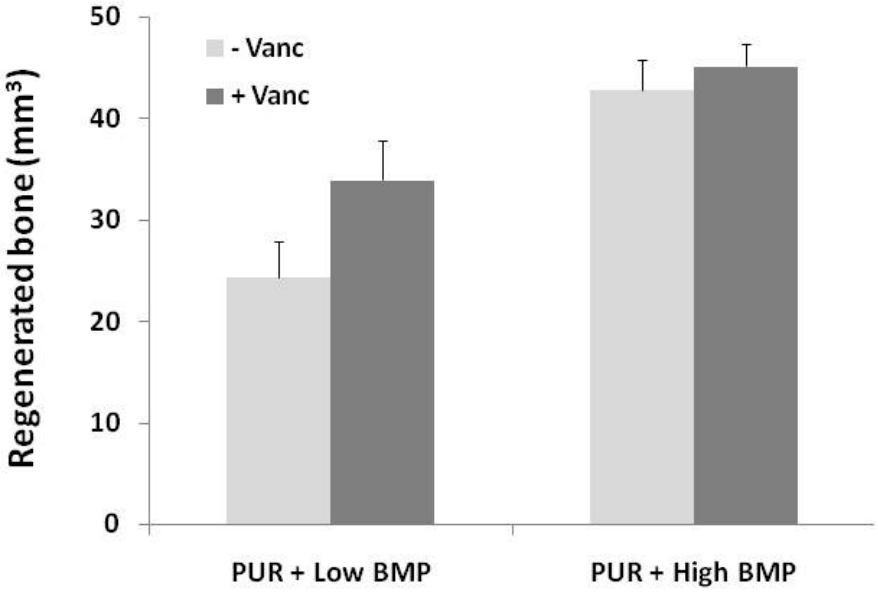

Figure V-3 Quantitative μCT analysis on new bone formation in the non-infected segmental defect study, showing no compromising effect of V-FB on the osteogenic effect of rhBMP-2.

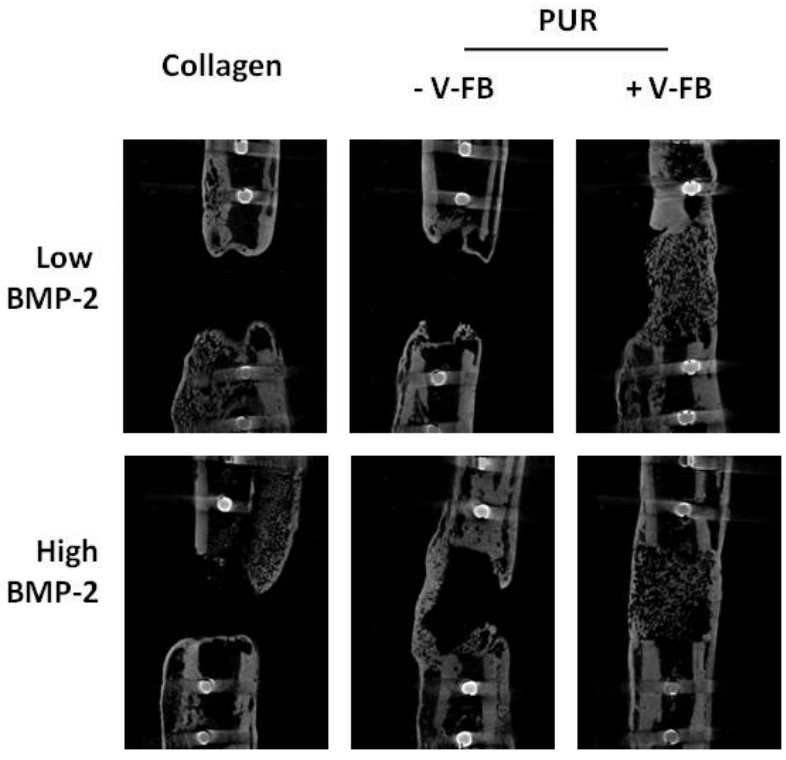

Figure V-4 Test of PUR with rhBMP-2 and V-FB in the infected rat segmental defect, using collagen adsorbed with rhBMP-2 as control. Two rhBMP-2 dosages were chosen.

Test of PUR/rhBMP-2/V-FB implants in an infected rat femoral segmental defect

Using collagen filled with rhBMP-2 as a clinical control, the PUR/rhBMP-2 and PUR/rhBMP-2/V-FB implants were tested in the infected rat femoral segmental defect to evaluate whether the presence of both the antibiotic and the growth factor would enhance the healing of an infected bone wound compared with the clinical standard of care which uses a collagen sponge filled with rhBMP-2 solution. Since the presence of infection could potentially compromise bone wound healing promoted by the growth factor (1), we again used two rhBMP-2 dosages as described previously.

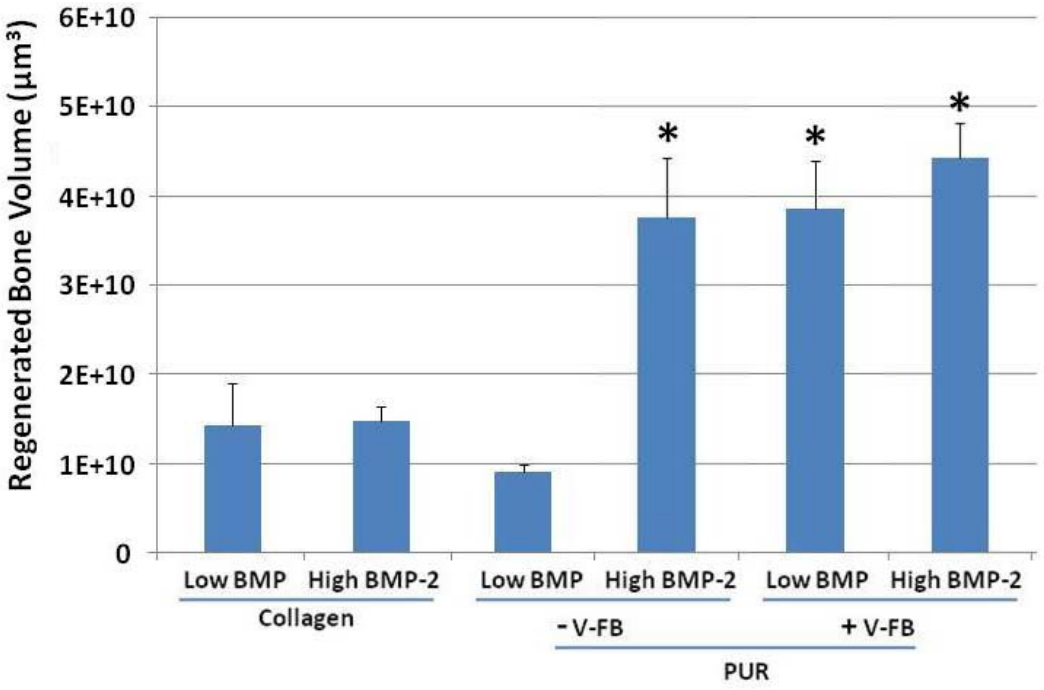

Figure V-5 Quantitative µCT analysis on new bone formation in the infected segmental defect study, and * denotes statistical significance of the group compared with collagen groups.

At 8 weeks, the defects were harvested and both X-ray and µCT images were acquired to examine the amount of new bone formation within the scaffolds. The representative µCT

images (Figure V-4) and quantitative analysis (Figure V-5) shows that collagen groups at either dosages of rhBMP-2 generated only a small amount of bone in the infected segmental defects. PUR with low rhBMP-2 dosage generated little bone, but PUR with high rhBMP-2 dosage generated significantly more bone volume compared with PUR with low rhBMP-2 dosage group and both collagen groups. When V-FB is present, PUR at either dosage generated significantly more new bone compared with collagen groups.

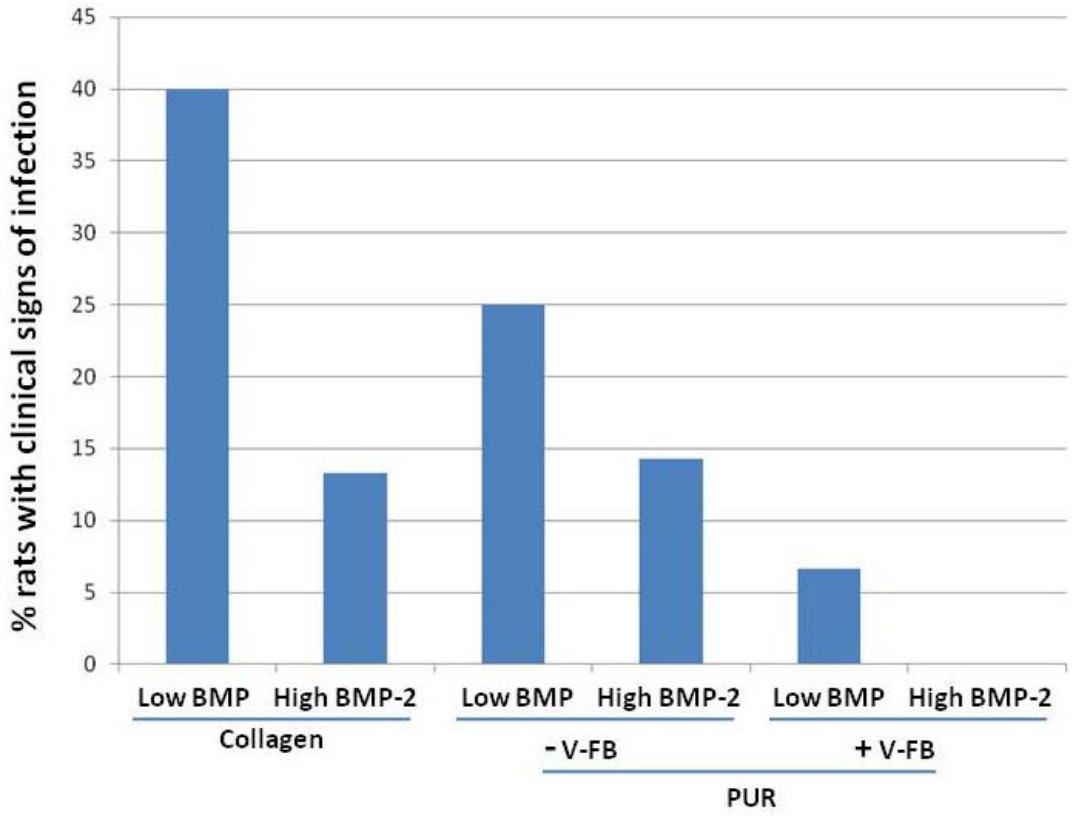

Figure V-6 Percentage of rats with signs of infection at week 8 in each treatment group from infected segmental defect study.

Interestingly, the trend of new bone formation is consistent with the clinical infection rate observed. As shown in Figure V-6, when counting the number of rats with infection at the end of the experiment, PUR treatment exhibited lower infection rate compared with collagen treatment at both dosages, and the infection decreased further when V-FB was

present in the scaffold. The PUR treatment group with both high BMP-2 dosage and V-FB showed no clinical signs of infection.

Discussion

Due to the fact that infection is the most observed cause of compromised bone wound healing (1), it is desired to inhibit contamination in wounds especially open fractures to allow bone regeneration to proceed normally. The current standard of care comprises a staged approach wherein a first stage of infection control typically through non-biodegradable PMMA beads is followed by a second bone grafting stage. A significant disadvantage of the approach is that a removal surgery is required for the PMMA beads to allow bone healing. We hypothesized that combining both a growth factor and an antibiotic in the same biodegradable and biocompatible scaffold, the controlled release of those biologics would be expected to control infection and promote bone healing simultaneously. Since the scaffold would disappear by itself during the wound healing process, there is no secondary removal surgery required, which is a significant contributor for the patient outcomes.

Due to the excellent properties of PUR, such as adjustable degradability to non toxic products (17), biocompatibility for cell infiltration and tissue ingrowth and ability to delivery drugs with controlled release kinetics (26-28), it is a promising candidate for bone tissue engineering and clinical applications. We have previously shown that rhBMP-2 release can be adjusted by a PLGA microspheres encapsulation strategy, and the animal studies showed that both a burst release and a sustained release are required to optimize new bone formation (28). Vancomycin was chosen as a model antibiotic and the decreased solubility through converting vancomycin hydrochloride to vancomycin free base resulted in better controlled release profile with extended effective concentration release for up to at

least 8 weeks (36). The strategies used for optimizing the release profiles of both rhBMP-2 and vancomycin were therefore combined in the same PUR scaffolds, which were tested in both an uninfected rat femoral segmental defect and an infected defect which reveal the synergistic effects of these drugs in promoting healing of infected fractures.

Vancomycin was reported to have a less negative effect on new bone formation than other antibiotics (37, 38), and has also been demonstrated not to compromise the morphogetic effect of rhBMP-2 in the present non-infected animal studies. In fact, the presence of vancomycin enhanced the performance of rhBMP-2 slightly, although the difference is not significant. It is conjectured that the leaching of 8 wt% of vancomycin created additional pores within the scaffold which allowed more cellular infiltration and thus new bone formation. In the infected segmental defect, we observed that increased rhBMP-2 dosage in PUR promoted more new bone formation and decreased infection rate of the animals, potentially due to the fact that the release of more rhBMP-2 enhanced angiogenesis, which both increased new bone formation and enhanced infection control (15, 39). The presence of V-FB in PUR decreased the infection rate at both rhBMP-2 dosages which relates to more new bone formation. There is a significant difference in terms of the amount of new bone between PUR/rhBMP-2(low)/V-FB and PUR/rhBMP-2(low). For the high dose of rhBMP-2, the presence of V-FB in the scaffold eliminated the clinical signs of infection completely. Therefore, the V-FB and rhBMP-2 performed synergistically to promote healing of infected bone defects by controlling infection and enhancing new bone formation simultaneously.

The biodegradable porous scaffold plus biologics system provides a suitable platform for cellular ingrowth and tissue formation. However, the initial cellular infiltration stage is a prerequisite for the wound healing process. Therefore, it would be advantageous if cells

could be delivered as well, which is expected to accelerate new bone formation. In the segmental bone defect studies, we observed very slow polymer degradation due to the absence of inflammatory cells which is essential in degrading polyurethanes through the release of reactive oxygen species and enzymes such as cholesterol esterase, esterase, and carboxyl esterase (40-43). The slow degradation of polymer appears to have impeded cellular infiltration. Therefore, it is desired to adjust the polymer degradation profiles to better match rate of ingrowth of new bone. In future studies, the potential of an injectable (44) dual delivery system will be investigated.

Conclusion

V-FB and rhBMP-2, when incorporated in the same biodegradable PUR scaffold, can be released at a controlled and sustained manner, and has been demonstrated to control infection and promote new bone formation simultaneously. Compared with the current two-stage clinical standard of care, the dual delivery approach requires only one surgical procedure. The concept of protecting the wound from contamination during the bone regeneration process could potentially change the clinical management of infected open fractures.

Acknowledgement

This work was funded by the Orthopaedic Extremity Trauma Research Program (DOD-W81XWH-07-1-0211), the Armed Forces Institute of Regenerative Medicine (sub-contract from the Rutgers-Cleveland Clinic Consortium Award DOD-W81XWH-08-2-0034), Vanderbilt Univeristy, and the US Army Institute of Surgical Research.

References

1. Johnson EN, Burns TC, Hayda RA, Hospenthal DR, Murray CK. Infectious complications of open type III tibial fractures among combat casualties. Clin Infect Dis. 2007 Aug 15;45(4):409-15.

2. Ostermann PA, Seligson D, Henry SL. Local antibiotic therapy for severe open fractures. A review of 1085 consecutive cases. J Bone Joint Surg Br. 1995 Jan;77(1):93-7.

3. Ristiniemi J, Lakovaara M, Flinkkila T, Jalovaara P. Staged method using antibiotic beads and subsequent autografting for large traumatic tibial bone loss: 22 of 23 fractures healed after 5-20 months. Acta Orthop. 2007 Aug;78(4):520-7.

4. Moehring HD, Gravel C, Chapman MW, Olson SA. Comparison of antibiotic beads and intravenous antibiotics in open fractures. Clin Orthop Relat Res. 2000 Mar(372):254-61.

5. Adams K, Couch L, Cierny G, Calhoun J, Mader JT. *In vitro* and *in vivo* evaluation of antibiotic diffusion from antibiotic-impregnated polymethylmethacrylate beads. Clin Orthop Relat Res. 1992 May(278):244-52.

6. Kuechle DK, Landon GC, Musher DM, Noble PC. Elution of vancomycin, daptomycin, and amikacin from acrylic bone cement. Clin Orthop Relat Res. 1991 Mar(264):302-8.

7. Mader JT, Calhoun J, Cobos J. *In vitro* evaluation of antibiotic diffusion from antibiotic-impregnated biodegradable beads and polymethylmethacrylate beads. Antimicrob Agents Chemother. 1997 Feb;41(2):415-8.

8. Nelson CL, Griffin FM, Harrison BH, Cooper RE. *In vitro* elution characteristics of commercially and noncommercially prepared antibiotic PMMA beads. Clin Orthop Relat Res. 1992 Nov(284):303-9.

9. Jeon O, Song SJ, Kang SW, Putnam AJ, Kim BS. Enhancement of ectopic bone formation by bone morphogenetic protein-2 released from a heparin-conjugated poly(L-lactic-co-glycolic acid) scaffold. Biomaterials. 2007;28(17):2763-71.

10. Boyne PJ, Marx RE, Nevins M, Triplett G, Lazaro E, Lilly LC, et al. A feasibility study evaluating rhBMP-2/absorbable collagen sponge for maxillary sinus floor augmentation. Int J Periodontics Restorative Dent. 1997 Feb;17(1):11-25.

11. Howell TH, Fiorellini J, Jones A, Alder M, Nummikoski P, Lazaro M, et al. A feasibility study evaluating rhBMP-2/absorbable collagen sponge device for local alveolar ridge preservation or augmentation. Int J Periodontics Restorative Dent. 1997 Apr;17(2):124-39.

12. Hoffmann A, Weich HA, Gross G, Hillmann G. Perspectives in the biological function, the technical and therapeutic application of bone morphogenetic proteins. Appl Microbiol Biotechnol. 2001 Oct;57(3):294-308.

13. Hogan BL. Bone morphogenetic proteins: multifunctional regulators of vertebrate development. Genes Dev. 1996 Jul 1;10(13):1580-94.

14. Malchau H, Herberts P, Eisler T, Garellick G, Soderman P. The Swedish Total Hip Replacement Register. J Bone Joint Surg Am. 2002;84-A Suppl 2:2-20.

15. Lienau J, Schmidt-Bleek K, Peters A, Haschke F, Duda GN, Perka C, et al. Differential regulation of blood vessel formation between standard and delayed bone healing. J Orthop Res. 2009 Sep;27(9):1133-40.

16. Geiger F, Bertram H, Berger I, Lorenz H, Wall O, Eckhardt C, et al. Vascular endothelial growth factor gene-activated matrix (VEGF165-GAM) enhances osteogenesis and angiogenesis in large segmental bone defects. J Bone Miner Res. 2005 Nov;20(11):2028-35.

17. Guelcher S, Srinivasan A, Hafeman A, Gallagher K, Doctor J, Khetan S, et al. Synthesis, *In vitro* degradation, and mechanical properties of two-component poly(ester urethane)urea scaffolds: Effects of water and polyol composition. Tissue Engineering. 2007;13(9):2321-33.

18. Guelcher SA. Biodegradable polyurethanes: Synthesis and applications in regenerative medicine. Tissue Engineering Part B-Reviews. 2008;14(1):3-17.

19. Guelcher SA, Patel V, Gallagher KM, Connolly S, Didier JE, Doctor JS, et al. Synthesis and *in vitro* biocompatibility of injectable polyurethane foam scaffolds. Tissue Engineering. 2006;12(5):1247-59.

20. Gorna K, Gogolewski S. Biodegradable polyurethanes for implants. II. *In vitro* degradation and calcification of materials from poly(epsilon-caprolactone)-poly(ethylene oxide) diols and various chain extenders. Journal of Biomedical Materials Research. 2002;60(4):592-606.

21. Gorna K, Gogolewski S. Preparation, degradation, and calcification of biodegradable polyurethane foams for bone graft substitutes. Journal of Biomedical Materials Research Part A. 2003;67A(3):813-27.

22. Bonzani IC, Adhikari R, Houshyar S, Mayadunne R, Gunatillake P, Stevens MM. Synthesis of two-component injectable polyurethanes for bone tissue engineering. Biomaterials. 2007 Jan;28(3):423-33.

23. Guan JJ, Sacks MS, Beckman EJ, Wagner WR. Synthesis, characterization, and cytocompatibility of efastomeric, biodegradable poly(ester-urethane)ureas based on poly(caprolactone) and putrescine. Journal of Biomedical Materials Research. 2002;61(3):493-503.

24. Zhang JY, Beckman EJ, Hu J, Yang GG, Agarwal S, Hollinger JO. Synthesis, biodegradability, and biocompatibility of lysine diisocyanate-glucose polymers. Tissue Engineering. 2002;8(5):771-85.

25. Zhang JY, Beckman EJ, Piesco NP, Agarwal S. A new peptide-based urethane polymer: synthesis, biodegradation, and potential to support cell growth *in vitro*. Biomaterials. 2000;21(12):1247-58.

26. Li B, Brown KV, Wenke JC, Guelcher SA. Sustained release of vancomycin from polyurethane scaffolds inhibits infection of bone wounds in a rat femoral segmental defect model. Journal of Controlled Release. In press.

27. Li B, Davidson JM, Guelcher SA. The effect of the local delivery of platelet-derived growth factor from reactive two-component polyurethane scaffolds on the healing in rat skin excisional wounds. Biomaterials. 2009 Jul;30(20):3486-94.

28. Li B, Yoshii T, Hafeman AE, Nyman JS, Wenke JC, Guelcher SA. The effects of rhBMP-2 released from biodegradable polyurethane/microsphere composite scaffolds on new bone formation in rat femora. Biomaterials. 2009 Dec;30(35):6768-79.

29. Hafeman AE, Zienkiewicz KJ, Carney E, Litzner B, Stratton C, Wenke JC, et al. Local delivery of tobramycin from injectable biodegradable polyurethane scaffolds. J Biomaterials Science. 2009;DOI:10.1163/156856209X410256.

30. Ruiz JC, Alvarez-Lorenzo C, Taboada P, Burillo G, Bucio E, De Prijck K, et al. Polypropylene grafted with smart polymers (PNIPAAm/PAAc) for loading and controlled release of vancomycin. Eur J Pharm Biopharm. 2008 Oct;70(2):467-77.

31. Adams CS, Antoci V, Jr., Harrison G, Patal P, Freeman TA, Shapiro IM, et al. Controlled release of vancomycin from thin sol-gel films on implant surfaces successfully controls osteomyelitis. J Orthop Res. 2009 Jun;27(6):701-9.

32. Chen X, Tsukayama DT, Kidder LS, Bourgeault CA, Schmidt AH, Lew WD. Characterization of a chronic infection in an internally-stabilized segmental defect in the rat femur. J Orthop Res. 2005 Jul;23(4):816-23.

33. Chen X, Kidder LS, Lew WD. Osteogenic protein-1 induced bone formation in an infected segmental defect in the rat femur. J Orthop Res. 2002 Jan;20(1):142-50.

34. Anglen JO. Comparison of soap and antibiotic solutions for irrigation of lower-limb open fracture wounds. A prospective, randomized study. J Bone Joint Surg Am. 2005 Jul;87(7):1415-22.

35. Brown KV, Walker JA, Cortez DS, Murray CK, Wenke JC. Earlier Debridement and Antibiotic Administration Decreases Infection. Journal of Surgical Orthopaedic Advances. 2009, Accepted.

36. Li B, Brown KV, Wenke JC, Guelcher SA. Sustained release of vancomycin from polyurethane scaffolds inhibits infection of bone wounds in a rat femoral segmental defect model. J Control Release. 2010 Apr 8.

37. Edin ML, Miclau T, Lester GE, Lindsey RW, Dahners LE. Effect of cefazolin and vancomycin on osteoblasts *in vitro*. Clin Orthop Relat Res. 1996 Dec(333):245-51.

38. Antoci V, Jr., Adams CS, Hickok NJ, Shapiro IM, Parvizi J. Antibiotics for local delivery systems cause skeletal cell toxicity *in vitro*. Clin Orthop Relat Res. 2007 Sep;462:200-6.

39. Gung YW, Cheng CK, Su CY. A stereomorphologic study of bone matrix apposition in HA-implanted cavities observed with SEM, being prepared by a microvascular cast and freeze-fracture method. Med Eng Phys. 2003 Sep;25(7):565-71.

40. Salthouse TN. Cellular enzyme activity at the polymer-tissue interface: a review. JBiomedMaterRes. 1976;10(2):197-229.

41. Santerre JP, Labow RS, Adams GA. Enzyme Biomaterial Interactions - Effect of Biosystems on Degradation of Polyurethanes. Journal of Biomedical Materials Research. 1993;27(1):97-109.

42. Labow RS, Duguay DG, Santerre JP. The Enzymatic-Hydrolysis of A Synthetic Biomembrane - A New Substrate for Cholesterol and Carboxyl Esterases. Journal of Biomaterials Science-Polymer Edition. 1994;6(2):169-79.

43. Labow RS, Erfle DJ, Santerre JP. Neutrophil-Mediated Degradation of Segmented Polyurethanes. Biomaterials. 1995;16(1):51-9.

44. Dumas JE, Zienkiewicz K, Tanner SA, Prieto EM, Bhattacharyya S, Guelcher S. Synthesis and Characterization of an Injectable Allograft Bone/polymer Composite Bone Void Filler with Tunable Mechanical Properties. Tissue Eng Part A. Mar 10.

CHAPTER VI

CONCLUSION AND FUTURE WORK

Summary of the dissertation

Starting from bioactive growth factor delivery from PUR scaffolds, dual release of both a growth factor and an antibiotic were demonstrated to enhance the healing of infected bone wounds successfully when the release profiles of both rhBMP-2 and Vancomycin were optimized to match their biological functions. The results show that sustained release of vancomycin above the MIC from biodegradable porous PUR for up to 8 weeks is desired to control infection in both soft tissue and bone tissue effectively. Additionally, both a burst release and sustained release of rhBMP-2 from PUR are desired to promote bone regeneration by promoting initial cellular infiltration and later cell differentiation into osteoblasts. The approach of combining both infection control and bone graft through a biodegradable PUR system, could potentially replace the current standard of care by eliminating an extra surgical procedure.

The first chapter presents the background based on which the studies designed, and the detailed experimental studies toward the final goal of achieving a dual delivery system. The project was divided into four specific aims, with each of them elaborated as a chapter in the dissertation.

The second chapter discusses PDGF-BB, a growth factor that primarily promotes cellular migration and proliferation, to optimize the release efficiency of growth factor from PUR. While protein in solution potentially reacts with isocyanate during polymerization, it

can be avoided through lyophilization and incorporation as a powder in the scaffold. The activity of PUR/PDGF-BB was tested in a rat skin excisional wound. While the release of PDGF-BB promoted tissue regeneration by recruiting cells into the scaffold as expected, the degradation rate of the polymer was also enhanced, due to the presence of more inflammatory cells attracted by the growth factor.

The third chapter relates to rhBMP-2, a growth factor used to enhance new bone formation. While bolus release of rhBMP-2 is neither performance- nor cost- effective, sustained release of rhBMP-2 has been reported in a number of studies to maximize its function as a morphogen. Since BMP-2 is also involved in early events of fracture healing such as cell recruitment and angiogenesis, a modest release in the early stage might be desirable. To test this hypothesis, a PLGA microsphere encapsulation approach was adopted, and the size of microspheres was observed to relate to the burst release of rhBMP-2. When tested in rat femoral defects, both the simple plug defect and the critical size segmental defect, our hypothesis was confirmed that both burst release and sustained release of rhBMP-2 were important in promoting bone regeneration.

The fourth chapter relates to antibiotic release from PUR. In order to effectively control infection of a bone wound, it is desirable to deliver effective concentration of antibiotic to the injury site for weeks to allow normal angiogenesis to happen which is a prerequisite for bone tissue formation. Most antibiotics are small molecules and very water soluble. In order to control/sustain the antibiotic release, vancomycin was chosen due to its adjustable solubility which is critical in determining its release profile from highly porous scaffolds. By converting vancomycin hydrochloride to free base, the solubility is significantly decreased and the release of effective concentration is extended to up to at least 8 weeks. The

improved release profile translated to better performance when tested in an infected rat femoral segmental defect.

The fifth chapter combines the best candidate delivery strategies observed for both rhBMP-2 and vancomycin, to incorporate both of them in the same PUR composite for the treatment of infected bone wounds. The composites were tested in the non-infected rat femoral segmental defect, to ensure that the presence of V-FB does not compromise the biological function of rhBMP-2. The composites were then tested in the infected segmental defect, and the bone regeneration rates were compared to the clinically used collagen sponge with rhBMP-2. Significantly more new bone formation was observed for the case of rhBMP-2 and V-FB dual delivery through the PUR sustained release system. Furthermore, the degree of bone regeneration was related to the rate of infection in the animals.

Future work

Overall, the concept of combining both infection control and bone graft through a biodegradable PUR system thus eliminating an extra surgical procedure in clinical standard care has been demonstrated in the present study. However, there are several directions under consideration or ongoing which could potentially be combined with the present biomaterials design, to make it more effective in promoting bone regeneration and more convenient for clinical applications.

Cell delivery from PUR

As evidenced by the present study, the presence of cells in the scaffolds is critical for tissue regeneration (1), and cellular infiltration can be promoted by release of growth factors. Therefore, it is anticipated that delivery of stem cells with the scaffolds would

accelerate bone wound healing through cell proliferation and differentiation promoted by the growth factor (1-3).

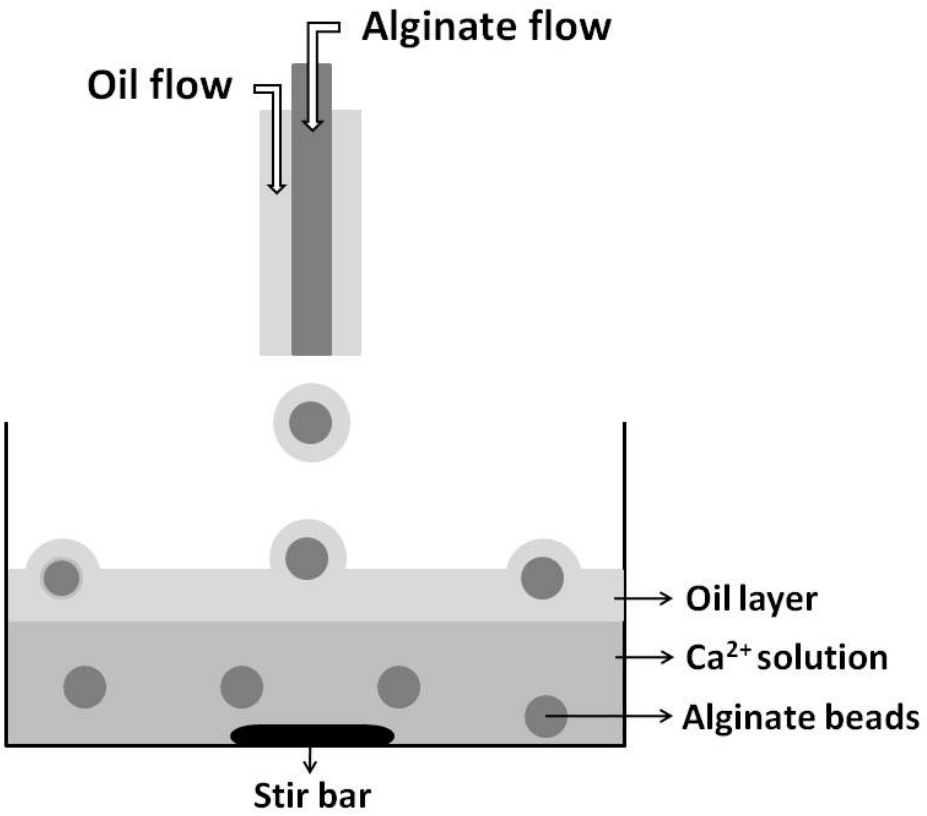

Figure VI-1 Alginate beads fabrication through crosslinking initiated by calcium

Some preliminary work has been performed to test the feasibility of delivering cells using PUR scaffolds. To protect cells from reacting with reactive PUR, MC3T3 cells were encapsulated in alginate beads before embedding into PUR. The alginate beads were fabricated by dropping the alginate solution (1-2 wt%, containting 10^6 cells per ml) into calcium chloride (100 mM) solution where the crosslinking occurs to form solid, hydrated beads (Figure VI-1) (4-6). By tuning parameters such as the flow rate of alginate and the

needle diameter of the flow, or introducing an outer oil flow, the alginate size bead can be adjusted from 500 μm to 2500 μm.

The encapsulated cells are viable as demonstrated by the green fluorescence when stained by LIVE/DEAD® Viability/Cytotoxicity Kit (Invitrogen, Carlsbad, CA) (Figure VI-2). The beads could then be embedded into PUR scaffolds by mixing with the polyol component before reacting with isocyanate. To react with excess amount of moisture on the bead surfaces, the index was chosen to be 180 (100 × ratio of NCO to OH) instead of 115 for regular PUR.

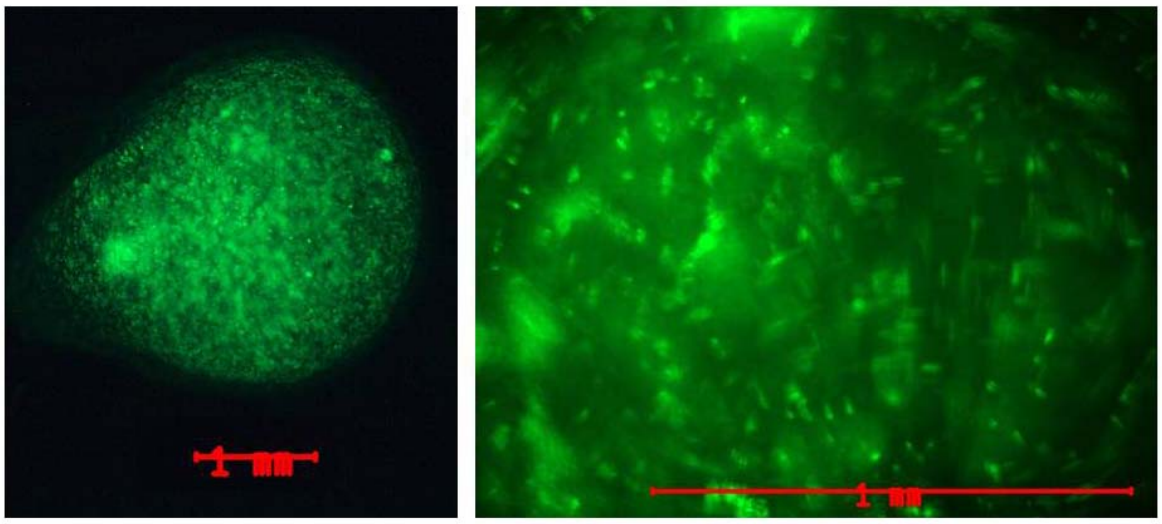

Figure VI-2 Live/dead staining of MC3T3 cells within alginate beads after fabrication

PUR degradation adjustment

In this project, PUR incorporated with growth factor has been tested in both skin tissue and bone tissue, and it was interesting to find that very different cellular responses have been observed for different tissue type and the degradation rate of polymer may depend on the wound type. In the skin excisional wound, the dominating cell types present in the

scaffolds are inflammatory cells and fibroblast cells. In this case, the polymer degradation was mainly mediated by the inflammatory cells that release both reactive oxygen species and enzymes (7-10).

However, in the femoral segmental defect, no inflammatory cells were observed, therefore the polymer has been demonstrated to degrade very slowly (e.g. about 40% polymer presence at week 8, and less than 10% degradation between weeks 4 and 8), which could have potentially impeded the process of new bone formation, and also drug release kinetics as well. A recent study by Yaszemski's lab (14) using isotope labeled BMP-2 showed that its retention profile observed *in vivo* was very similar to that tested on cell culture *in vitro*, but the release rate is faster *in vivo* (e.g. it takes 6~7 weeks and ~5 weeks for the release to reach plateau for *in vitro* and *in vivo* respectively). Since the polymer usually degrades slower *in vitro*, the enhanced release *in vivo* could have been due to the increased degradation. In the present study, the PUR/rhBMP-2 sustained release system which degrades very slowly, promoted more new bone formation than the collagen/rhBMP-2 bolus release system which disappears very quickly *in vivo* (e.g. no evidence of collagen presence was observed at week 4). Therefore, PUR/rhBMP-2 is expected to perform better if it is degraded faster due to 1) more space created allowing more cellular infiltration and 2) increased growth factor release promoting cellular differentiation.

Ideally, the polymer has to degrade gradually to allow the recruitment of cells which are responsible to develop into bone tissue. Polyurethane is a tunable system (11, 12). By carefully selecting the components (such as polyester triol) for polymerization, the degradation profile can be adjusted. There are several strategies to speed up the polymer degradation. The choice of isocyanate affect degradation rate, and PUR synthesized from LTI usually degrades faster than that synthesized from HDIt. Alternatively, we can also

increase the molecular weight of polyester triol, and the elongated soft segments are more susceptible to hydrolysis. Additionally, the ratio of different components (caprolactone, glycolide, and lactide) involved in synthesizing polyester triol could be adjusted, and the increase of glycolide percentage would increase the degradation rate of PUR as well.

A recent study in our lab, which tested bone particles bearing PUR composites (with a porosity of 50% of the scaffolds) in a rabbit calvaria defect, showed few amount of polymer presence at weeks 6 and complete polymer degradation at weeks 12. The formulation used in this study could be a promising candidate for future studies with dual delivery of both growth factor and antibiotic.

Injectable dual delivery PUR composites

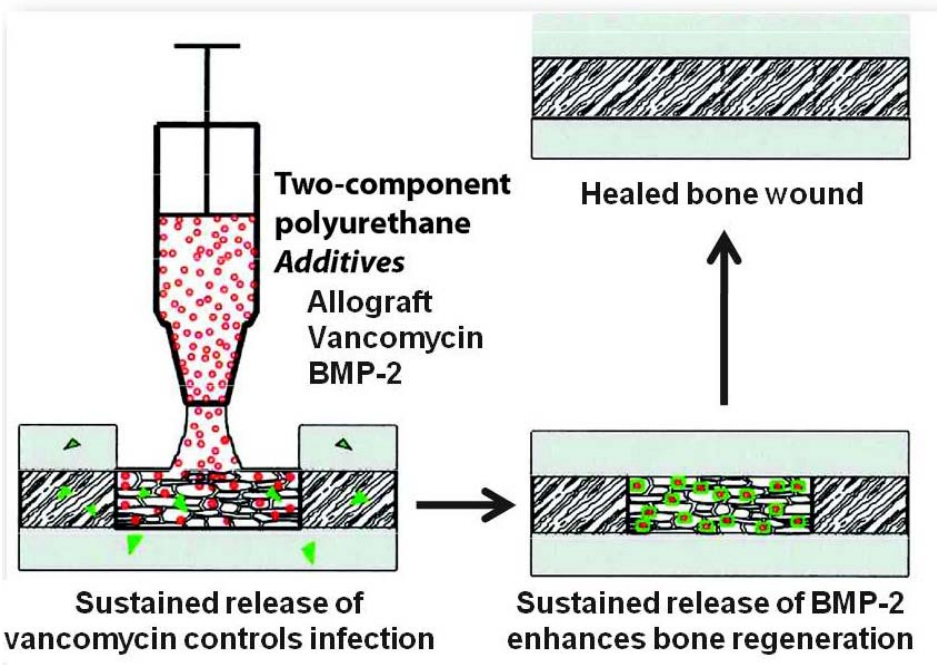

Figure VI-3 Injectable dual delivery PUR for infected bone wound healing

All the scaffolds tested under the present study are premade implants. For easier application, it is desirable to make it an injectable system. Upon mixing of the two reactive components, the isocyanate and the hardener, the mixture can be injected through a syringe as a liquid, and then hardens *in situ* (13). By carefully choosing the amount of catalyst, the working time can be adjusted to be around 3-5 minutes which is appropriate for operation. Combining the injectability and dual delivery outcomes, PUR/bone graft composite containing vancomycin and rhBMP-2 can be applied as an injection liquid to inhibit infection and enhance bone wound healing (Figure VI-3).

References

1. Ikada Y. Challenges in tissue engineering. J R Soc Interface. 2006 Oct 22;3(10):589-601.

2. Barrientos S, Stojadinovic O, Golinko MS, Brem H, Tomic-Canic M. Growth factors and cytokines in wound healing. Wound Repair Regen. 2008 Sep-Oct;16(5):585-601.

3. Pedersen JA, Swartz MA. Mechanobiology in the third dimension. Ann Biomed Eng. 2005 Nov;33(11):1469-90.

4. Mandal BB, Kundu SC. Calcium alginate beads embedded in silk fibroin as 3D dual drug releasing scaffolds. Biomaterials. 2009 Oct;30(28):5170-7.

5. Goren A, Dahan N, Goren E, Baruch L, Machluf M. Encapsulated human mesenchymal stem cells: a unique hypoimmunogenic platform for long-term cellular therapy. Faseb J. Jan;24(1):22-31.

6. Hunt NC, Shelton RM, Grover LM. Reversible mitotic and metabolic inhibition following the encapsulation of fibroblasts in alginate hydrogels. Biomaterials. 2009 Nov;30(32):6435-43.

7. Salthouse TN. Cellular enzyme activity at the polymer-tissue interface: a review. JBiomedMaterRes. 1976;10(2):197-229.

8. Santerre JP, Labow RS, Adams GA. Enzyme Biomaterial Interactions - Effect of Biosystems on Degradation of Polyurethanes. Journal of Biomedical Materials Research. 1993;27(1):97-109.

9. Labow RS, Duguay DG, Santerre JP. The Enzymatic-Hydrolysis of A Synthetic Biomembrane - A New Substrate for Cholesterol and Carboxyl Esterases. Journal of Biomaterials Science-Polymer Edition. 1994;6(2):169-79.

10. Labow RS, Erfle DJ, Santerre JP. Neutrophil-Mediated Degradation of Segmented Polyurethanes. Biomaterials. 1995;16(1):51-9.

11. Guelcher S, Srinivasan A, Hafeman A, Gallagher K, Doctor J, Khetan S, et al. Synthesis, *In vitro* degradation, and mechanical properties of two-component poly(ester urethane)urea scaffolds: Effects of water and polyol composition. Tissue Engineering. 2007;13(9):2321-33.

12. Guelcher SA. Biodegradable polyurethanes: Synthesis and applications in regenerative medicine. Tissue Engineering Part B-Reviews. 2008;14(1):3-17.

13. Dumas JE, Zienkiewicz K, Tanner SA, Prieto EM, Bhattacharyya S, Guelcher S. Synthesis and Characterization of an Injectable Allograft Bone/polymer Composite Bone Void Filler with Tunable Mechanical Properties. Tissue Eng Part A. Mar 10.

14. Kempen DH, Lu L, Hefferan TE, Creemers LB, Maran A, Classic KL, et al. Retention of *in vitro* and *in vivo* BMP-2 bioactivities in sustained delivery vehicles for bone tissue engineering. Biomaterials. 2008 Aug;29(22):3245-52.